

Non-linear multivariate analysis of the global solar radiation  
received across five cities in South Africa

by

TAMARA ROSEMARY GOVINDASAMY

209540135

Submitted in partial fulfillment of the academic requirements of

Doctor of Philosophy in Physics

School of Chemistry and Physics

College of Agriculture, Engineering and Science

University of KwaZulu-Natal

Pietermaritzburg

2018



<b>Contents</b>	<b>Page</b>
Declaration	6
Acknowledgments	7
List of figures and tables	8
Nomenclature	12
Abstract	15
Chapter 1: Introduction	17
1.1. Current state of energy in South Africa	18
1.2. South Africa's investigation into alternate energy resources	20
1.3. The potential of solar energy	22
1.4. Research and skills which may assist in the adoption of solar renewable systems	25
Chapter 2: Solar radiation	28
2.1. Components of solar radiation	29
2.1.1. Long wave radiation	31
2.1.2. Short wave radiation	31
2.1.3. The solar constant ( $I_{sc}$ )	32
2.2. Geometric solar angles	33
2.3. Quantification of solar radiation	36
2.3.1. Pyrheliometers	38
2.3.2. Pyranometers	38
2.4. Considerations when evaluating global solar radiation	39
2.4.1. Cloud and surface albedo	40
2.4.2. Atmospheric factors	40
2.4.2.1. Clouds	40
2.4.2.1. Aerosols	41
2.5. Photovoltaic (PV) applications of solar radiation	42

	<b>Page</b>
2.5.1. Conversion of solar to PV energy	44
Chapter 3: Background and theory	47
3.1. Models to estimate GSR	47
3.2. Prediction models	47
3.2.1. Forecasting horizons	47
3.3. Statistical models	48
3.3.1. ANNs	49
3.3.2. NWP	49
3.4. Physical models	50
3.4.1. Temperature based models	50
3.4.1.1. Hargreaves-Samani (H-S) model	51
(i) Empirical coefficient ( $K_r$ )	52
3.4.1.2. Bristow and Campbell model	53
3.4.1.3. Allen model	53
3.4.1.4. Samani model	53
3.4.2. Sunshine duration models	54
3.4.2.1. Angstrom model	54
(i) Clearness Index ( $K_T$ )	54
(ii) Angstrom coefficients	55
3.4.2.2. Adaptations of the Angstrom model	56
3.5. Multivariate models	57
3.5.1. Proposed models for South Africa	58
Chapter 4: Method and materials	59
4.1. Weather and climate in South Africa	59
4.2. Study site details	62

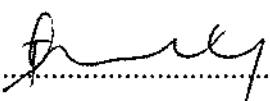
	<b>Page</b>
4.2.1. Bloemfontein, Free State	62
4.2.2. Cape Town, Western Cape	63
4.2.3. Durban, KwaZulu-Natal	63
4.2.4. Johannesburg, Gauteng	64
4.2.5. Pietermaritzburg, KwaZulu-Natal	64
4.3. Experimental technique	65
4.4. Statistical error analysis	66
Chapter 5: Results and Discussion	69
5.1. Single variable analysis	69
5.1.1. Bloemfontein (BFN)	69
5.1.2. Cape Town (CT)	73
5.1.3. Durban (DBN)	77
5.1.4. Johannesburg (JHB)	79
5.1.5. Pietermaritzburg (PMB)	82
5.2. Multivariate analysis	86
5.2.1. Bloemfontein (BFN)	87
5.2.2. Cape Town (CT)	88
5.2.3. Durban (DBN)	90
5.2.4. Johannesburg (JHB)	91
5.2.5. Pietermaritzburg (PMB)	93
Chapter 6: Conclusions	95
References	98
Appendix A: Fortran programs	107
Program to calculate $H_o$	107
Program to calculate $S_o$	109

	<b>Page</b>
Appendix B: Research article Quantifying the global solar radiation received in Pietermaritzburg, KwaZulu-Natal to motivate the consumption of solar technologies	110
Appendix C: Monthly average measurements	120
Appendix D: Research article (under review)	140

## Declaration


This dissertation describes the work undertaken in the School of Chemistry and Physics, University of KwaZulu-Natal (Pietermaritzburg), under the supervision of Prof. N. Chetty between April 2016 - December 2018. I declare this to be my original work except where due reference and credit is given.

Student : Tamara Rosemary Govindasamy

Signature:  .....

Date: 4 September 2019.....

Supervisor: Prof. Naven Chetty

Signature:  .....

Date: 4 September 2019.....

## Acknowledgments

We would like to acknowledge the South African Weather Service (SAWS) and Agricultural Research Council (ARC) for providing the measured meteorological variables required for this research.

I am grateful for the support and guidance received from Prof. Naven Chetty. I would like to express gratitude to my colleagues at Allan Gray for making provisions for me to complete my studies.

<b>List of Figures and Tables</b>	<b>Page</b>
Figure 1: PV potential across South Africa	23
Figure 2: Earth's energy budget	28
Figure 3: Intersections of the celestial sphere	33
Figure 4: Depiction of the declination and hour angle	35
Figure 5: Instruments used to measure solar radiation	39
Figure 6: The electron-hole pair after photon is absorbed	46
Figure 7: Maximum and minimum air temperatures across South Africa	59
Figure 8: High pressure belt over Africa	60
Figure 9: Köppen climate classification	61
Figure 10: Map of South Africa illustrating study sites	65
Figure 11: Graph of calculated $\frac{H}{H_o}$ using the H-S model for Bloemfontein	71
Figure 12: Graph of calculated $\frac{H}{H_o}$ using the A-P model for Bloemfontein	73
Figure 13: Graph of calculated $\frac{H}{H_o}$ using the H-S model for Cape Town	75
Figure 14: Graph of calculated $\frac{H}{H_o}$ using the A-P model for Cape Town	76



	<b>Page</b>
Figure 15: Graph of calculated $\frac{H}{H_o}$ using the H-S model for Durban	78
Figure 16: Graph of calculated $\frac{H}{H_o}$ using the A-P model for Durban	79
Figure 17: Graph of calculated $\frac{H}{H_o}$ using the H-S model for Johannesburg	81
Figure 18: Graph of calculated $\frac{H}{H_o}$ using the A-P model for Johannesburg	82
Figure 19: Graph of calculated $\frac{H}{H_o}$ using the H-S model for Pietermaritzburg	84
Figure 20: Graph of calculated $\frac{H}{H_o}$ using the A-P model for Pietermaritzburg	85
Figure 21: Proposed model for the estimation of $\frac{H}{H_o}$ for Bloemfontein	88
Figure 22: Proposed model for the estimation of $\frac{H}{H_o}$ for Cape Town	89
Figure 23: Proposed model for the estimation of $\frac{H}{H_o}$ for Durban	91
Figure 24: Proposed model for the estimation of $\frac{H}{H_o}$ for Johannesburg	92
Figure 25: Proposed model for the estimation of $\frac{H}{H_o}$ for Pietermaritzburg	94
Table 1: Classification of day type using clearness index	55
Table 2: Geographical details of study sites	62
Table 3: Regression equations using air temperature	70

	<b>Page</b>
Table 4: Regression equations using relative humidity	71
Table 5: Regression equations using sunshine duration	72
Table 6: Regression equations using air temperature	74
Table 7: Regression equations using relative humidity	75
Table 8: Regression equations using sunshine duration	76
Table 9: Regression equations using air temperature	77
Table 10: Regression equations using relative humidity	78
Table 11: Regression equations using sunshine duration	79
Table 12: Regression equations using air temperature	80
Table 13: Regression equations using relative humidity	81
Table 14: Regression equations using sunshine duration	82
Table 15: Regression equations using air temperature	83
Table 16: Regression equations using relative humidity	84

	<b>Page</b>
Table 17: Regression equations using sunshine duration	85
Table 18: Proposed multivariate equations	87
Table 19: Error indicators for proposed equations	87
Table 20: Proposed multivariate equations	88
Table 21: Error indicators for proposed equations	89
Table 22: Proposed multivariate equations	90
Table 23: Error indicators for proposed equations	90
Table 24: Proposed multivariate equations	91
Table 25: Error indicators for proposed equations	92
Table 26: Proposed multivariate equations	93
Table 27: Error indicators for proposed equations	93
Table 28: Summary of multivariate equations for each study site	95

## Nomenclature

PV	Photovoltaic
IRP	Integrated Resource Plan
DoE	South African Department of Energy
SAREC	South African Renewable Energy Council
SESSA	Sustainable Energy Society of South Africa
CSIR	Council for Scientific and Industrial Research
CSP	Concentrated Solar Power
SETRM	Solar Energy Technology Road Map
SA-STTRM	South African Solar Thermal Technology Road Map
GSR	Global Solar Radiation
$H_D$	Diffuse radiation
ETR ( $H_o$ )	Extraterrestrial radiation
$I_{sc}$	The solar constant
$H_B$	Direct beam radiation
$H_T$	Total radiation incident on a non-horizontal surface
$H_R$	Ground reflected radiation
$K_T$	Clearness index
$\rho_{sun}$	Sun's radiative power
WMO	World Meteorological Organization
$\theta_z$	Solar zenith angle
$\theta_i$	Angle of incidence
$\alpha$	Altitude
$\gamma$	Azimuth angle
$\phi$	Latitude
$t$	Time of day
$t_o$	Solar noon
$\delta$	Declination angle
$D_n$	Julian calendar day

$\omega_s$	Hour angle
$S_o$	Day length
$E_o$	Eccentricity coefficient ( $MJ/m^2.day$ )
WRC	World Radiation Center
BSRN	Baseline Surface Radiation Network
AOT	Aerosol Optical Thickness
UV	Ultraviolet
IR	Infrared
NWP	Numerical Weather Prediction
ANN	Artificial Neural Network
ARIMA	Auto Regressive Integrated Moving Average
AI	Artificial Intelligence
MLP	Multi-Layer Perceptron
RBF	Radial Basic Function
GCM	General Circulation Models
H-S	Hargreaves-Samani model
$K_r$	Empirical Hargreaves-Samani coefficient
$\Delta T$	Temperature difference ( $\Delta T = T_{max} - T_{min}$ )
$T_{max}$	Maximum air temperature ( $^{\circ}C$ )
$T_{min}$	Minimum air temperature ( $^{\circ}C$ )
$S$	Sunshine duration ( <i>hours</i> )
A-P	Angstrom-Prescott model
$K_T$	Clearness index ( $K_T = \frac{H}{H_o}$ )
$RH$	Relative humidity
SAWS	South African Weather Service
ARC	Agricultural Research Council
MBE	Mean Bias Error
MABE	Mean Absolute Bias Error
MPE	Mean Percentage Error
MAPE	Mean Absolute Percentage Error

RMSE	Root Mean Square Error
MARE	Mean Absolute Relative Error
$H_m$	Measured value of GSR
$H_c$	Calculated value of GSR
$H_{m,ave}$	Average measured value of GSR

## Abstract

South Africa is considered one of the most developed countries in Africa, however with more than 80% of its electricity being generated from coal, this country is considered one of the highest contributors to greenhouse gas emission throughout the continent. The impacts of this fossil fuel dependency are prominent in the environmental degradation experienced – climate change conditions as well as the current state of emergency faced by the national power utility, ESKOM. While provisions such as load shedding are being made to avoid the country from facing black out, the consequences of these resolves significantly influence the economy of the country.

Although the cost of applicable renewable energy technologies has decreased considerably over the past few years, South Africa continues to lag in the adoption of renewable energy systems in a global comparison. Most applications of potential solar renewable energy systems are currently in the investigation stages, leaving this readily accessible resource's capacity idle. This makes research in solar renewable energy highly significant with regards to progressing the country's uptake of green energy technologies.

Our study proposes linear and non-linear analysis of multivariate models for the estimation of global solar radiation (GSR) received across five major cities in South Africa. The significance of this study is to allow for effective GSR estimation in the application of solar technologies, while increasing implementation of these alternatives. Measured quantities such as sunshine duration and solar radiation for certain regions are limited due to the expensive equipment required and maintenance thereof. Local meteorological sources are unable to provide historic data which is complete, as these quantities are scarcely quantified.

The dependency of GSR on meteorological variables such as air temperature, relative humidity and relative sunshine duration was evaluated for the period January 2007 – June

2018 to realize estimation models for each of the study sites. The Hargreaves-Samani and Angstrom-Prescott empirical models served as the foundation for our single variable analysis of GSR reliance on each meteorological parameter and their relative variations. Our results have indicated that our proposed multivariate, non-linear equations perform better than the empirical models as well as single variable, linear regression equations. Our suggested models are site specific and demonstrate a strong correlation to historic GSR values with low, acceptable error indicators.

Further to this, we have recognized that second and third order relationships between  $H/H_0$  and multiple meteorological variables provide a more accurate description of GSR for most of the cities under study. This analysis could potentially contribute significantly to the investigation of solar radiation alternatives and photovoltaic (PV) technologies in South Africa. We believe that integration of estimation models within the design and installation stages of PV technologies will be largely beneficial in ensuring their optimum intake. The models discussed in this study verify the reliability and accuracy of GSR estimation through readily accessible meteorological factors in a cost effective manner.



## Chapter 1: Introduction

Ensuring that growing energy demands are met while providing secure energy supply and reducing greenhouse gas emission is a global undertaking, which South Africa is actively pursuing. In this chapter, we introduce South Africa, its current energy state of emergency and the developments being made to investigate the potential contributions of renewable energy resources. We will focus on the contribution of solar photovoltaic (PV) technologies and their implementation throughout the country.

South Africa is the southernmost country in the southern hemisphere and is considered a developing country with a population greater than 55,9 million (as at 2016, Worldbank statistics [1]). While trying to maintain the economic and social development of the country, many issues such as energy security, pose dire challenges for sustainability of the state. With the recent reintroduction of the load shedding program, citizens are once again left in darkness while fitting higher electricity bills. Little or no information is provided regarding any development plans which government and municipalities are investigating in order to alleviate the energy crisis, which often leads to a lack of support from citizens. It is vital to keep the communities and country aware of the current situations and mitigation plans which are intended.

South Africa, being one of the most coal dependent countries, needed to assess the status of available resources and whether or not this would be a sustainable option for future energy sourcing a long time ago. While the world is moving towards greener energy sources in an attempt to reduce our carbon footprint and hopefully alleviate the effects of global warming on climatic and environmental conditions, South Africa still trails behind when it comes to discovering an exploring the potential of alternative energy resources.

Certain areas in Africa receive more than double the amount of radiation as compared to countries in the northern hemisphere of the continent [2]. South Africa is no exception. It is well suited for the harnessing of solar radiation with sunshine being available throughout the year. Disregarding this potential, there are various financial and technical limitations associated with solar energy technologies, which restrict its use to private, off-grid networks. These boundaries need to be resolved in order to increase the impact and contribution of solar power to the country's energy supply. Thus, our work aims to provide an indication of the amount of underutilized solar potential is available in this country, while trying to increase the knowledge and implementation of such solar technologies.

### **1.1. Current state of energy in South Africa**

South Africa is considered one of the most developed countries in the continent of Africa, however with more than 80% of the electricity in South Africa being generated from coal, this classifies the country as the highest contributor to greenhouse gas emission in Africa [3,4]. Together with this, the intensive dependency on coal also results in a high level of environmental degradation as the depletion of this fossil fuel and environmental impacts are prominent. While being the 7<sup>th</sup> largest coal producer and 5<sup>th</sup> largest coal exporter globally, South Africa is still facing a dire energy crisis, with the current grid infrastructure taking strain while meeting day-to-day demands, and a significant proportion of the population not having access to electricity [3]. Energy security and sustainability remains one of the biggest challenges to be addressed by government.

The initial crisis began in late 2007, where a state of emergency called upon the implementation of the load shedding program (2008) to avoid the country facing a total black-out [5]. At the time, this was the only manner in which ESKOM (National electricity utility) could meet the current electricity demand. The extremity of the situation was one which had been brewing for some time and some of the contributing factors which led to this include; shortfalls in the management of the energy system, the increased demand of the continuously

growing South African population, increased energy consumption from industries such as mining, agriculture and transportation and little to no investment in the power infrastructure by government over the past decades [3,5].

Existing coal-fired power stations, Medupi and Kusile are experiencing intense strain as they are aging infrastructure and are unable to undergo routine maintenance. The available electricity reserve margins do not make allowance for these units to be serviced as the country's daily demands need to be met and any excess in supply is to be reserved for unplanned situations [5,6]. Meeting the country's internal demands is a residing challenge for ESKOM which has resulted in load shedding being carried out in periods of peak demand, for example: the winter months. Furthermore, ESKOM faces severe financial constraints in addition to its production capacity.

The energy sector has been neglected for the past few decades, with underinvestment from the state towards this sector [5,7,8]. Existing infrastructure now proves inadequate and unable to manage the current load. These are issues which could have been better anticipated, had the necessary resources and investments been directed towards managing resources, regulations and processes for the long-term [7]. The above is a brief description of the conditions which have given rise to escalated energy costs in South Africa. In addition, there remain countless households which have no access to grid electricity. Approximately 11% of the South African population (as at 2012) had no access to electricity [7]. This with the increased electricity costs only increases the gap in energy poverty

Municipalities have been making attempts to introduce electricity to rural households as the government believes that access to electricity is one of the main limiting factors affecting the country's economic growth [7]. Access to secure electricity supply is a key driver for development and innovation within the country, while creating employment and increasing the country's value. In order to improve the economy of the country, the progress of its people

is of utmost importance. Limited access to electricity and said resources in remote locations leaves part of the society with a lot less than just a deprivation of electricity supply. Lack of development in these areas, results in higher unemployment rates as access to educational resources and infrastructure is also low in these areas.

The government is introducing numerous efforts to alleviate the limitations faced by residents [7]. These are but a few of the socio-economic consequences arising from the disruption of energy supply and under performance of the national grid. While resolves to electrify the country may be on the forefront, the state utility continues to face increased demand resulting in higher electricity costs for the country as a whole. The improvement of these energy challenges is essential for the economic growth of a developing country such as South Africa.

## **1.2. South Africa's investigation into alternate energy resources**

Following the dissection of the current energy crisis, government together with the relevant departments began seeking alternatives to complement the heavy fossil fuel dependency and to diversify the sourcing of energy. Some of the viable renewable resources which are under study include; wind, solar, hydro, biomass and wave energy. Renewable resources are the ideal alternative to fossil fuels, as these will help reduce South Africa's greenhouse gas emission levels and potentially the cost of electricity production, while leading the energy sector to a sustainable path.

Although South Africa lags in acceptance of energy generation through renewables when compared to other countries, government has introduced policies and projects under the Integrated Resource Plan (IRP 2010) to address the current state of the energy sector and promote the use of diverse energy sources [6]. The South African Department of Energy (DoE) is delegated to facilitate the secure and sustainable delivery of energy for social and economic development of the country [10]. The IRP is a proposition to regulate and develop

an integrated energy plan for the energy industry as a whole. This ensures sustainability and development of the sector in both the short and long-term.

Renewable energy resources are under investigation and implementation in some instances, however in the case of solar technologies, these applications are limited to private, off-grid connections. Embracing green energy resources will reduce the costs of energy production, increase employment levels which will directly impact the rural parts of South Africa and attract investments into the country [3]. Universities across the state have invested multiple resources to the study of renewable energy potential in South Africa. Institutions such as the South African Renewable Energy Council (SAREC) and the Sustainable Energy Society of South Africa (SESSA) influence the research and policies surrounding renewable energy sources, through engagement with national and international stakeholders [3]. As the price of renewable energy technologies continues to decline, alternative sources prove to be more feasible for electricity generation.

Though the above factors drive and promote the use of diverse energy sources, there are numerous deficiencies which constrain the adaptation process. Economic and social challenges have a considerable influence on the introduction and research process. Alongside infrastructure and regulatory restraints, funding for the procurement of large-scale renewable energy systems remains one of the biggest challenges faced by the South African energy institutions [6].

The adaptation of renewable energy systems is largely dependent on the available financial support. The costs associated with developing and maintaining renewable energy systems which are able to contribute to grid demand are particularly high and hence require financial support from international stakeholders. Investments towards these systems are considered high risk with a lot of uncertainty, which make them unappealing. The shortage of financial security obstructs the positioning of such systems.

The IRP outlines strategies to address these challenges in the medium to long-term, while municipalities aim to reduce the socio-economic limitations [9]. Renewable energy systems have been introduced to some rural areas in the form of solar geysers, but this cannot be classified as grid application. Deliberate research and testing into the available renewable energy sources (specifically wind and solar energy) in South Africa is also largely affected by the lack of financial support [11]. Renewable resources are the ideal energy alternatives to significantly decrease South Africa's carbon footprint while salvaging the remaining available fossil fuels. The development of such systems in the energy industry will promote job creation and scarce skill development within the country and consequently encourage economic growth. Proper policies and support thereof need to be implemented at government level to ensure the advancement of diverse energy sourcing.

### **1.3. The potential of solar energy**

Of the renewable resources available, wind and solar power are the most abundant in South Africa. Studies by the Council for Scientific and Industrial Research (CSIR) identify these two renewables as the cheapest sources with generation capacity [12]. Receiving an average of 2500 hours of sunshine per year, including ample sunshine during the winter months, makes this country's solar potential one of the highest in the world [3,6]. The amount of solar radiation received varies in each province and has an average radiation level between 4.5 and 6.6  $KWh/m^2$  [3].

# PHOTOVOLTAIC POWER POTENTIAL SOUTH AFRICA

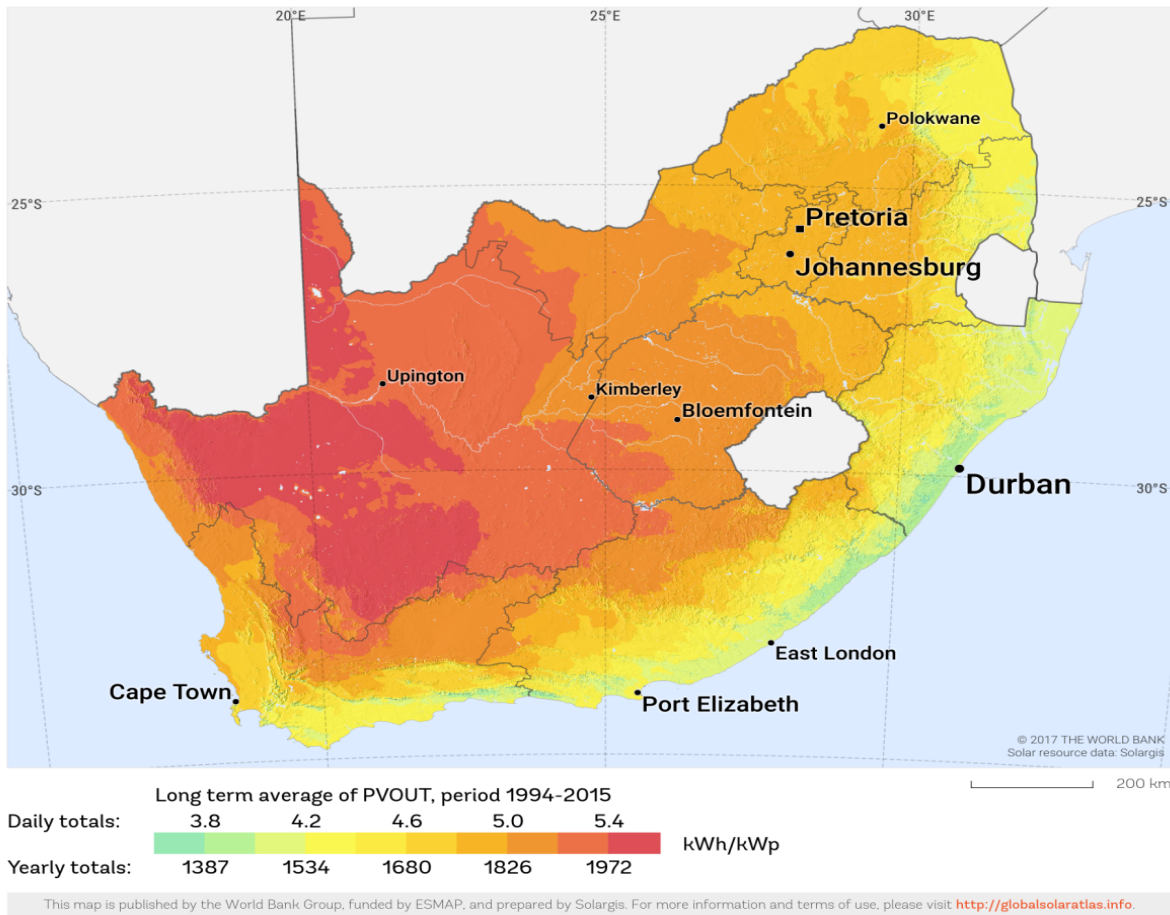


Figure 1: PV potential across South Africa [13]

There has been a noticeable rise in the use of off-grid, solar PV systems within the private sector. This may be due to the increased cost of conventional electricity as well as the disrupted energy supply experienced over the past few years (load shedding). Currently, registered solar PV systems only contribute 43.81MW and majority of usage lies within the commercial sector while there is no utility-scale contribution from Concentrated Solar Power (CSP) plants [3,6]. Some of the small-scale applications are for telecoms and electronic media [5]. Small-scale solar PV technologies have been introduced to rural and disadvantaged households, for basic electrification uses such as water heating and lighting. An existing 24

KW solar dish stirling plant was built as a demonstration in Johannesburg, Gauteng.

Recent studies being pursued in the realization of solar technologies include; the development of solar maps using measured radiation to improve on satellite solar data, Solar Energy Technology Road Map (SETRM) which aims to provide guidelines for the developing the solar technology industry and the South African Solar Thermal Technology Road Map (SA-STTRM) which intends to promote solar heating and cooling utilization [3]. A CSP feasibility study is underway in the Northern Cape province [6]. Implementation of large-scale solar technologies is subject to the following: energy strategies which are supported by the government, improvement of existing grid infrastructure and efficient use of grid electricity supply, a lack of suitable renewable energy skills at governmental level [3].

The growth of solar and other renewable energy systems will affect the initiatives and funding currently made towards existing coal stations and potential nuclear power plants [11]. The benefits of green energy sources will introduce variation to the energy supply and significantly reduce the strain experienced by current infrastructure. In order for renewables to produce a supply capacity which can supplement the current grid supply, sufficient financial support needs to be made available. As adoption of green energy systems depends heavily on the rate of economic growth and the state's energy demands, efficient use of grid supply will allow for additional supply to be stored while more attention and resources can be directed towards said renewable energy systems. Development of CSPs and other renewable energy systems will also extend as an energy saving opportunity while supplementing the grid supply.

The DoE began a CSP bid window which resulted in reduced prices of renewable energy technologies and contracting (these are considered internationally competitive) [14]. Developments within the solar energy sector on a global level have led to the decrease in costs of these technologies. Currently, China's bulk supply of solar PV technologies at low production costs has been one of the main contributors to the rapid progress of the solar PV industry



over the past few years.

Internationally, companies within the solar PV industry are exploring vertical integration opportunities in addition to manufacturing [14]. These advances have accompanied the decrease in costs of utility-scale solar PV projects which is considerable when investigating the potential use of these technologies. Solar PV technologies have become more commercialized while CSP technologies remain relatively expensive with limited suppliers [14].

Fresnel mirrors as well as storage capacity of the plant, have high production costs which make this a rare option. The procurement of CSP plants could be used to support utility grid supply, while significantly reducing the electricity tariffs in the long-term [14]. Energy security is crucial for economic growth and the above considerations show that the utility-scale potential of solar energy resources in South Africa is possible but requires a large amount of investment.

#### **1.4 Research and skills which may assist in the adoption of solar renewable systems**

Several tertiary institutions and organizations within South Africa have been researching the potential and various applications of solar renewable energy in South Africa. These findings are often used in strategy development and decision making by the relevant national stakeholders. Other institutions who make solar PV technologies available to consumers (commercial and residential) often study and provide courses which illustrate the feasibility of such systems based on the cost of PV energy yields. These courses outline the process of PV system installation, explain current and potential legislation surrounding these technologies in the private and commercial sectors and also expand on the optimization of systems depending on the requirements of a given site [15].

While these studies are crucial for the development of the renewable energy industry, suf-

ficient technical skills which are required to implement and enhance such systems is still lacking [3]. The lack of financial support towards this aspect of the adoption of renewable energies restricts the strategies which have been outlined by government and the relevant national departments. Research and the development of skills focused on the acquisition of renewable energy systems in South Africa should be one of the key focuses.

Solar radiation measurements and data are crucial for the development and performance estimation of CSP plants and PV technologies [16]. Analysis of available solar resources and estimations of yield have to be conducted before implementation of such technologies, especially due to the high associated costs. Application of solar PV technologies largely depends on the amount of solar radiation available at a given site, hence research in this regard is imperative. Although solar tracking PV technologies are existent, these often lose energy in the process. Evaluating the optimum tilt angle before installing PV modules can be performed by analyzing the available solar radiation of a location [17].

With solar radiation data not being readily available for most regions in South Africa, most research involves the use of meteorological variables and mathematical relations to investigate the solar potential for sites of interest [16,17]. The cost of equipment associated with the measurement of ground solar radiation levels are relatively high and it is often remote locations which receive high levels of solar radiation – where there is no access to solar radiation data. Various international studies over the past two decades have led to the development of solar radiation estimation models and time-series weather prediction models using available, measured meteorological factors [16,17,18]. Obtaining accurate models for locations is important and hence has become a field of large interest.

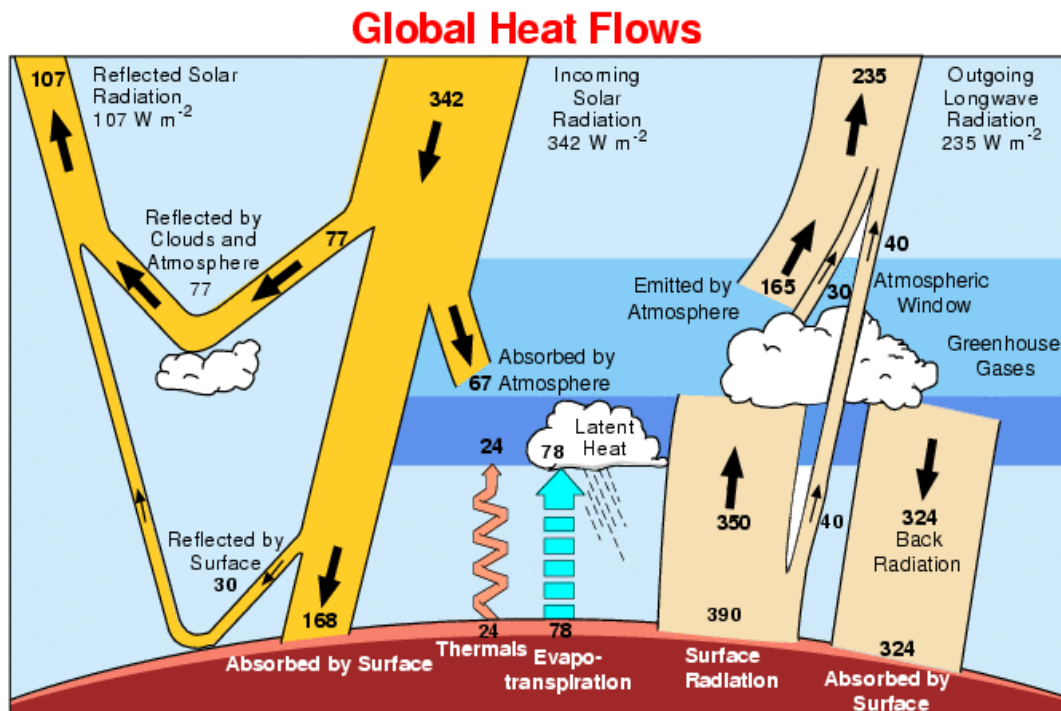
In this study, we analyze and enhance the existing linear models for five major cities in South Africa. Based on the available meteorological conditions provided by local weather stations, we introduce non-linear regression models for these cities, whilst evaluating their

efficiency and accuracy over a period longer than ten years. Further, we propose a multivariate model for each of these cities and test its performance in accordance to single variable models, as well as non-linear variations thereof. Based on our proposed models, we aim to encourage the use of solar radiation estimation models in the procurement of large-scale solar energy technologies. These cost-effective methods and skills are easily accessible and can be included in the assessment of the feasibility of solar PV technologies within the country.

## Chapter 2: Solar radiation

The sun, located approximately  $1.5 \times 10^{11}\text{m}$  away from the earth, emits electromagnetic radiation generated from nuclear fusion which is the primary source of the earth's energy [19]. The amount of solar insolation received at the surface of the earth is quantifiable variable, while variations of this quantity widely influence the earth's climate based on solar activity [20,21]. The solar constant is the radiation incident at the exterior of the earth's atmosphere, which is measured at surface normal to the incident radiation [20,22]. This constant is determined from space, via satellite data and has a value of  $1367\text{Wm}^{-2}$ . This quantity varies by approximately 0.01% over a period of around 30 calendar years [22-26].

The amount of solar irradiance at the earth's surface is exhausted by about 50% as compared to its original value as depicted in Figure 2 below. This is a result of attenuation which occurs in the atmosphere and accounts for almost 30% of the incident radiation being reflected before reaching the earth's surface [23,24].



*Kiehl and Trenberth 1997*

Figure 2: Earth's energy budget [27]

Global solar radiation (GSR) is the total solar radiation incident on a horizontal surface and it consists of two components; diffuse solar radiation and direct solar radiation [19-25]. When the incoming radiation passes through the atmosphere, it undergoes the effects of reflection, absorption and scattering. The irradiance which is scattered from all directions is referred to as diffuse solar radiation. While some of the incident radiation is also scattered back into space by the earth's surface, the radiation that enters the earth's surface in a straight line is known as direct solar radiation [20-23,25-28].

### 2.1. Solar radiation components

The solar radiation entering the earth's atmosphere is subject to attenuation. Only a portion of the incident radiation is absorbed by the earth's surface [19, 20-23,29-31]. Scattering of the radiation mainly occurs at short wavelengths due to the gaseous particles (greenhouse gases) which constitute the atmosphere [22,23]. Water vapor (clouds), aerosols and other particles which form the earth's atmosphere, cause the incident radiation to be scattered into random directions [20,23,31] and this is referred to as diffuse radiation ( $H_D$ ) [23,29-31]. Radiation experienced outside the atmosphere is known as extraterrestrial radiation (ETR) ( $H_o$ ). ETR incident on a surface outside the earth's atmosphere and normal to the incident radiation from the sun is known as the solar constant ( $I_{sc}$ ) [20,23,29,30].

Together with reflecting the incident radiation, these particles also absorb the radiation as illustrated in Figure 2. Reflection occurs at the surface of the earth at an atmospheric level, where a portion of the incident radiation is reflected back into space. Surface albedo is defined as the ratio of the reflected solar radiation to the actual incoming solar radiation [31]. The remaining radiation which is incident on a horizontal surface on the earth is called direct beam radiation ( $H_B$ ) [20,23,29-31].

The total radiation incident on a horizontal surface (the sum of the diffuse and direct beam radiation components) [23,30,32];

$$H = H_D + H_B \quad (1)$$

is known as the global solar radiation (GSR) and denoted by  $H$  ( $MJ/m^2$ ).

Since this represents radiation received from all angles, it is termed global [30]. The total radiation incident on a non-horizontal surface on earth ( $H_T$ ) has to include the ground reflected radiation ( $H_R$ ) [20,23,30];

$$H_T = H_D + H_B + H_R \quad (2)$$

Lambert's Cosine Law describes the GSR incident on a horizontal surface in terms of to its angle of incidence with the surface. The angle at which the nearly parallel radiation beams irradiate the horizontal surface is called the solar zenith angle ( $\theta_z$ ) [23,29,30]. For a horizontal surface, GSR can be described by;

$$H = H_D + H_o \cos\theta_z \quad (3)$$

and for a non-horizontal surface, the total incident radiation is;

$$H_T = H_D + H_o \cos\theta_i + H_R \quad (4)$$

where  $\theta_i$  is the angle of incidence between the radiation beam and is measured normal to the tilted surface [30]. The ratio of the GSR ( $H$ ) to the ETR ( $H_o$ ) gives a description of the atmosphere's transparency and is called the clearness index ( $K_T$ ) [11]. We discuss this quantity further in section 3.4.2.1.

$$K_T = \frac{H}{H_o} \quad (5)$$

The study of GSR is significant in providing insights on the earth's climatic conditions and

effects thereof. This quantity is also important in the study of renewable alternate energy sources which enables successful implementation and design of solar radiation systems. GSR has units of energy per square meter per day ( $W/m^2.day$ ) or ( $MJ/m^2.day$ ).

### **2.1.1. Long wave radiation**

This is the radiation which is absorbed by gaseous particles in the atmosphere and then re-emitted [27]. The long wave radiation is dependent on the temperature and absorption efficiency of the greenhouse gases ( $H_2O$ ,  $CO_2$ ,  $O_3$ ,  $O_2$  and water vapor) at certain wavelengths [19,27]. The transfer of long wave radiation in the presence of clouds depends on the cloud (top and base) temperatures as well as the cloud emissivity which relates the efficiency with which the clouds are able to absorb and reflect the long wave radiation [27]. The cloud emissivity is dependent on the cloud type and constituents.

### **2.1.2. Short wave radiation**

Short wave radiation is absorbed and scattered by the earth's atmosphere. The incident short wave radiation is either absorbed by the atmosphere and provides a heating effect or back scattered into space [27]. Similarly scattering occurs between clouds and the surface of the earth. Scattering of the incident radiation by clouds has greater significance in comparison to the scattering caused by gaseous particles and is known as Rayleigh scattering [20, 22,27]. Absorption and scattering of short wave radiation due to aerosols which exist in the atmosphere, depends largely on their optical and chemical characteristics.

### **2.1.3. The solar constant ( $I_{sc}$ )**

The solar constant ( $I_{sc}$ ) is the radiant energy experienced at normal incidence outside the earth's atmosphere and is measured at the mean sun-earth distance [19]. This quantity depends on the temperature of the sun, its size and the distance between the earth and sun [33]. According to the Stefan-Boltzmann law, if the sun is considered as a black-body, and we assume that the radiant energy expelled from the sun is the same energy which is incident

at the earth's surface, the solar constant can be calculated by the following:

$$I_{sc} = \frac{\rho_{sun}}{4\pi r^2} \quad (6)$$

where  $\rho_{sun}$  is the sun's solar radiation power and the area of the sphere is calculated using the radius of the sun-earth [33].

Since the distance between the earth and sun experiences annual regular variations,  $I_{sc}$  is agreed as an average value over a period of time. In 1982, the World Meteorological Organization (WMO) accepted the average value of  $1367\text{W}/\text{m}^2$  for the solar constant [19,20,22,27,33]. Variations in the earth-sun distance stem from the earth's elliptical orbit around the sun, resulting in the sun and earth being closer and further during periods of the year [33]. This is termed the eccentricity effect and the solar constant makes provision for this factor [20,22]. Typical variations from the mean sun-earth distance during the year approximate to  $\pm 1.7\%$  [33].

## 2.2. Geometric solar angles

The position of the sun has to be considered when determining the actual amount of solar radiation received on earth. As the position of the sun varies throughout the day, locating the sun's position relative to the earth is dependent on the following; the sun's zenith angle ( $\theta_z$ ), altitude ( $\alpha$ ) and the azimuth angle ( $\gamma$ ) which are further illustrated in Figure 3 [22,32-34].



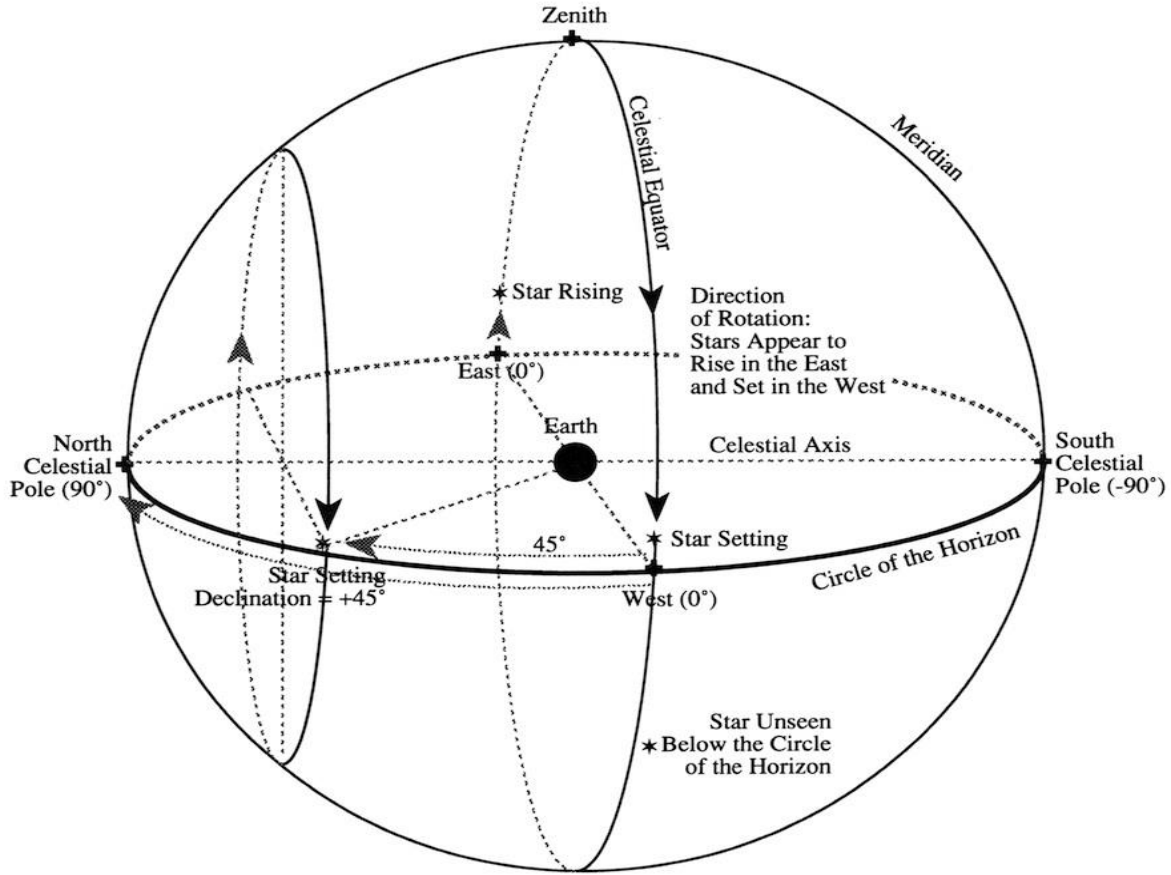


Figure 3: Intersections of the celestial sphere [38]

As briefly mentioned in the prior, the earth's orbit around the sun is elliptical with an axial tilt of  $23.45^\circ$  [33-37]. This is described as the inclination of the earth axis to the orbit. As the earth orbits the sun, its axis of rotation remains in a fixed position which leads to seasonal variation [36,37]. The celestial equator is the projection of the earth's equatorial plane, which is used to translate its position.

When the celestial equator intersects with the ecliptic plane, the earth experiences 'Equinoxes' which are indicators of season change [33,36,37]. When the sun passes the earth's equator (while south-bound) this is known as the Vernal Equinox in the southern hemisphere [22,36,37]. This occurs on the 23rd of September each year, while the Autumnal Equinox on the 21st of March [22,36,37].

Solstices are experienced when the earth is closest or furthest away from the sun and occur twice a year. June 21st is known as the Winter Solstice in the southern hemisphere and this is when the shortest day and longest night is experienced, due to the lowest sun angle of the year [36,37]. On December 21st the Summer Solstice consequences the longest day corresponding to the largest sun angle for the year [22,36,37].

Solar radiation incident at a given surface on the earth is also dependent on the latitude of that location. A specific site will receive the highest amount of solar radiation when the sun reaches its zenith which is its highest point in the sky for that particular day [33-37]. The specific time when the sun is at its peak, is known as the solar noon and the zenith angle is dependent on the latitude of the location ( $\phi$ ), the time of day ( $t$ ), solar noon ( $t_o$ ) as well as the the solar declination angle ( $\delta$ ) [32,33].

$$\cos\theta_z = \sin\phi\sin\delta + \cos\phi\cos\delta\cos[15(t - t_o)] \quad (7)$$

The time of solar noon and time of day need to be converted from hours to degrees, which shows that the earth rotates at a rate of  $15^\circ$  per hour ( $\frac{360^\circ}{24\text{hours}} = 15$ ) [23,32,33].

The latitude of a site ( $\phi$ ) is negative if it is in the southern hemisphere, positive for the northern hemisphere and its value ranges from  $0^\circ - 90^\circ$  [22,23,32]. This quantity is available for all geographical locations in any standard atlas.

The declination angle ( $\delta$ ), is defined as the angle at which the sun is located directly above the site, or at its zenith [23,32,33] and is described in [23,32,39,40] as;

$$\delta = 23.45^\circ \sin \left[ 360^\circ \frac{(284 + D_n)}{365} \right] \quad (8)$$

$\delta$  is a function of the day of the year  $D_n$  (Jan 1st = 1, Dec 31st = 365) [32,33,39,40], as well as the obliquity of the earth's orbit which is shown in Figure 4. The hour angle ( $\omega_s$ ) is the time deviation (in degrees) from solar noon [23,37,40];

$$\omega_s = \cos^{-1}(-\tan\phi \tan\delta) \quad (9)$$

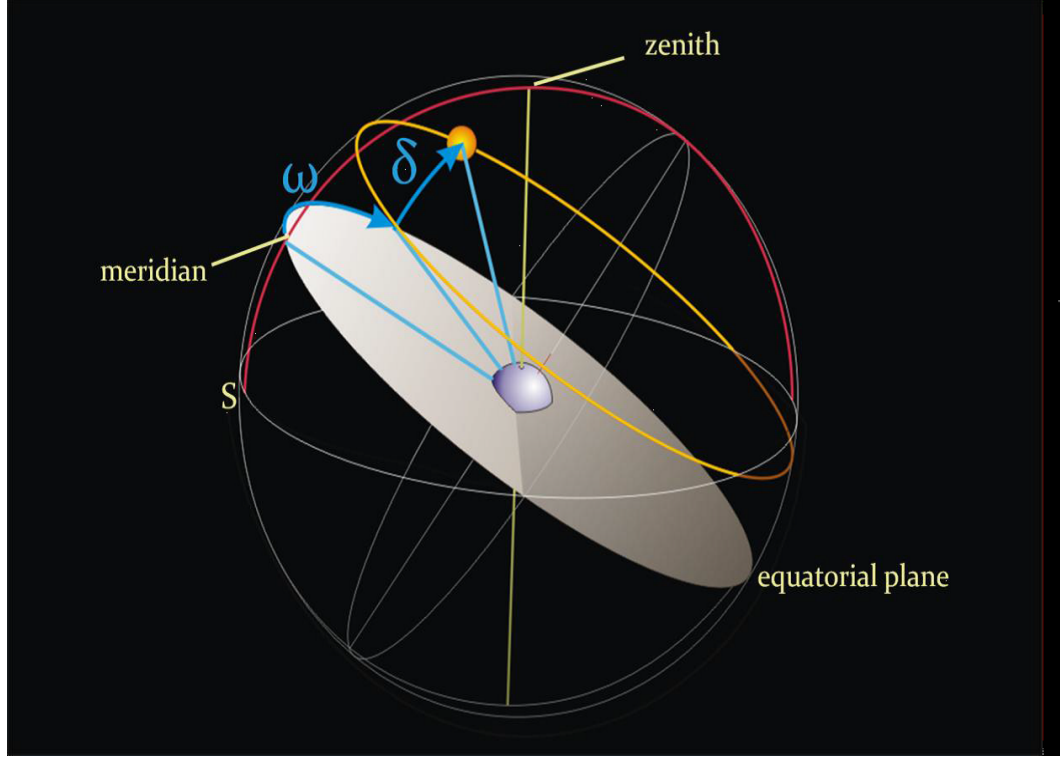


Figure 4: Depiction of the declination and hour angle [33]

The solar azimuth angle ( $\gamma$ ) is the angle measured from the north or south of the earth in the horizontal plane [32]. This angle is measured with respect to the south and increases, counter-clockwise [23,32];

$$\cos\gamma = -\frac{(\sin\delta - \cos\theta_z \sin\phi)}{\cos\phi \sin\theta_z} \quad (10)$$

The day length ( $S_o$ ) is used to translate time (in hours) between sunrise and sunset [23,32,33,40,41].

The duration of the sun appearing in the sky, at a given site;

$$S_o = \frac{2\omega_s}{15} \quad (11)$$

ETR ( $H_o$ ) is significantly dependent on many of these factors including;  $I_{sc}$ , the earth's obliquity and the above mentioned solar angles [22,23,29,40,41];

$$H_o = \frac{24 \times 3.6 \times 10^{-3} I_{sc}}{\pi} \left[ 1 + 0.033 \cos \left( \frac{2\pi D_n}{365} \right) \right] [\cos\phi \cos\delta \sin\omega_s + \omega_s \sin\phi \sin\delta] \quad (12)$$

The eccentricity coefficient,  $E_o$  ( $MJ/m^2.day$ ) is defined in terms of the earth-sun distance [22,23,29];

$$E_o = \left[ 1 + 0.033 \cos \left( \frac{2\pi D_n}{365} \right) \right] \quad (13)$$

Understanding of the geometrical location of the sun relative to the earth is significant in the research of solar radiation and its components.

### 2.3. Quantification of solar radiation

Knowledge of the available solar resources at a specific location helps to create an understanding of the nature and distribution of the incident radiation, as well as the climatic conditions experienced in that region [30]. Quantification of GSR is of economic importance in the review of renewable energy resources as it enables effective design and application of solar radiation systems. However, solar radiation data is not always available for every location and often in areas with the most solar potential. Meteorological stations which measure solar radiation data and sunshine duration, often require costly equipment and consequence high maintenance costs to record this data timeously [23,30].

Currently it is not possible to establish an accurate global coverage of solar radiation statistics as there aren't many active meteorological stations for most locations [31]. This results from the high associated costs and shortage of available infrastructure. The World Radiation Center (WRC) and Baseline Surface Radiation Network (BSRN), are two international net-

works which monitor the solar radiation received on earth by collecting recorded data from meteorological stations across the world. The findings from these centers serve as a reference database for solar radiation measurements throughout the world [30]. Due to the scarce number of meteorological stations which actively record solar radiation data, solar radiation estimation models which are accurate and efficient are constantly being pursued, developed and improved [30,40,41].

Some of the desired prediction methods focus on estimation through the use of more accessible meteorological factors such as air temperature, relative humidity, dew point, etc. [40,42,43]. Physical measurements of solar radiation can be conducted by the application of broadband radiometers which are designed to detect this electromagnetic radiation including its specific components, or by recording the sunshine duration using solar tracking devices [23,44].

Radiometry is the study of the measurement of electromagnetic radiation using radiometric devices that absorb solar radiation [23]. The detectors used in radiometers can be listed under the following types; thermopile detectors, black-body cavity detectors and semiconductor detectors [23]. It is vital that the radiometers used to measure solar radiation at a site be calibrated against an absolute radiometer [44]. Most of these instruments consist of a thermal detector, a glass dome (provides protection from environmental elements), a silica cartridge (absorbs any water particles), electric circuits and a narrow aperture [23,30,44]. Thermopile detectors are used to detect radiation in the short wavelength spectrum [23].

For accurate measurements, these radiometers need to record data at least every hour, while older methods of solar radiation measurements include the “Burning Card Method”, which works on the principle of the Campbell-Stokes sunshine recorder [23,44]. The direct beam radiation incident on this instrument is focused on a glass sphere containing a card inside. The course of the sun during the day burns a trace on the card, which is then examined to conclude

the sunshine duration as well as the time and position of the sun at sunrise and sunset [23,44].

### **2.3.1. Pyrheliometers**

These radiometers measure the direct beam radiation incident at a specific location and its marginal periphery (outer limits) [23,30,44]. The detector of a pyrheliometer tracks the sun during the day and is arranged normal to the direction of the incident solar radiation [23]. All radiometers consist of a thermal sensor or tracker which detects the energy of the incident radiation and converts it into electric signals [23,44].

The detection of the incident electromagnetic radiation is first conducted and then it is classified into direct or diffuse beam radiation by examining the energy and wavelength of the beams [30,44]. Pyrheliometers disregard the diffuse sky radiation and record only the direct beam radiation. For this reason, pyrheliometers have been accepted as a reliable device for the measurement of direct solar radiation.

### **2.3.2. Pyranometers**

Pyranometers are able to measure both direct and diffuse components of radiation through its horizontal radiation-sensing surface which absorbs GSR [23,30,44]. Certain pyranometers measure only the diffuse component by eliminating the direct beam radiation [44]. These require a shading disk which conceals the direct beam component and measures only the diffuse sky radiation. The shading disk is placed over the radiometer, along the path of the direct beam radiation [23].

Satellites have proven to be accurate in their ability to observe the solar radiation distribution along the earth's atmosphere through satellite images [30]. The images from geostationary satellites are processed to describe the solar radiation conditions at certain locations and are useful in monitoring and predicting the amount of cloud cover at a site [30]. Uncertainties in the measurements from radiometers depend on the structure of the instrument such as

sensitivity levels and thermal offsets which are the main sources of errors [23]. Spectral effects together with meteorological factors can also play a part in any discrepancies in recordings [23,30,44]. Atmospheric parameters such as temperature fluctuations, wind and rain impact the efficiency of the radiometer, and these errors have to be accounted for by correction methods [23,30].

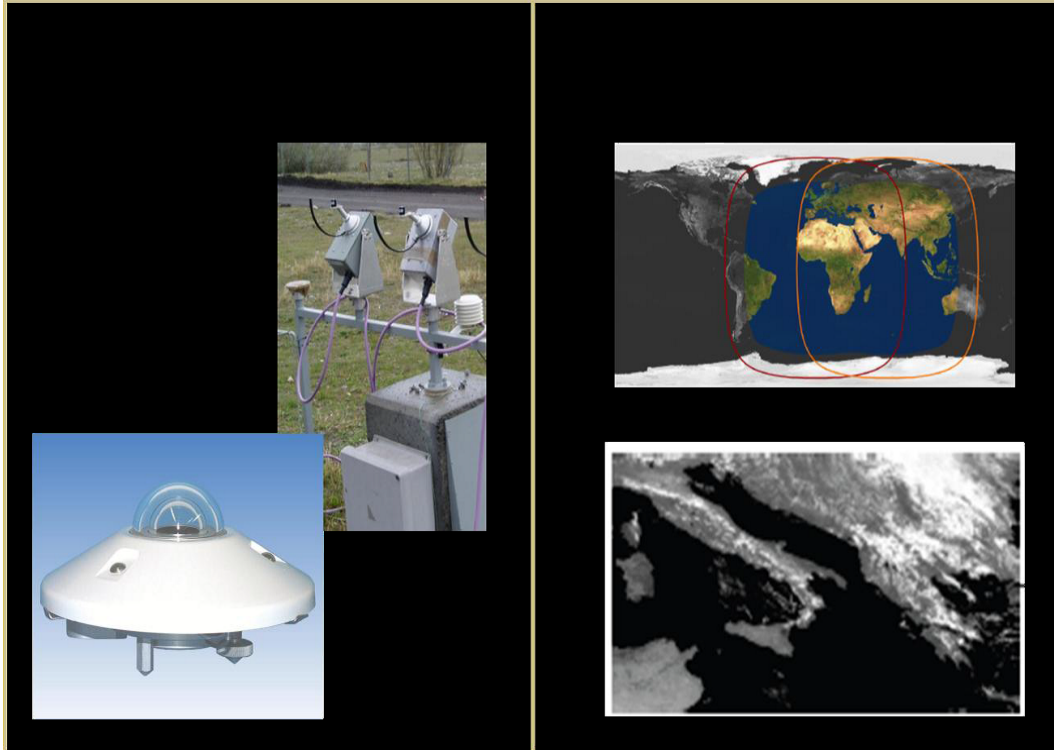


Figure 5: Instruments used to measure solar radiation [33]

#### 2.4. Considerations when evaluating global solar radiation

ETR which enters the atmosphere is depleted by attenuation processes such as absorption, reflection and scattering [20,23,32,44,45]. Various gaseous particles, aerosols and clouds constitute the atmosphere, and each of them can absorb, reflect or scatter the incident radiation [20,23,33]. Scattering occurs according to the Rayleigh Theory of scattering and is due to the concentration of gases in the atmosphere [23,33]. Elements such as pollutants, aerosol concentrations, atmospheric gas concentrations and clouds reduce the ETR into diffuse solar radiation by absorbing the incident solar radiation or reflecting it back into space [20,23].

### 2.4.1. Cloud and surface albedo

The ratio of solar radiation which is reflected and back-scattered ( $H_R$ ) to the incident radiation ETR ( $H_o$ ) at a surface, is known as the Surface-Albedo [20,23,45];

$$Albedo = \frac{H_R}{H_o} \quad (14)$$

The  $H_R$  component is specular (uniform reflection) and diffuse (random variation in reflected rays) in nature [45]. When the incident radiation is scattered and absorbed, the variation accompanying these processes is called the 'Direct Radiative Forcing' [23].

Cloud-Albedo describes the atmospheric transparency by quantifying the degree of cloudiness [20,23]. This proportion is dependent on the type of clouds and can be determined by considering the observed amount of cloud cover, sunshine duration or by computing the Aerosol Optical Thickness (AOT) of the cloud [23,27,33]. The eccentricity effect causes a change in the amount of solar radiation incident at a specific location during the year [45]. The amount of GSR available on a surface at the earth depends on the atmospheric conditions mentioned above. Hence, the transparency of the atmosphere (Albedo) is described in terms of aerosol and atmospheric gas concentrations [23].

### 2.4.2. Atmospheric factors

#### 2.4.2.1. Clouds

Clouds are perceived as regulators of solar radiation with nearly 65% of the atmosphere being covered by them [20]. Cloud types and effects are detected by using meteorological satellite images [32,42]. The Cloud-Albedo effect is defined as the instance when clouds reflect the incident solar radiation back into space whilst reducing the temperature of the atmosphere [20]. If clouds completely obscure the sun, there will be no direct beam radiation and the total GSR will be equal to the diffuse radiation [32].



The type of cloud depends on its constituents and causes fluctuations in the available GSR and subsequently affects the climate experienced in a given area [20,32,44,45]. Satellite observations of clouds together with models which account for the transparency, reflectivity and absorbency of the atmosphere are used to address the effects of all aspects which influence the amount of GSR received at the earth's surface.

#### **2.4.2.2. Aerosols**

The effect of aerosols on solar radiation depends significantly on the physical composition of the aerosol. This includes the size and shape, chemical characteristics and interaction properties specific to the type of aerosol [27]. Aerosols are gaseous particles which are found in the atmosphere and are usually liquid or solid in nature [20]. Some examples of aerosols include; dust, sulphates and carbon molecules. Aerosols can both absorb and scatter incident solar radiation while increasing the diffuse radiation component [20,23].

The atmosphere is made up of air molecules and gases such as;  $CO_2$ ,  $O_2$ ,  $N_2$ ,  $O$ ,  $N$ , Ozone and water vapor [20,23,46]. At certain wavelengths these atmospheric molecules absorb solar radiation. Ozone in the stratosphere absorbs ultraviolet (UV) radiation, while  $H_2O$ ,  $CO_2$  and  $O_2$  absorb radiation in the visible and near-infrared regions [23,33,47]. These gases scatter solar radiation when their particle size is considerably small in comparison to the wavelength of the incident solar radiation which is referred to as Rayleigh scattering [20,23,33,47].

Water vapor in the atmosphere decreases the total amount of GSR by absorbing both the direct and diffuse radiation components [23]. Aerosols can also interact with radiation which has already been scattered, this is dependent on their spectral properties [47]. Mie scattering occurs when the wavelength of the incident radiation and aerosol particle size are equal [33,47]. Aerosols have the ability to scatter and absorb any thermal infrared (IR) radiation emitted from the earth's surface and emit infrared radiation [47].

Much of the reservations surrounding research in global radiative forcing and climate sensitivity stems from the uncertainties in aerosol forcing [47]. Due to limitations which inhibit accurate estimation of aerosol properties and their spatio-temporal profiles, the understanding of aerosol-radiation interactions is considered complex [47].

## **2.5. Photovoltaic (PV) applications of solar radiation**

In order to maximize the consumption of the sun's radiation, solar power can be harnessed and converted into thermal and electrical energy [48,23,49]. 'Active' applications of solar radiation which make use of solar energy conversion systems include thermoelectric and PV technologies [23,48]. Evolution of PV technology has been significant over the past few decades since its introduction in 1954, with solar PV cells being more widely used today due to the increase in their efficiency [48,50,51].

Standard PV cells are made from semiconductor materials such as silicon and work on the basis of the photo-electric effect [23,48]. The radiation incident on a PV cell is responsible for electron excitation and results in a steady current which may be stored. Currently there are two types of PV cells on the market namely; crystalline silicon-based PV cells and thin film cells [48]. Semiconductor materials such as; amorphous silicon, cadmium-tellurium are the dominant materials used in the composition most PV cells [48].

Crystalline silicon-based PV cells are more expensive as compared to thin film cells and their price is justified considering their vastly outperforming efficiency [48]. The energy seized by these cells can be converted into electricity and used to run appliances, for lighting purposes, and to power motors and generators [48,49]. This electricity can be stored and used during power outages. PV systems are extremely economical in broader contexts given that their applications will assist in decreasing the consumption costs of grid electricity. Thermal electric applications of PV technologies involves the collection, storage and conversion of solar energy [23,48].

A solar panel consists of a large number of small, connected PV cells to increase the surface area for sunlight exposure. Large scale deployment of these solar panels in CSP plants is only viable for certain areas, depending on the amount of direct normal radiation received at that location [48,52]. Technologies which lend themselves to thermal electric applications in CSP plants include; parabolic troughs, solar dish collectors and Fresnel mirrors [48,53].

Fresnel mirrors consist of reflecting mirrors which are complexly designed to capture and store radiation. The mirrors are manufactured from glass which has an absorber insulation and offers a longer lifespan (more than 25 years) [53]. These mirrors are arranged in parallel rows forming a horizontal layout which proves to be more efficient in capturing the maximum amount of incident radiation [53]. Parabolic troughs and solar dish collectors are also made from some of these reflecting mirrors. However, their design is far more complicated as the mirrors and glass are curved to form troughs [53].

These technologies can be placed at higher altitudes to experience a reduced impact from atmospheric aerosols [53]. CSP plants currently make use of these structured devices which are efficient and economical as they have the potential to reduce the strain and costs of grid electricity [48,52,53].

Since these technologies are highly suitable for remote locations which have difficulties in accessing the grid supply, PV cells can be implemented in both the industrial and residential (urban and rural) sectors [50]. Solar radiation has the potential to meet the world's energy requirements through active solar technologies such as those mentioned above. New advances to solar cells allow for the optimal amount of radiation to be captured.

Features like tracking and tilting are fitted into the solar collectors to allow automated adjustment relative to the sun's position [49]. Placement of solar panels has direct implications

on the energy output and efficiency of the cell [49]. Limitations in the application of PV cells arise from their uncertainty and variability [51]. Hence, methods to predict the amount of solar insolation incident at a given site are beneficial for the design and manufacturing of PV technologies [50,51].

Accurate and effective forecasting methods may guide the optimal placement of PV panels, customized design of these technologies and allow for better management of grid electricity [54]. These technologies are at our disposal and can be used to supplement the national grid supply, for example in times of load shedding and blackouts [50,54].

For successful assessment of the PV potential for a prospective region, knowledge of the atmospheric conditions and solar radiation for the region must be available [55]. PV cell performance models are used to evaluate the potential of PV application for a site. These models generally require ground measurements of solar radiation, or satellite radiation data and numerical weather prediction models to evaluate the proposed performance [55]. For this purpose, establishing accurate and efficient GSR prediction models may serve as input when identifying the performance of a PV cell. These prediction models can be extended to be included in the performance analysis algorithms of PV cells.

### **2.5.1. Conversion of solar to PV energy**

A solar cell is considered a large p-n junction diode which allows light to be coupled into distinct regions [56,57,58]. PV cells enable production of electrical energy through the absorption of light energy [58]. These cells are made from semiconductor materials which are capable of absorbing photons of light with energies equal or greater than its band width [57,58]. The PV cell is a p-n junction between two thin layers of different semiconductor materials [56,57].

The first is the positive semiconductor (p-type) which is usually made from crystalline silicon

that is chemically doped with an impurity (e.g. boron) to create a deficit of free electrons in the material. The second semiconductor layer is the negative (n-type) which also constitutes crystalline silicon but instead is chemically doped with an impurity which enables a surplus of electrons (e.g. phosphorus) [57,58].

The realization of practical current in a solar cell takes place at the atomic level as light photons incident on the cell are absorbed. The absorption of this energy causes electrons in the valence band to be excited to the conduction band which results in an electron-hole pair being created [56-58]. The flow of electrons from the n-type semiconductor to the p-type semiconductor is known as the PV effect and is illustrated in Figure 6 below [57].

Electrons in the conduction band are movable and in order for this charge to be collected, recombination with the hole in the valence band has to be avoided [57,58]. Separation of these positive and negative charges is obtained by the built-in potential gradient within the cell [57]. An electric field is created when an organic semiconductor is placed between the two semiconductors explained above as a result of the discrepancy in their energy levels.

Since the electron-hole pair is bound together by Coulomb attraction, the electric field is necessary to ensure charge separation [57,58]. The free charge can then be captured for current generation. The structure and composition of PV cells is thus of significant importance.

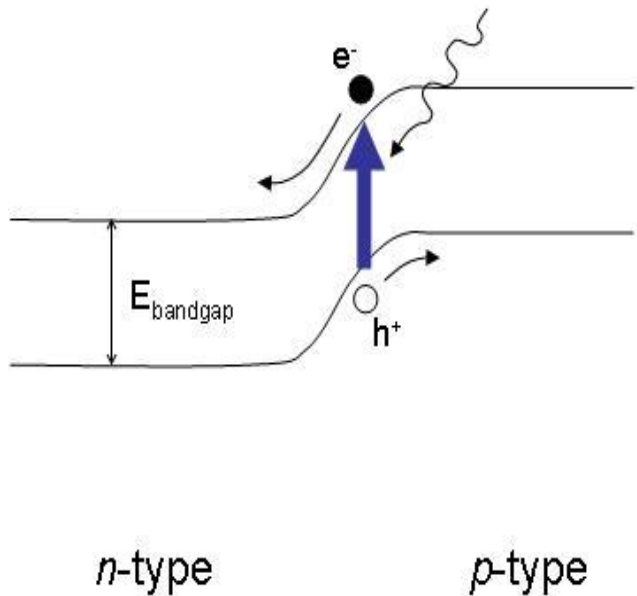


Figure 6: The electron-hole pair after photon is absorbed [58]

Individual PV cells range in size between 1-15cm and produce typical power of around 1 to 2W [57]. PV cells are connected in series to produce PV modules and increase the power output. Typical PV modules consist of 36 individual PV cells and have a power output rating of approximately 60W [57]. PV cells and modules are laminated in order to prevent impact from environmental factors such as penetration of water and gases. Solar PV arrays are formed by integrating PV modules to form a DC power producing unit. The above is a summarized description of the energy conversion process which occurs in PV cells.

## Chapter 3: Background and theory

### 3.1. Models to estimate GSR

Competent solar radiation estimation models are consistently being pursued, especially in areas where GSR data is not measured. This chapter explores the various models which have previously been studied and which prove to be sufficient in estimating GSR. Knowledge of the available solar radiation is fundamental for the management of energy resources as well as the development of solar PV technologies [59]. We also discuss models which forecast and predict solar availability in the below. Techniques used to quantify the available solar resources, depend on the time scale validation of the prediction - forecasting horizon [60]. Inaccurate models can lead to significant discrepancies in the estimation of the annual energy yield of a PV system [61].

### 3.2. Prediction models

#### 3.2.1. Forecasting horizons

Before discussing the types of prediction models in consumption, it is important to take note of the various forecasting horizons which directly influence the prediction model required for a specific PV system. The real-time acquisition of predicted data is crucial for solar power plants (e.g. CSP) which may supply the demand of the national grid [30,60].

The time interval for which values of solar radiation are predicted is referred to as the forecast horizon. CSPs require quantifying stations to assess and forecast the incident solar radiation to allow for proper management of resources [30]. While the uptake in solar technology continues to rise, the need for accurate short-term predictions of solar radiation becomes more pertinent [62].

Now casting refers to predictions made in a short time interval usually between 0-3 hours

[30,60]. These predictions can be made by analyzing measurements made at a particular instant and a few hours before. Short-term forecasts are made every 3-6 hours and can be acquired from models which incorporate meteorological variables such as precipitation, wind, temperature and sunshine duration [30,60,61].

Predictions made between 6-72 hours or longer are referred to as ‘forecasting’. These estimates are conducted by various techniques which include both numerical and physical approaches [30]. For accurate predictions to be made, models which are suitable for the specific forecasting horizon need to be considered. (e.g. some Numerical Weather Prediction (NWP) models do not perform well in now casting, as these models may not account for variations in the weather conditions within the interval of 3 hours) [30,60].

### **3.3. Statistical models**

Statistical analysis of the weather parameters previously observed in a definite site is important for implementing modeling techniques [23]. For the prediction of solar radiation, factors such as GSR, ETR and meteorological parameters need to be observed for a period longer than one calendar year [23]. Satellite observations (sunshine duration, cloud cover, etc.) can be used as variables in the analysis and models used for solar radiation forecasting [23,43]. Statistical methods include; time-series forecasts, Numerical Weather Prediction (NWP) models and Artificial Neural Networks (ANN).

Stochastic weather models can be developed from observed meteorological data [43]. To make provision for seasonal variations while considering short-term fluctuations due to cloud cover, Auto-Regressive Integrated Moving Average (ARIMA) models may be implemented [62]. Majority of the statistical models developed require complex and tedious numerical analysis based on historical observed data, but are highly accurate in their forecasts [63]. Statistical research techniques and models are fast becoming the preferred method of forecasting solar radiation as they require less computational effort and do not require much



internal system variables [23,43,59-64].

### **3.3.1. Artificial Neural Networks (ANNs)**

Artificial Neural Networks (ANNs) are used to solve for the intense computing power required by most statistical models which forecast GSR [59,61]. An ANN is a massive processor which performs functions on the basis of Artificial Intelligence (AI) [52]. They consist of a group of processing units which store and process exponential data sets [65]. There are two main categories of ANNs; Multi-Layer Perceptron (MLP) and Radial Basic Function (RBF) [43,65].

Like other statistical methods, these networks require the input of observed historical meteorological data. These models stand out from others as a result of their high level of accuracy and efficiency [43]. ANNs are able to accurately forecast cloud cover and formation, which make them advantageous in describing the atmosphere [59]. The future of statistical forecasting of GSR lies within the realm of ANNs due to its time saving and exponential storage capabilities [43,59,65].

### **3.3.2. Numerical Weather Prediction (NWP)**

NWP models are mathematical models which use current weather parameters as input variables, for initial and boundary conditions [30,63]. These models are able to predict GSR on a global scale and are used to forecast GSR in the 'forecasting' horizon (up to 48 hours) which is referred to as General Circulation Models (GCM) [63]. For regional and local predictions, the choice of NWP depends on its efficiency, cost and accessibility to meteorological data [30].

While NWP models are popular methods for estimating GSR and describing the dynamics of the earth's atmosphere, they require extensive computations [64]. In some short-term forecast horizons, NWP models perform poorer in comparison to simple forecast approaches which assume that consecutive days are identical [62]. These models are advantageous for PV systems which necessitate longer forecast horizons as the analysis of historically observed

data allows for improved long term predictions.

### **3.4. Physical models**

Physical models consider the influence of atmospheric conditions, site topography and weather conditions in the estimation of GSR [23,42]. The physical approach is based largely on processes that occur in the earth-atmosphere system, while these models require observed meteorological data as input variables [23,64]. Examples of the dependent meteorological considerations include; astronomical factors such as the solar constant, solar angles, physical factors like surface and cloud albedo, attenuation processes, geographical considerations which are the latitude and altitude of the site, and meteorological variables - temperature, relative humidity, vapor pressure, precipitation, sunshine duration [23,42,64].

Required meteorological variables are easily available as they are recorded at most local weather stations (with the exception of some parameters e.g. sunshine duration) or can be measured with the use of basic instruments and/or calculations. Satellite image data can be used in models which depend on atmospheric transmittance [44]. Physical models which are dependent on meteorological parameters are viable for the estimation of solar radiation in regions where solar radiation data is not measured as they have lower computation costs and fewer input data requirements [66]. Although solar radiation data is not extensively quantified, majority of physical models require this data for validation and calibration of estimation models.

#### **3.4.1. Temperature based models**

The air temperature on the earth's surface is directly influenced by the solar insolation absorbed by the atmosphere [67]. Models which use air temperature as a parameter to predict GSR at a location, require measurements of maximum and minimum air temperatures depending on the forecast horizon [23,42,43]. Since measurements of solar radiation and sunshine duration are limited at many meteorological stations, temperature based models are

considered [43,66,68].

It is important to note that areas which use recorded data from stations which are not in proximity, compromise the reliability and accuracy of their data [42,43]. This has led to the development of models which use easily available and measurable parameters such as air temperature [43,63,69-71].

Temperature based models estimate GSR through the assumption of atmospheric transmissivity - clear sky days correspond to higher incident solar insolation (greater short wave radiation) and result in increased maximum air temperature and decreased minimum air temperature (due to reduced long wave radiation emission from the atmosphere) [66,69-74]. Similarly, maximum air temperature decreases with reduced atmospheric transmissivity (i.e. higher cloud cover) while minimum air temperature increases due to cloud emissivity [72-74]. In the following, we give a brief description of a few well-established temperature based models, with a main focus on the Hargreaves-Samani model.

#### **3.4.1.1. Hargreaves-Samani (H-S) model**

Limitations in the availability and accessibility of solar radiation data resulted in the air temperature approach which was developed by Hargreaves and Samani [71]. The main assumption of this model is that the GSR at a site is responsible for the temperature range [42]. The difference in the daily measured maximum and minimum air temperatures are related to the amount of GSR received by the following equation [68-74];

$$H = H_o K_r (\Delta T)^{0.5}, \quad (15)$$

where  $K_r$  is an empirical coefficient that is dependent on the site and various meteorological parameters [25], and  $\Delta T$  refers to the difference between maximum and minimum temperatures ( $\Delta T = T_{max} - T_{min}$ ).

This model allows for solar radiation estimation through use of minimal meteorological data and is advantageous for locations where availability of measured data is limited. However, the risks associated with implementing this model lie in the assumption that the extraterrestrial ( $H_o$ ) and global solar radiation values ( $H$ ) are directly related to the air temperature difference [69-71].

For a specific location, significant errors may arise due to the influences of various meteorological factors such as elevation, storm patterns, cloudiness, humidity and advection on the air temperature [69,70].

**(i) Empirical coefficient ( $K_r$ )**

Studies conducted in [70,71] indicate that the value of the empirical coefficient  $K_r$  in the H-S equation depends on the location's humidity as well as its geographical situation with respect to large masses of water (lakes, dams, oceans). For inland/interior regions, the recommended value of  $K_r$  is 0.162, while for coastal regions  $K_r = 0.19$  [42,43,69-71,76,77].

A location is classified as coastal if the location is situated on or close to the coast (interaction between land and sea) [70]. The effects of relative humidity, pressure and cloudiness were investigated to recalibrate the value of  $K_r$ , but diverted the equation from its simplicity and main purpose [70,77,78].

Further studies resulted in a temperature dependent equation for the estimation of this empirical coefficient [54,69,76];

$$K_r = 0.00185(\Delta T)^2 - 0.0433(\Delta T) + 0.4023 \quad (16)$$

The H-S relation implicitly accounts for the relative humidity at a site in the temperature range  $\Delta T$  [43,46,69-71,76,78].

The evaluation of this empirical coefficient is solely based on the temperature difference. If the air temperature is affected by other climatic factors such as; location topography, elevation, proximity to a large body of water, then the  $K_r$  coefficient has to be corrected to avoid errors [69,70].

#### 3.4.1.2. Bristow and Campbell Model

This model relates GSR as an exponential asymptotic function of  $\Delta T$ ;

$$\frac{H}{H_o} = a [1 - \exp(-b(\Delta T)^c)], \quad (17)$$

where  $a$  represents the maximum radiation that can be received on a clear sky day, which is dependent on the site's pollution and elevation [68,72,75].

#### 3.4.1.3. Allen Model

As an extension of the H-S model, Allen proposed that the empirical coefficient  $K_r$  is influenced by the mean atmospheric pressure ( $P$ ) of the site. This factor was introduced to reason for the elevation effects on the heat capacity of the atmosphere, which resulted in proposed empirical coefficients:  $K_r = 0.17$  for interior regions and  $K_r = 0.2$  for coastal regions [70,72].

$$\frac{H}{H_o} = A \left( \frac{P}{1013} \right)^{0.5} (\Delta T)^{0.5} \quad (18)$$

#### 3.4.1.4. Samani Model

Samani further proposed that the empirical coefficient  $K_r$  is a function of daily ( $\Delta T$ ) to minimize the estimation error [69,72].

$$\frac{H}{H_o} = [A(\Delta T)^2 + B(\Delta T) + C(\Delta T)^{0.5}] \quad (19)$$

### 3.4.2. Sunshine duration models

#### 3.4.2.1. Angstrom model

Sunshine duration is a widely used variable in GSR estimation models. Measurement of this parameter has a direct correlation to the amount of GSR incident at the earth's surface [40,41,79,80]. This parameter is a reliable indicator, however measured data is not always available [23,68]. The earliest known correlation of solar radiation and sunshine duration was established by Angstrom in 1924 [80]. His work was the fundamental basis of many models which are still currently used to estimate solar radiation [23,39-41,63,79,80]. Angstrom recorded the incoming solar radiation data using a pyranometer and developed the following linear relationship [80];

$$Q_H = Q_o(0.25 + 0.75)S, \quad (20)$$

$Q_o$  represents the total incoming clear sky radiation,  $Q_H$  denotes the total incoming solar radiation, and  $S$  is the relative sunshine duration (sunshine duration/maximum possible sunshine duration ( $S_o$ )).

Clear sky conditions were difficult to classify and define without a dependence on other atmospheric and geographical factors which resulted in Prescott modifying the Angstrom correlation by replacing the clear sky radiation with the Extraterrestrial radiation  $H_o$  [23,39,63-65,80,81]. This relation became generally known as the **Angstrom-Prescott (A-P)** relation [23,38-41,63,79,80,38];

$$\frac{H}{H_o} = a + b \left( \frac{S}{S_o} \right), \quad (21)$$

where  $a$ ,  $b$  are known as the Angstrom coefficients and  $\frac{S}{S_o}$  is the relative sunshine duration.

#### (i) Clearness Index ( $K_T$ )

Equation (5) represents the ratio of total incoming GSR to the incoming ETR. This is a

measure of the atmosphere's transmissivity and also indicates fraction of available solar radiation at a location [63,82].

The atmosphere can be described in terms of the clearness index as explained in Table 1 [23];

**Table 1: Classification of day type using clearness index [23]**

Sky type	$K_T$
Clear	$0.7 \leq K_T \leq 0.9$
Partially cloudy	$0.3 \leq K_T \leq 0.7$
Cloudy	$0.0 \leq K_T \leq 0.3$

### (ii) Angstrom Coefficients

The  $a, b$  coefficients in equation (21) are empirical values that are dependent on the site geography (latitude, elevation, etc.) [11,50,52,53]. These empirical values range between  $0.089 \leq a \leq 0.460$  and  $0.208 \leq b \leq 0.851$  for various different locations in the world [23].

The physical significance of these empirical quantities gives a partial measure of the atmosphere's transmissivity [63].

Coefficient  $a$  is a function of cloud cover, while  $b$  is the fraction by which the sky's clearness index is affected due to sunshine duration [41,63]. The relative sunshine duration  $\frac{S}{S_o}$  is also known as the 'cloud cover index' [23,63]. For days when  $\frac{S}{S_o} = 1$  (clear day - no cloud cover obscuring the sun),  $\frac{H}{H_o} = a + b = K_T$ .

The sum of the Angstrom coefficients yields the atmospheric transmittance for that day [23,63]. On overcast days  $\frac{S}{S_o} = 0$ , then  $\frac{H}{H_o} = a = K_T$ . For areas where the Angstrom coefficients have not been defined, the recommended coefficients are;  $a = 0.25$  and  $b = 0.50$  [67]. The A-P model is renowned for its high degree of precision in estimating GSR for many

global locations, with the model's main advantage being that it only requires one input variable [23,79-82].

### 3.4.2.2. Adaptations of the Angstrom Model

Measurements of short wave radiation can be used to accurately predict the amount of solar radiation received at any location on the earth's surface [67]. Over the years, recent models which account for the effects of various meteorological factors, have been developed [67,83-85]. These parameters include; precipitation, relative humidity, air temperatures and sunshine duration to improve the accuracy of predictions [43,44,67,68,72,83].

These models have been derived from the fundamental A-P relation, and are referred to Angstrom based relations [23]. A generalized model which was developed for world-wide use is described by [84] as;

$$\frac{H}{H_o} = 0.23 + 0.48 \frac{S}{S_o}, \quad (22)$$

which makes use of a global average of the Angstrom coefficients. Work done in [42], describes an exponential relationship between the relative sunshine duration and the clearness index for Spain and is described in eq. (23). The climate in this country is considered to be similar to that of South Africa (semi-arid and mediterranean) [42].

$$\frac{H}{H_o} = a + b \exp\left(\frac{S}{S_o}\right). \quad (23)$$

The Angstrom coefficients are crucial for the proper application of Angstrom based models. Since these coefficients are site dependent, historically observed solar radiation data need to be analyzed to derive a reliable set of Angstrom coefficients [23,63,65]. An example of a model which omits the Angstrom coefficients is found in [84];

$$\frac{H}{H_o} = K \left(\frac{S}{S_o}\right)^{0.63} \sin(\theta_z)^{-0.19}. \quad (24)$$

The site parameters are explicitly included in the relation in the form of a zone factor  $K$  and



the model requires the solar noon (zenith) angle ( $\theta_z$ ) [84].

While the A-P model requires minimal computational input in estimating GSR, sunshine data and cloud observations are not easily available. Previously observed sunshine and GSR data is essential for the derivation of the empirical coefficients which allow for proper application of the model. Further, the model proves less efficient in the presence of clouds and other extensive atmospheric factors.

### 3.5. Multivariate models

Physical models which are used to estimate GSR at a specific location, largely depend on the meteorological data available [43,83,84]. Models which integrate factors such as sunshine duration, air temperature and relative humidity are known as combination (multivariate) models [40,42,50,83,92]. Relative humidity is defined as the amount of water vapor present in the air, and is greatly influenced by the air temperature [44,83]. Relative humidity ( $RH$ ) is described as a percentage and reaches a daily minimum around midday (solar noon) and a maximum at sunrise [83]. The development of models which correlate more than one variable are extremely dependent on the site of interest [40,83,86]. Nigeria, which is situated in the northern hemisphere and has a tropical climate with high rainfall in the summer season, has similar climatic conditions to that which is experienced in South Africa [40]. Studies in [40] proposed the following linear model for estimating the average monthly GSR in Nigeria;

$$\frac{H}{H_o} = 1.387 + 1.592 \frac{\bar{S}}{\bar{S}_o} - 0.045 \overline{T_{max}} + 0.004 \frac{\overline{RH}}{100}, \quad (25)$$

Here  $\overline{T_{max}}$  is the average daily maximum temperature and  $\overline{RH}$  is the average daily relative humidity [40]. These multivariate regression equations were found to have a higher correlation when compared to models using just one meteorological variable [40,83,86].

#### 3.5.1. Proposed models for South Africa

Further research on the estimation of GSR in South Africa through multiple meteorological

variables was completed in [87], which proposed linear models for the 9 provinces in South Africa. It was shown that the wind speed had a negligible impact on the prediction models for certain provinces [87].

Following a similar approach, our work focuses on the regression analysis of these meteorological factors as well as the non-linear impact of multivariate models and variations of these parameters. Extensive studies in [75,88-92] detail the non-linear analysis of GSR estimation models across various countries in the world. As an extension of our linear, single variable analysis conducted in Appendix B, and based on the above studies we chose to observe the performance of multivariate models of the form;

$$\frac{H}{H_o} = a(T) + b\left(\frac{RH}{100}\right) + c\left(\frac{S}{S_o}\right) + d, \quad (26)$$

where  $a, b, c$  and  $d$  are site dependent regression coefficients and  $T$  represents temperature variables such as;  $\Delta T, \sqrt{\Delta T}, T_{max}$  and  $\sqrt{T_{max}}$ . We extended this relation to investigate higher order variations and observed that quadratic models relating  $T_{max}$  are best suited for cities in South Africa. Our results are detailed in Chapter 5 and we present our proposed models for South Africa below. These models are unique to each of the five study sites.

## GC models for the estimation of GSR for cities in South Africa

### Bloemfontein

$$\frac{H}{H_o} = 0.040(T_{max}) - 0.307\left(\frac{RH}{100}\right) + 1.151\left(\frac{S}{S_o}\right) - 0.979 \quad (27)$$

### Cape Town

$$\frac{H}{H_o} = 4 \times 10^{-4}(T_{max})^3 - 0.03(T_{max})^2 + 0.71(T_{max}) + 13.33\left(\frac{RH}{100}\right)^3 - 19.66\left(\frac{RH}{100}\right)^2 + 7.52\left(\frac{RH}{100}\right) + 2.25\left(\frac{S}{S_o}\right)^3 - 0.46\left(\frac{S}{S_o}\right)^2 - 0.37\left(\frac{S}{S_o}\right) - 5.41 \quad (28)$$

### Durban

$$\frac{H}{H_o} = -1.4 \times 10^{-3}(T_{max})^2 + 0.108(T_{max}) + 13.097\left(\frac{RH}{100}\right)^2 - 16.833\left(\frac{RH}{100}\right) - 1.180\left(\frac{S}{S_o}\right)^2 + 1.603\left(\frac{S}{S_o}\right) + 3.399 \quad (29)$$

### Johannesburg

$$\frac{H}{H_o} = 7.5 \times 10^{-4}(T_{max})^3 - 0.06(T_{max})^2 + 1.27(T_{max}) - 6.14\left(\frac{RH}{100}\right)^3 + 11.25\left(\frac{RH}{100}\right)^2 - 6.43\left(\frac{RH}{100}\right) - 18.59\left(\frac{S}{S_o}\right)^3 + 36.74\left(\frac{S}{S_o}\right)^2 - 23.70\left(\frac{S}{S_o}\right) + 15.80 \quad (30)$$

### Pietermaritzburg

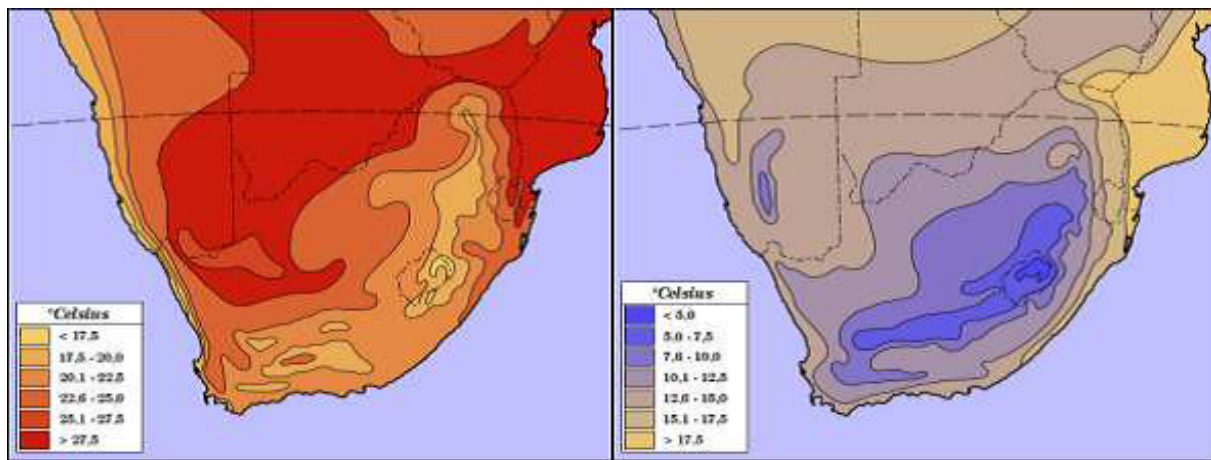
$$\frac{H}{H_o} = 0.002(T_{max})^2 - 0.085(T_{max}) + 7.513\left(\frac{RH}{100}\right)^2 - 8.183\left(\frac{RH}{100}\right) - 0.91\left(\frac{S}{S_o}\right)^2 - 1.11\left(\frac{S}{S_o}\right) + 3.533 \quad (31)$$

## Chapter 4: Method and materials

### 4.1. Weather and climate in South Africa

Before discussing the experimental method followed for this study, it is beneficial to introduce the climatic conditions related to South Africa and each of the selected study regions. Climate describes the average effect of meteorological conditions in a specific region over the long term [93]. Due to South Africa's wide-ranging landscape and oceanic influence, the country's climate may be considered diverse and is best described by the climate experienced across various regions of the country (climate zones) [94-96]. The eastern coastline experiences a semi-arid and mild, sub-tropical climate while the southwestern region is considered mediterranean. The northeastern part of South Africa experiences sub-tropical conditions while a small region in the North West is a desert climate zone [95].

Air temperature and rainfall patterns across the various climate zones are influenced by the region's topography, terrain and sea proximity [94,95]. While the majority of the country's rainfall occurs during the summer months (October to March), sunshine is obtainable all through the year. This is inclusive of the the winter season (April to September). Average air temperatures range between 15°C and 30°C during summer and often exceed 38°C. Figure 7 depicts the typical air temperatures experienced across the country [97,98].



Figures 7: Maximum and minimum air temperatures across South Africa [98]

South Africa experiences large fluctuations of annual rainfall which is a consequence of the change in solar radiation and north to south shift of the Hadley cell [94,96]. These weather trends differ in accordance to the movement of the high-pressure belt (circles the globe between 25 and 30 degrees south, latitude) during the winter and a low-pressure system that occurs during summer which is illustrated in Figure 8 below [94-96].

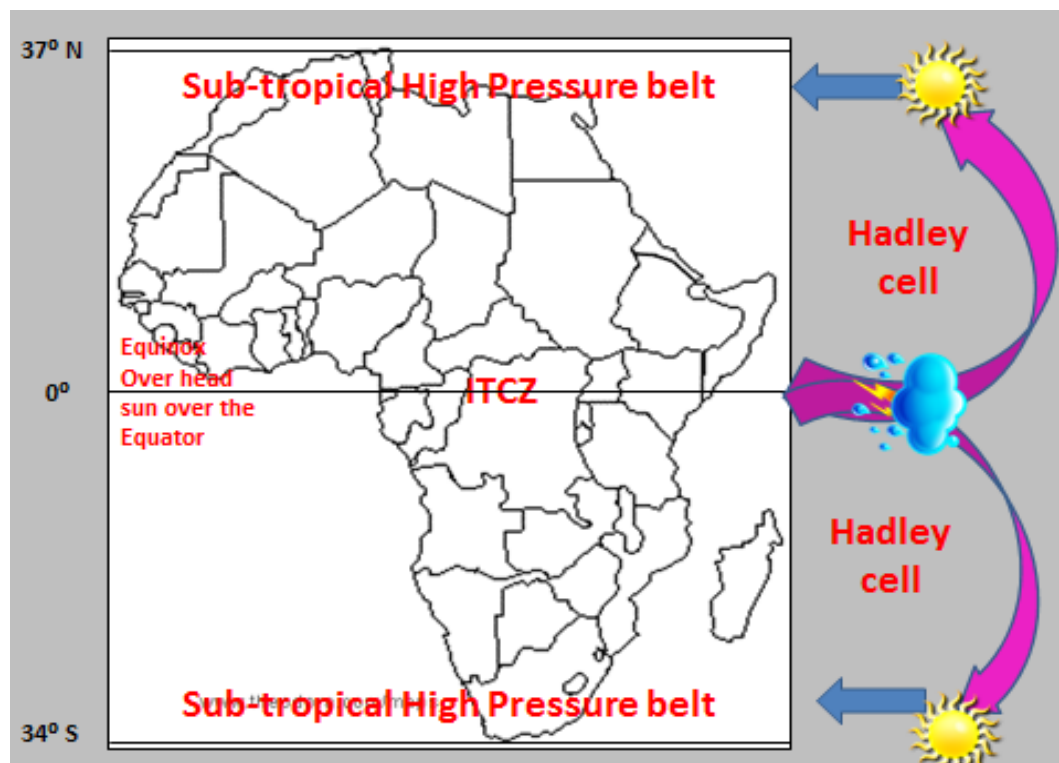
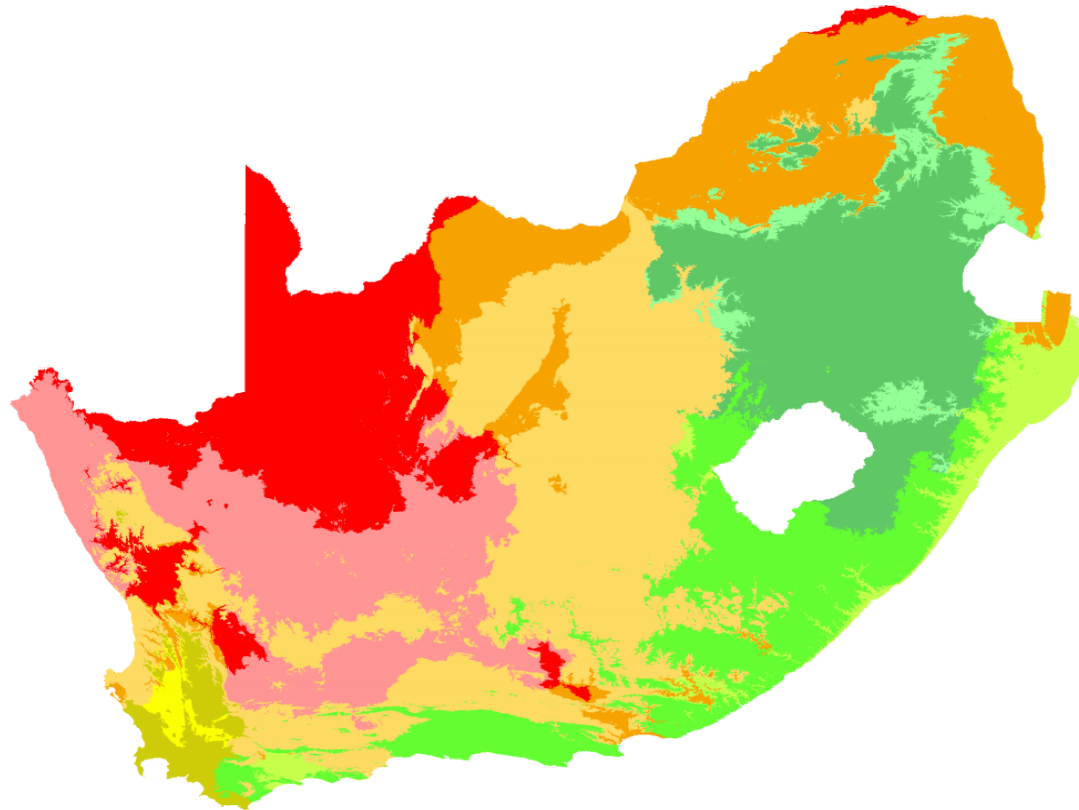


Figure 8: High pressure belt over Africa [96]

Proximity to the coast largely influences the climate of a region. The Agulhas current flows southward along the Indian Ocean which forms the coastline of the eastern parts of South Africa (KwaZulu-Natal), while the cold Benguela current flows northward along the Atlantic Ocean coastline along the Western Cape [96,97]. Along with this factor, variations in rainfall and air temperature are used to describe the climate of a region in accordance to the Köppen climate classification scheme shown below [93].

## Köppen climate types of South Africa



### Köppen climate type

<span style="color: red;">■</span> BWh (Hot desert)	<span style="color: yellow;">■</span> Csa (Hot-summer mediterranean)	<span style="color: lightyellow;">■</span> Cfa (Humid subtropical)
<span style="color: pink;">■</span> BWk (Cold desert)	<span style="color: olive;">■</span> Csb (Warm-summer mediterranean)	<span style="color: lightgreen;">■</span> Cfb (Oceanic)
<span style="color: orange;">■</span> BSh (Hot semi-arid)	<span style="color: lightgreen;">■</span> Cwa (Humid subtropical)	<span style="color: green;">■</span> Cfc (Subpolar oceanic)
<span style="color: lightorange;">■</span> BSk (Cold semi-arid)	<span style="color: mediumgreen;">■</span> Cwb (Subtropical highland)	

\*Isotherm used to separate temperate (C) and continental (D) climates is -3°C  
Data source: Climate types calculated from data from WorldClim.org

Figure 9: Köppen climate classification [99]

This is a brief introduction to the average climate and weather conditions which are experienced over South Africa. Further in depth discussions can be found in [93-97]. Weather and climate conditions are significant contributors to the amount of solar radiation received across regions of the country. In addition, climate change which has been noticed over the past few decades is also an important factor to consider, as it directly impacts the amount of GSR available in South Africa together with having a large influence over other meteorological factors which cause GSR to vary [95,100-102]. Climate change trends are used to

explain the weather conditions experienced, environmental degradation (pollution) as well as the country’s global warming impacts [94,95].

## 4.2. Study site details

For this study we have selected five major cities across various climate zones in South Africa; Bloemfontein, Cape Town, Durban, Johannesburg and Pietermaritzburg. In the following, we provide details on each city’s climatic conditions and land use. Table 2 shows the geographical specifics for each study site.

**Table 2: Geographical details of study sites**

Site	Province	Latitude ( <sup>o</sup> south)	Longitude ( <sup>o</sup> east)	Elevation (m)
Bloemfontein	Free State	29.1030	26.3263	1400
Cape Town	Western Cape	33.9630	18.4194	670
Durban	KwaZulu-Natal	29.9650	30.4849	670
Johannesburg	Gauteng	26.1430	28.3971	1800
Pietermaritzburg	KwaZulu-Natal	29.6270	30.4062	750

### 4.2.1. Bloemfontein, Free State

The spatial distribution of the capital city of the Free State province – Bloemfontein lends itself to three main land use types; formal stands (urban areas), smallholdings and farms [103,104]. An access barrier exists between the northern and southern parts of Bloemfontein, which segregates the developed areas from the rural [103]. Approximately 52% of Free State’s population occupy residence in Bloemfontein due to its relatively high level of development, while occupants of the rural and surrounding areas lack access to resources such as water, sanitation, electricity, transport and employment opportunities [103].

The Free State province is considered a semi-arid region, with high precipitation received during the summer [97,104]. The Köppen climate classification lists Bloemfontein as a BSk climate zone which corresponds to a cold, semi-arid region [104]. The annual mean air tem-

perature of this city is  $24.6^{\circ}\text{C}$ , while the average annual rainfall experienced is around 550mm [97,104]. Semi-arid regions experience high fluctuations in air temperatures [97]. The meteorological conditions native to this region are typical to that of an interior plateau region with rain during summer, cold winters and sunshine in abundance [97,104].

#### **4.2.2. Cape Town, Western Cape**

The land use and resource management across the Western Cape varies across the 30 municipalities. Cape Town, being the capital city of the province falls within the City of Cape Town Metropolitan Municipality [105]. Only 13% of the spatial distribution of this city is used for settlement and infrastructure while the remaining land is used for agricultural purposes [105]. This city is well known for its vast production of wines, citrus fruits and certain crops. Municipalities are currently working towards mitigating the inadequate water resource management.

Cape Town typically experiences a mediterranean climate which is described by its dry summers with low precipitation and moist winters [97,105]. This city is classified as Csb (warm, summer mediterranean) according to Köppen. Along the west coast dry conditions are usually felt, while it becomes wetter approaching the escarpment along the east coast and drier (semi-arid) towards the interior Karoo [105]. The province experiences a strong, humid south-easterly wind which often clears pollution [97]. Average annual maximum temperatures are around  $27^{\circ}\text{C}$  while inland temperatures fall between  $3\text{-}5^{\circ}\text{C}$  [97].

#### **4.2.3. Durban, KwaZulu-Natal**

The city of Durban experienced rapid urbanization to metropolitan status over the past few years [106]. This growth primarily stems from Durban being a coastal city. It is now considered one of the three largest cities in South Africa with a population exceeding 3.5 million [106]. Durban is the economic hub of KwaZulu-Natal due to its densely populated industrial core with few of the surrounding areas being considered rural. Economic diversity is a consequence of the spatial distribution across the city. Most of the disadvantaged areas

still lack access to resources such as water, electricity and transportation [106].

Durban is well known for its sub-tropical climate with high humidity levels [97]. On average, this town receives around 320 days of sunshine throughout the year, with air temperatures exceeding 33°C in the summer [97]. The influence of the Indian Ocean plays a role in the summer precipitation obtained, in addition to the mild temperatures in winters [97]. Durban corresponds to a Cfa (humid, sub-tropical) climate from Figure 9.

#### **4.2.4. Johannesburg, Gauteng**

Johannesburg is located on the north-eastern plateau of South Africa, in the Province of Gauteng and is known as the 'Highveld' (an elevation above sea level of 1 700m) [107]. It is the largest and wealthiest city in South Africa, being the commercial, industrial and financial hub of South Africa. Johannesburg is considered a landlocked city with a population of approximately 4.4 million as at 2016 [107,108]. Land use in Johannesburg is dependent on location and income groups, with the highest densities found in the city's informal settlements. Urban areas are highly dense while rural and semi-urban regions have a low density.

Johannesburg experiences a relatively dry and sunny climate. Due to the city's high altitude, temperatures in Johannesburg are usually fairly mild with an average maximum temperature of 25 °C in summer [97,104]. An annual average rainfall of around 700mm is common in Johannesburg, with majority of this rainfall taking place in the summer [107]. From Figure 9, Johannesburg has a Cwb – sub-tropical, highland climate classification.

#### **4.2.5. Pietermaritzburg, KwaZulu-Natal**

Pietermaritzburg which is also known as the Midlands is the capital city in the province of KwaZulu-Natal. It is situated in a hollow that is surrounded by the Drakensburg mountain range escarpment, which implicates lower temperatures and humidity levels in comparison to Durban due to the higher altitude [97]. The sub-tropical climate is still experienced with



warm summers and mild winters [97]. The Köppen classification for Pietermaritzburg is Cwa – humid, sub-tropical. The midlands is considered as one of the warmest cities in KwaZulu-Natal. The spatial distribution of this town lies between mixed residential and commercial.



Figure 10: Map of South Africa illustrating study sites [109]

### 4.3. Experimental technique

For each of the selected study sites, historic meteorological data was obtained from the South African Weather Service (SAWS) and Agricultural Research Council (ARC). Records of sunshine duration, air temperature, relative humidity and solar radiation for the period January 2007 – June 2018 was provided by these independent sources. We analyzed the average monthly GSR incident at each site for the specified period based on;

- i. dependence on a single meteorological variable
- ii. dependence on multiple meteorological variables

using the H-S and A-P equations (eqs. 15 and 21) as the foundation models.

As previously discussed, sunshine duration and solar radiation measurements are not undertaken for many locations across South Africa. This is due to the cost of relevant equipment and its maintenance. Historic data from the SAWS and ARC was limited for certain regions (e.g. Pietermaritzburg and Durban), as sunshine duration was not measured for the full period. Measurements were recorded for a few months and then stopped; this led us to making use of only the available monthly averages. For Durban, sunshine duration was measured for the period May 2010 - June 2018; Johannesburg: January 2007 - October 2017 and Pietermaritzburg: January 2007 - December 2014.

ETR ( $H_o$ ) was calculated based on the latitude ( $\phi$ ) of each site, using a fortran program which is provided in Appendix A. Similarly, sun angles were used to find values for  $S_o$ , see Appendix A. This study is an extension of our previous research findings which is presented in the research paper which is provided in Appendix B (Govindasamy, Tamara Rosemary and Chetty, Naven. Quantifying the global solar radiation received in Pietermaritzburg, KwaZulu-Natal to motivate the consumption of solar technologies. Open Physics, De Gruyter. Vol 16 (1).2018. pp. 786 - 794. ID: 10.1515/phys-2018-0098).

#### **4.4. Statistical error analysis**

Understanding of the accuracy of our analysis and proposed models is quantified in terms of the statistical error analysis. The mean bias error (MBE) specifies the mean deviation between the calculated and observed values and is an indicator of a model's long-term performance [72,110]. Positive MBE indicators describe over-estimation, while negative MBEs correspond to an under-estimation. The root mean square error (RMSE) gives insight into the short-term performance of a correlation.  $R^2$ , the coefficient of determination, is a measure of the correlation between the dependent variables which are predicted from the independent variables. Low statistical error measures are aspired [111]. Previous studies prescribe that error indicators in the range -10% and 10% are accepted [111,112]. The statistical error analysis described in our results was obtained using the following;

Mean bias error (MBE) and mean absolute bias error (MABE)

$$MBE = \frac{1}{n} \sum_{i=1}^n (H_{c,i} - H_{m,i}) \quad (32)$$

$$MABE = \frac{1}{n} \sum_{i=1}^n (| H_{c,i} - H_{m,i} |) \quad (33)$$

Mean percentage error (MPE) and mean absolute percentage error (MAPE)

$$MPE = \frac{1}{n} \sum_{i=1}^n \left( \frac{H_{c,i} - H_{m,i}}{H_{m,i}} \right) \times 100\% \quad (34)$$

$$MAPE = \frac{1}{n} \sum_{i=1}^n \left| \left( \frac{H_{c,i} - H_{m,i}}{H_{m,i}} \right) \right| \times 100\% \quad (35)$$

Root mean square errors (RMSE)

$$RMSE = \sqrt{\frac{\sum_{i=1}^n (H_{c,i} - H_{m,i})^2}{n}} \quad (36)$$

Mean absolute relative error (MARE)

$$MARE = \frac{1}{n} \sum_{i=1}^n \left| \frac{H_{m,i} - H_{c,i}}{H_{m,i}} \right|, \quad (37)$$

Coefficient of determination ( $R^2$ )

$$R^2 = 1 - \frac{\sum_{i=1}^n (H_{m,i} - H_{c,i})^2}{\sum_{i=1}^n (H_{m,i} - H_{m_{ave}})^2} \quad (38)$$

where  $H_{c,i}$  and  $H_{m,i}$  are the  $i^{th}$  calculated and measured values of GSR, respectively.  $H_{m_{ave}}$

is the average of the measured  $H$  values.

Averaging and rounding of hourly, daily measurements to obtain monthly averages, may influence the statistical indicators. Further to this, measured data obtained from the external sources may be subject to inconsistencies (no measured quantities when equipment malfunctions, heating effects, etc.). We present an analysis of the applicable statistical indicators within our discussion (Chapter 5) for each study site.

## Chapter 5: Results and discussion

In this chapter, we present the findings of our study in two main sections; 5.1. Single variable analysis and 5.2. Multivariate analysis.

### 5.1. Single variable analysis

We discuss the dependence of GSR on meteorological variables which include; air temperature, relative humidity and sunshine duration for each of the study sites. Regression equations for each of the above-mentioned meteorological variables are presented in Tables 3 - 5 below. Graphs showing empirical relationships for the H-S and A-P models for each site are also provided. A full data set for monthly averages is provided in Appendix C.

#### 5.1.1. Bloemfontein (BFN)

Average monthly values of air temperature ( $\Delta T$ ,  $T_{max}$ ,  $T_{ave}$ ), relative humidity ( $RH$ ), relative sunshine duration ( $\frac{S}{S_o}$ ) and  $\frac{H}{H_o}$  are detailed in Appendix C due to the large number of observations. These quantities were investigated to obtain the regression models listed in Tables 3 - 5 below.

**Table 3: Regression equations using air temperature**

Variable (x)	Equation	RMSE	MBE	MABE	MPE	MAPE	MARE	$R^2$
<b>Linear</b>								
$\Delta T$	$\frac{H}{H_o} = 0.0069x + 0.671$	0.43767	-0.05717	0.32538	17.29265	44.46985	0.44470	0.02216
$T_{max}$	$\frac{H}{H_o} = 0.051747x - 0.59003$	0.39306	-0.05722	0.26360	6.92935	31.82398	0.31824	0.17562
$T_{ave}$	$\frac{H}{H_o} = 0.0433x + 0.026$	0.39701	-0.05704	0.26436	7.94668	31.77643	0.31776	0.15893
<b>Quadratic</b>								
$\Delta T$	$\frac{H}{H_o} = -0.0145x^2 + 0.5131x - 3.6589$	0.43222	-0.05750	0.32051	16.26518	44.27964	0.44280	0.00316
$T_{max}$	$\frac{H}{H_o} = 0.003113x^2 - 0.11034x + 1.444947$	0.38234	-0.06881	0.24842	4.62127	28.69110	0.28691	0.21995
$T_{ave}$	$\frac{H}{H_o} = 0.0018x^2 - 0.0195x + 0.5092$	0.39248	-0.07159	0.25716	5.79130	30.27540	0.30275	0.17805
<b>Cubic</b>								
$\Delta T$	$\frac{H}{H_o} = -0.0006x^3 + 0.014x^2 + 0.0437x - 1.1372$	0.50642	-0.26906	0.35897	-15.99310	38.74866	0.38749	0.36851
$T_{max}$	$\frac{H}{H_o} = 0.000258x^3 - 0.017218x^2 + 0.41128x - 2.903922$	0.38204	-0.06218	0.25554	5.75200	29.94900	0.29949	0.22117
$T_{ave}$	$\frac{H}{H_o} = 0.0003x^3 - 0.0156x^2 + 0.2633x - 0.9128$	0.53309	-0.33011	0.37733	-24.45094	36.75987	0.36760	0.26509
<b>Power</b>								
$\Delta T$	$\frac{H}{H_o} = 0.152x^{0.5}$	0.48023	-0.19967	0.34792	-3.34831	40.29660	0.40297	0.23061
$T_{max}$	$\frac{H}{H_o} = 0.152x^{0.5}$	0.40952	-0.05802	0.29027	14.00557	38.37048	0.38370	0.27840
$T_{ave}$	$\frac{H}{H_o} = 0.152x^{0.5}$	0.45314	-0.21025	0.30286	-9.43931	31.35986	0.31360	0.22908
<b>H-S</b>								
$\Delta T$	$\frac{H}{H_o} = 0.16x^{0.5}$	0.47077	-0.17512	0.34131	0.28710	40.70602	0.40706	0.18260

Table 3 describes the regression equations for temperature variables  $\Delta T$ ,  $T_{max}$ , and  $T_{ave}$ . Low RMSE values are indicated for the above relations, however the  $R^2$  values are also low. This suggests that the temperature dependent relations have a low correlation to the measured clearness index,  $K_T = \frac{H}{H_o}$  values. Since Bloemfontein is considered an interior region,

the proposed H-S empirical coefficient is  $K_r = 0.16$ . Figure 11 below shows the H-S empirical model's prediction of  $\frac{H}{H_o}$  for this city. This model underestimated  $K_T$  values for majority of the months which is indicated by the high RMSE value of 0.47077. Over a study period longer than one calendar year, the H-S model was unable to account for outliers which is a result of it's dependency on  $\Delta T$  alone. We applied the H-S model to  $T_{max}$  using 0.152 as the empirical coefficient ( $K_r$ ) and found that this variable produced a lower overall error across indicators and higher  $R^2$  measure when compared to  $\Delta T$ .

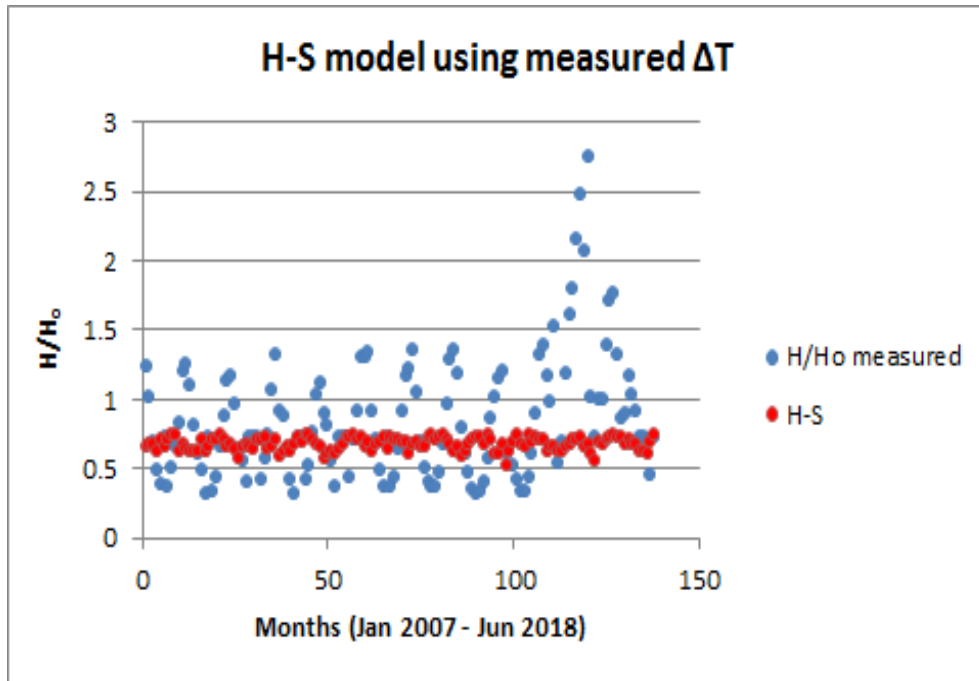


Figure 11: Graph of calculated  $\frac{H}{H_o}$  using the H-S model for Bloemfontein

Table 4: Regression equations using relative humidity

Equation	RMSE	MBE	MABE	MPE	MAPE	MARE	$R^2$
$\frac{H}{H_o} = -1.3594 \left( \frac{RH}{100} \right) + 1.4864$	0.43118	-0.05714	0.32663	16.35068	44.99671	0.44997	0.06320
$\frac{H}{H_o} = -8.926 \left( \frac{RH}{100} \right)^2 + 7.5561 \left( \frac{RH}{100} \right) - 0.6701$	0.42960	-0.05725	0.32736	16.33660	46.18015	0.46180	0.08840
$\frac{H}{H_o} = 43.753 \left( \frac{RH}{100} \right)^3 - 73.788 \left( \frac{RH}{100} \right)^2 + 38.857 \left( \frac{RH}{100} \right) - 5.5765$	0.42912	-0.05734	0.32694	16.38457	46.21127	0.46211	0.09450
$\frac{H}{H_o} = 0.4084 \left( \frac{RH}{100} \right)^{-0.7}$	0.46556	-0.18382	0.34458	-2.09859	40.43938	0.40439	0.15658

Table 4 above shows the regression models found from GSR dependence on RH alone. The statistical error indicators above suggest that there is low correlation between RH only and  $\frac{H}{H_o}$ , other variables need to be considered.

**Table 5: Regression equations using sunshine duration**

Equation	RMSE	MBE	MABE	MPE	MAPE	MARE	$R^2$
$\frac{H}{H_o} = 0.7 \left( \frac{S}{S_o} \right) + 0.26$	0.41954	0.07025	0.30092	-13.72015	40.33662	0.40337	0.10622
$\frac{H}{H_o} = 5.3465 \left( \frac{S}{S_o} \right)^2 - 5.399404 \left( \frac{S}{S_o} \right) + 1.8062$	0.40140	0.05720	0.28839	-11.18023	38.55370	0.38554	0.82371
$\frac{H}{H_o} = -13.657 \left( \frac{S}{S_o} \right)^3 + 35.366 \left( \frac{S}{S_o} \right)^2 - 27.109 \left( \frac{S}{S_o} \right) + 6.6972$	0.51450	0.32734	0.37738	28.64690	40.43981	0.40440	0.71037
$\frac{H}{H_o} = 1.616044 \left( \frac{S}{S_o} \right)^{2.514954}$	0.40589	0.05868	0.29281	-11.19233	39.41057	0.39411	0.80672
<b>A-P:</b> $\frac{H}{H_o} = 0.5 \left( \frac{S}{S_o} \right) + 0.25$	0.47708	0.22943	0.33822	9.30640	36.88015	0.36880	0.75097

Sunshine based equations in Table 5 indicate higher  $R^2$  correlation coefficients and low MBEs which emphasize the relationship between sunshine duration and clearness index. Considering the period for which data was analyzed, high MAPE values can be explained by over and underestimation of the regression equations when compared to the actual measured values of  $\frac{H}{H_o}$ . Figure 12 below describes the A-P empirical model's estimation of GSR for the period. Again, we notice the multiple outliers of  $K_T$  which are not included in the prediction trend. From the above analysis we can notice that sunshine models have a stronger correlation to  $\frac{H}{H_o}$  in Bloemfontein as opposed to temperature and RH.



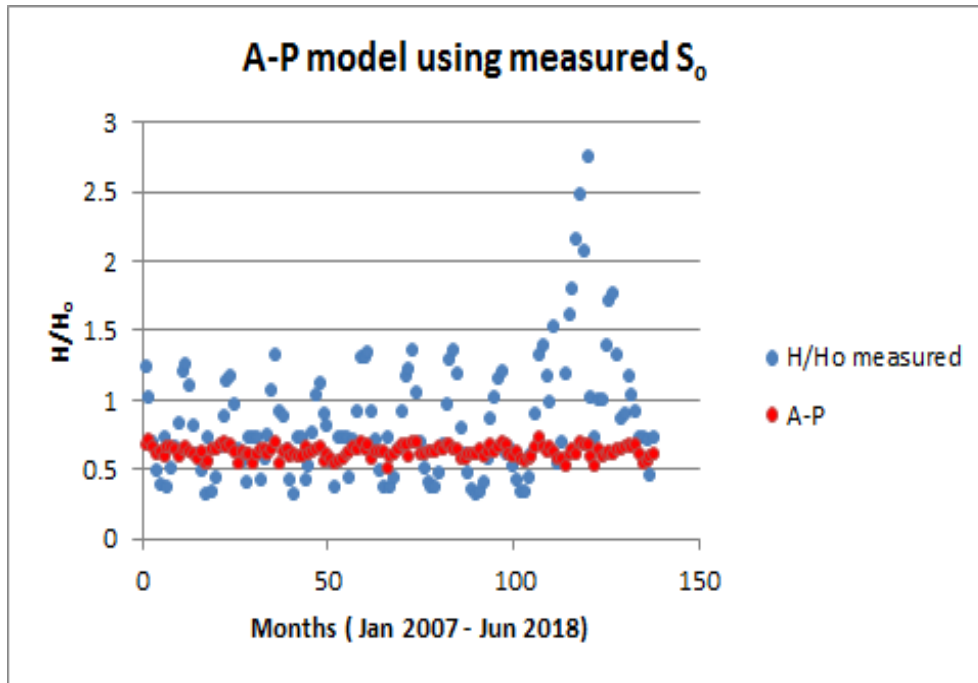


Figure 12: Graph of calculated  $\frac{H}{H_0}$  using the A-P model for Bloemfontein

### 5.1.2. Cape Town (CT)

Monthly average values can be found in Appendix C. Table 6 below shows the temperature dependent regression equations. Since  $\Delta T$  showed a low correlation and high RMSE in the linear equation, we decided to exclude this variable up until the H-S model. For Cape Town,  $T_{ave}$  showed a stronger relationship to  $\frac{H}{H_0}$ , with the highest correlation being a power equation. Cubic relations produced lower RMSE and higher  $R^2$  values. High MAPE values are noticed and are due to the over and underestimation of  $K_T$  values using these equations.

**Table 6: Regression equations using air temperature**

Variable (x)	Equation	RMSE	MBE	MABE	MPE	MAPE	MARE	R <sup>2</sup>
<b>Linear</b>								
$\Delta T$	$\frac{H}{H_o} = 0.1707x - 0.7339$	0.42198	-0.06373	0.32300	28.18197	58.54130	0.58541	0.16708
$T_{max}$	$\frac{H}{H_o} = 0.1032x - 1.5745$	0.35822	-0.06460	0.28738	11.12107	46.81940	0.46819	0.39977
$T_{ave}$	$\frac{H}{H_o} = 0.1222x - 1.4803$	0.35489	-0.06306	0.28812	11.77766	48.39380	0.48394	0.41085
<b>Quadratic</b>								
$T_{max}$	$\frac{H}{H_o} = 0.0001x^2 + 0.0968x - 1.506$	0.36239	-0.08726	0.28850	7.00088	45.57831	0.45578	0.38570
$T_{ave}$	$\frac{H}{H_o} = 0.0019x + 0.0558x - 0.9503$	0.35351	-0.05235	0.28698	13.98320	48.37756	0.48378	0.41543
<b>Cubic</b>								
$T_{max}$	$\frac{H}{H_o} = -0.00107x^3 + 0.070182x^2 - 1.4174x + 9.26389$	0.35810	-0.06245	0.28705	11.79253	46.15665	0.46157	0.40015
$T_{ave}$	$\frac{H}{H_o} = -0.00117x^3 + 0.06437x^2 - 1.0398x + 5.40071$	0.35420	-0.06079	0.28734	12.29520	47.44155	0.47441	0.41313
<b>Power</b>								
$\Delta T$	$\frac{H}{H_o} = 0.19x^{0.42197}$	0.53544	-0.28850	0.40325	-3.19296	57.26803	0.57268	0.34107
$T_{max}$	$\frac{H}{H_o} = 0.19x^{0.3}$	0.52533	-0.27367	0.39903	0.43857	59.01393	0.59014	0.29092
$T_{ave}$	$\frac{H}{H_o} = 0.17x^{0.3}$	0.57003	-0.35045	0.42671	-15.72890	55.08234	0.55082	0.51993
<b>H-S</b>								
$\Delta T$	$\frac{H}{H_o} = 0.19x^{0.5}$	0.49183	-0.20509	0.37574	13.62268	61.73122	0.61731	0.1315

The empirical H-S model using  $K_r = 0.19$  (Cape Town is a coastal region) is illustrated in Figure 13 below. This model produced the highest MAPE value which can also be seen below. The model was unable to include most of the data points which may suggest that additional meteorological variables should be considered for better correlation.

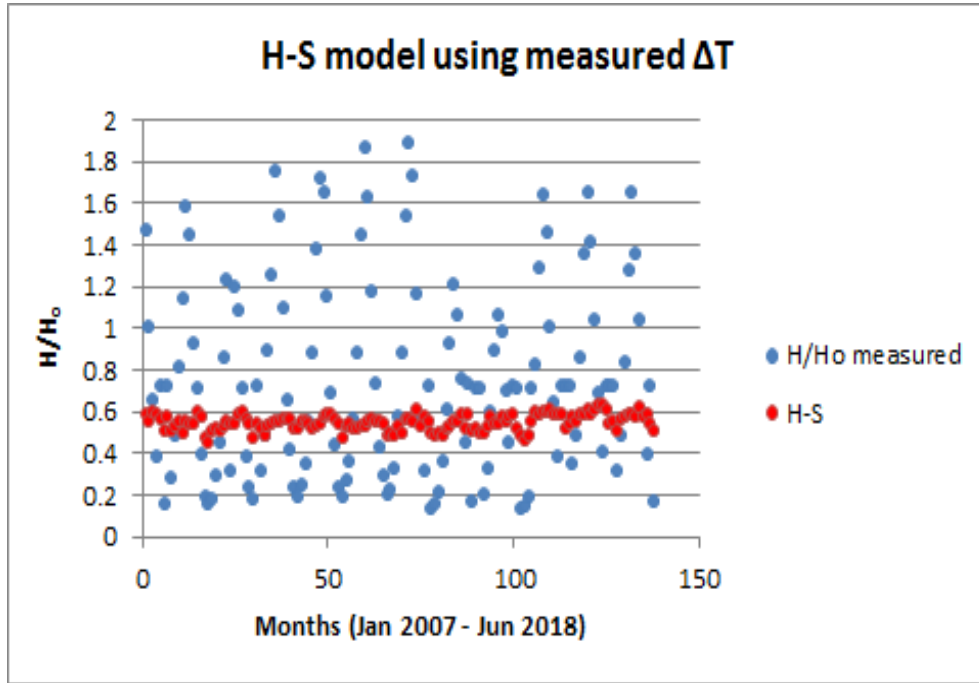


Figure 13: Graph of calculated  $\frac{H}{H_o}$  using the H-S model for Cape Town

Table 7: Regression equations using relative humidity

Equation	RMSE	MBE	MABE	MPE	MAPE	MARE	$R^2$
$\frac{H}{H_o} = -0.69601 \left( \frac{RH}{100} \right) + 1.03217$	0.49947	-0.20208	0.38589	16.07106	64.87663	0.64877	0.16695
$\frac{H}{H_o} = -7.0613 \left( \frac{RH}{100} \right)^2 + 5.5049 \left( \frac{RH}{100} \right) + 0.0085$	0.56112	-0.35252	0.40740	-25.72610	47.63227	0.47632	0.42778
$\frac{H}{H_o} = -49.5741 \left( \frac{RH}{100} \right)^3 + 61.45687 \left( \frac{RH}{100} \right)^2 - 17.9676 \left( \frac{RH}{100} \right) + 0.01144$	0.50315	-0.25837	0.37333	-7.31371	51.40359	0.51404	0.18420
$\frac{H}{H_o} = 0.11164 \left( \frac{RH}{100} \right)^{-3.53848}$	0.56404	-0.34597	0.41643	-17.96540	51.76938	0.51770	0.11360

The quadratic regression equation using RH shows a moderate correlation between RH and  $K_T$ ,  $R^2 = 0.42778$ . The remaining regression relations found suggest that RH alone is not a good predictor for  $\frac{H}{H_o}$ . These regression equations were investigated based on the relationship between the measured RH and GSR values.

**Table 8: Regression equations using sunshine duration**

Equation	RMSE	MBE	MABE	MPE	MAPE	MARE	R <sup>2</sup>
$\frac{H}{H_o} = 0.6 \left(\frac{S}{S_o}\right) + 0.26$	0.38900	0.05820	0.31613	-36.69623	65.92395	0.65924	0.29218
$\frac{H}{H_o} = 4.01239 \left(\frac{S}{S_o}\right)^2 - 3.24101 \left(\frac{S}{S_o}\right) + 0.8203$	0.26996	0.05629	0.20114	0.16194	30.44986	0.30450	0.90653
$\frac{H}{H_o} = -0.9535 \left(\frac{S}{S_o}\right)^3 + 6.04913 \left(\frac{S}{S_o}\right)^2 - 4.64358 \left(\frac{S}{S_o}\right) + 1.30602$	0.28975	-0.11910	0.23813	-37.52875	50.41317	0.50413	0.89232
$\frac{H}{H_o} = 1.591774 \left(\frac{S}{S_o}\right)^{3.083798}$	0.27253	0.05833	0.20403	1.52485	31.56772	0.31568	0.90474
<b>A-P:</b> $\frac{H}{H_o} = 0.5 \left(\frac{S}{S_o}\right) + 0.25$	0.42090	0.14054	0.32934	-21.07497	59.46378	0.59464	0.77278

Table 8 above shows strong correlation equations for  $\frac{H}{H_o}$  using relative sunshine. The high  $R^2$  and low RMSE indicators are desirable. The high MAPE values can be explained by the over and underestimation of the models, which is a result of the large number of data points. Figure 14 below shows the performance of the A-P empirical model for Cape Town for Jan 2007 - Jun 2018. The model is consistent with estimating  $\frac{H}{H_o}$  values which are less than 1, however, there is a large number of outliers which are disregarded by the model.

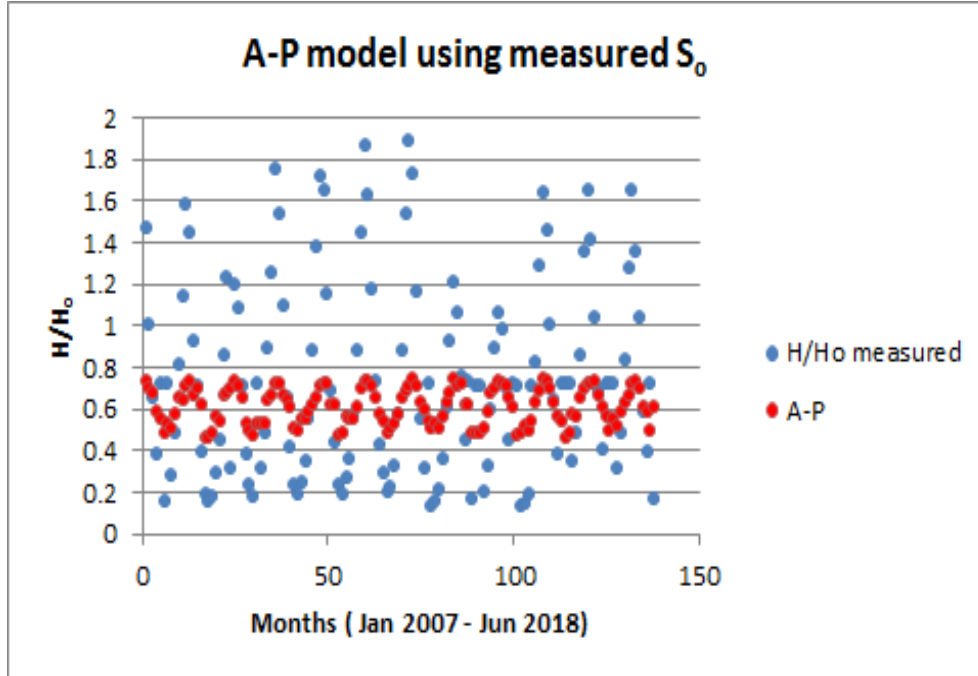


Figure 14: Graph of calculated  $\frac{H}{H_o}$  using the A-P model for Cape Town

### 5.1.3. Durban (DBN)

Regression relations in Table 10 show a weak correlation between  $\Delta T$  and  $\frac{H}{H_o}$ , hence further analysis of  $T_{max}$  and  $T_{ave}$  are listed. The cubic relation describing  $T_{ave}$  shows the strongest relation, which is still moderate,  $R^2 = 0.50574$ . Though RMSE values are low, the correlation between temperature variables and clearness index is also low. This proposes that further meteorological variables should be included for better estimation.

**Table 9: Regression equations using air temperature**

Variable (x)	Equation	RMSE	MBE	MABE	MPE	MAPE	MARE	$R^2$
<b>Linear</b>								
$\Delta T$	$\frac{H}{H_o} = -0.0205x + 0.7637$	0.19526	-0.00673	0.16199	28.18197	58.5430	0.58541	0.16133
$T_{max}$	$\frac{H}{H_o} = 0.0244x - 0.1558$	0.19867	-0.01306	0.16471	13.99678	37.55833	0.37558	0.13181
$T_{ave}$	$\frac{H}{H_o} = 0.4434x - 0.37429$	0.16041	-0.01155	0.12165	7.47170	5.83383	0.48394	0.43399
<b>Quadratic</b>								
$T_{max}$	$\frac{H}{H_o} = -0.0021x^2 + 0.1619x - 2.2706$	0.18498	0.00413	0.15043	14.06562	34.44608	0.34446	0.24732
$T_{ave}$	$\frac{H}{H_o} = -0.0026x^2 + 0.1486x - 1.3807$	0.15433	-0.00005	0.12266	8.86645	27.26062	0.27261	0.46712
<b>Cubic</b>								
$T_{max}$	$\frac{H}{H_o} = 7 \times 10^{-5}x^3 - 0.0091x^2 + 0.3875x - 4.5885$	0.19482	0.04172	0.16206	22.47673	39.36829	0.39368	0.16515
$T_{ave}$	$\frac{H}{H_o} = -0.00038x^3 + 0.02263x^2 - 0.3888x + 2.30057$	0.14990	-0.01095	0.11367	6.18120	23.85143	0.23851	0.50574
<b>Power</b>								
$\Delta T$	$\frac{H}{H_o} = 0.18x^{0.25}$	0.27044	-0.15046	0.20627	-14.6782	37.37487	0.37375	0.10210
$T_{max}$	$\frac{H}{H_o} = 0.18x^{0.25}$	0.22597	-0.08712	0.17787	-0.86772	35.86964	0.35870	0.10860
$T_{ave}$	$\frac{H}{H_o} = 0.18x^{0.25}$	0.23439	-0.11691	0.17786	-8.78169	33.06749	0.33068	0.20845
<b>H-S</b>								
$\Delta T$	$\frac{H}{H_o} = 0.19x^{0.5}$	0.3347	0.19894	0.28607	74.46372	85.12727	0.85127	0.0722

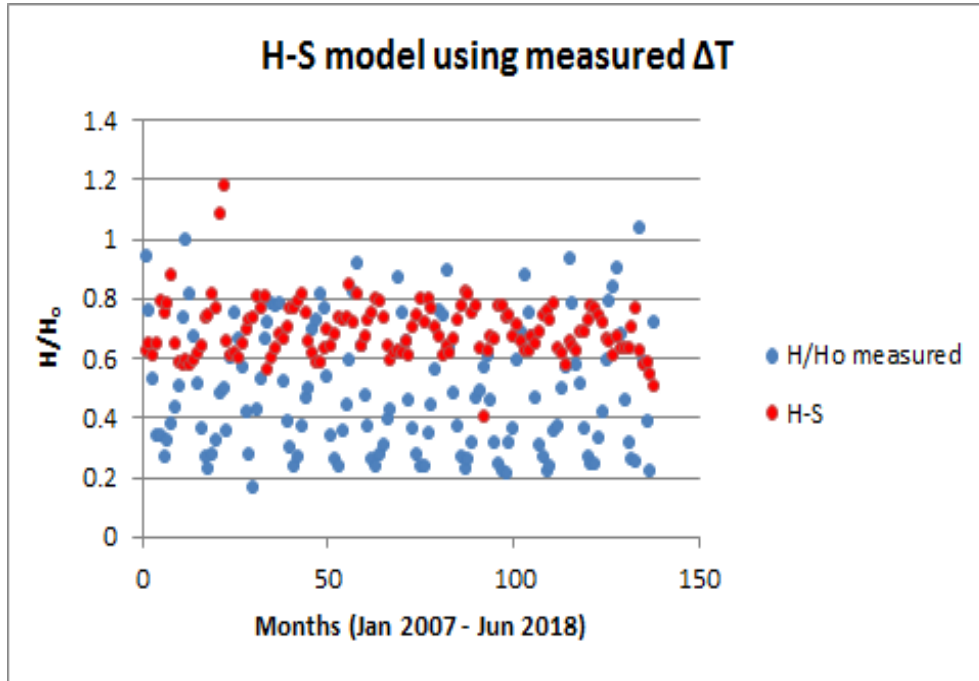


Figure 15: Graph of calculated  $\frac{H}{H_o}$  using the H-S model for Durban

$K_r = 0.19$  was used in the H-S empirical model to estimate the GSR for Durban and is illustrated above. It can be noticed that the model was inadequate in estimating the lower values of  $\frac{H}{H_o}$ , which could be result of the high humidity and temperature values experienced in Durban. Table 10 indicates low variance in  $K_T$  consequencing from RH.

Table 10: Regression equations using relative humidity

Equation	RMSE	MBE	MABE	MPE	MAPE	MARE	$R^2$
$\frac{H}{H_o} = 0.5766 \left( \frac{RH}{100} \right) + 0.0162$	0.21951	-0.07849	0.17109	0.31672	35.06654	0.35067	0.0162
$\frac{H}{H_o} = 2.613905 \left( \frac{RH}{100} \right)^2 - 2.96288 \left( \frac{RH}{100} \right) + 1.44087$	0.23476	-0.12778	0.17686	-12.94040	32.25880	0.32259	0.15200
$\frac{H}{H_o} = -11.702 \left( \frac{RH}{100} \right)^3 + 23.80885 \left( \frac{RH}{100} \right)^2 - 14.9551 \left( \frac{RH}{100} \right) + 3.22227$	0.21012	-0.09342	0.16287	-5.08930	31.94627	0.31946	0.22090
$\frac{H}{H_o} = 0.676346 \left( \frac{RH}{100} \right)^{1.504722}$	0.23404	-0.10604	0.17637	-6.98257	33.97975	0.33980	0.01620

**Table 11: Regression equations using sunshine duration**

Equation	RMSE	MBE	MABE	MPE	MAPE	MARE	$R^2$
$\frac{H}{H_o} = 0.4 \left(\frac{S}{S_o}\right) + 0.25$	0.23396	0.04411	0.19611	-11.01770	43.18372	0.43184	0.25314
$\frac{H}{H_o} = 0.831998 \left(\frac{S}{S_o}\right)^2 - 1.25011 \left(\frac{S}{S_o}\right) + 0.921591$	0.19568	0.02188	0.16085	-12.59010	36.55315	0.36553	0.87666
$\frac{H}{H_o} = 6.435316 \left(\frac{S}{S_o}\right)^3 - 9.65304 \left(\frac{S}{S_o}\right)^2 + 4.270518 \left(\frac{S}{S_o}\right) - 0.0113$	0.19523	0.02188	0.16082	-12.49590	36.48033	0.36480	0.87723
$\frac{H}{H_o} = 0.4987 \left(\frac{S}{S_o}\right)^{0.3223}$	0.24508	0.10626	0.19619	3.96200	31.04578	0.38046	0.80652
<b>A-P:</b> $\frac{H}{H_o} = 0.5 \left(\frac{S}{S_o}\right) + 0.25$	0.23677	-0.01163	0.20600	-24.33390	49.75277	0.49753	0.81943

The sunshine regression equations indicate high  $R^2$  and low RMSE values, with the cubic model showing the strongest relation. The A-P model’s estimation is illustrated in Figure 16, which contributed the highest MAPE. Overestimation from this model is noticed.

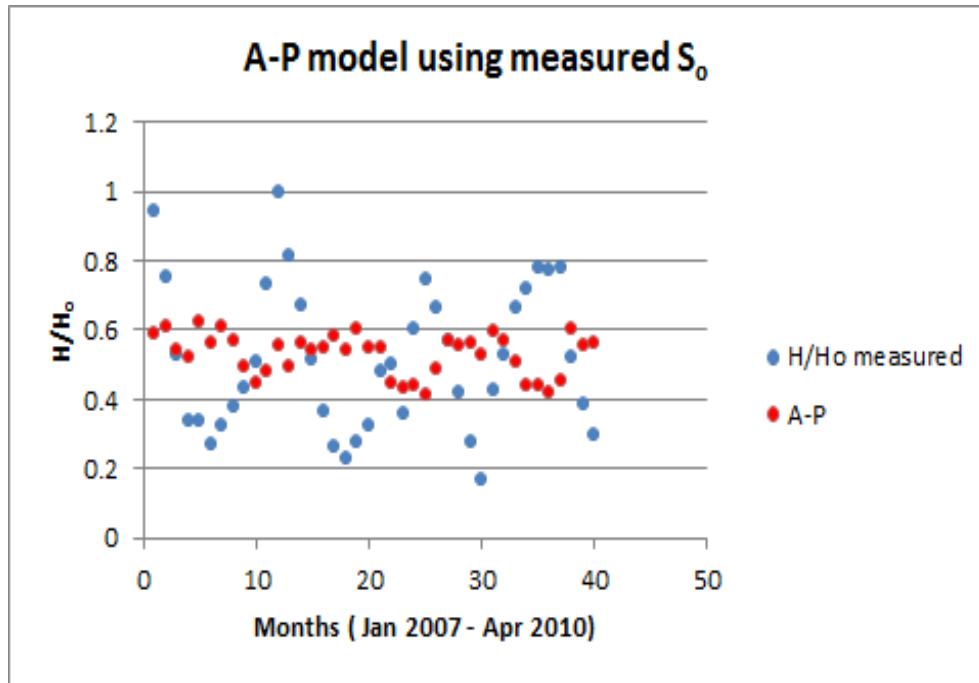


Figure 16: Graph of calculated  $\frac{H}{H_o}$  using the A-P model for Durban

#### 5.1.4. Johannesburg (JHB)

Temperature dependent relations listed in Table 12 describe a stronger relationship for Johannesburg as compared to the previous three sites. This could be a result of the dry, sunny climate experienced in this city, which reduces the impact of RH on measured air temper-

ature. Moderate to acceptable  $R^2$  values are noticed while the overall error indicators are considerably low.

**Table 12: Regression equations using air temperature**

Variable (x)	Equation	RMSE	MBE	MABE	MPE	MAPE	MARE	$R^2$
<b>Linear</b>								
$\Delta T$	$\frac{H}{H_o} = -0.0416x + 1.0903$	0.22854	-0.08250	0.17698	-3.37257	30.57129	0.30571	0.14500
$T_{max}$	$\frac{H}{H_o} = 0.0498x - 0.65056$	0.15908	-0.04745	0.11614	-4.05413	19.67910	0.19680	0.51498
$T_{ave}$	$\frac{H}{H_o} = 0.04898x - 0.23334$	0.13006	-0.00149	0.10245	3.43022	19.11542	0.19115	0.67579
<b>Quadratic</b>								
$T_{max}$	$\frac{H}{H_o} = -0.0019x^2 + 0.1363x - 1.61$	0.15673	-0.04330	0.11908	-3.13917	21.15946	0.21159	0.56377
$T_{ave}$	$\frac{H}{H_o} = 0.004523x^2 - 0.09123x - 0.781591$	0.11906	0.00208	0.08739	3.03414	15.72060	0.15721	0.73436
<b>Cubic</b>								
$T_{max}$	$\frac{H}{H_o} = 0.0008x^3 + 0.0581x^2 - 1.3354x + 10.164$	0.14117	-0.05549	0.10399	-6.39981	16.40648	0.16407	0.61805
$T_{ave}$	$\frac{H}{H_o} = -4.05 \times 10^{-5}x^3 + 0.006404x^2 - 0.1193x + 0.915382$	0.11906	-0.00178	0.08762	3.05150	14.85376	0.14854	0.72834
<b>Power</b>								
$\Delta T$	$\frac{H}{H_o} = 0.16x^{0.336425}$	0.30207	-0.18455	0.22808	-19.88230	33.47207	0.33472	0.17120
$T_{max}$	$\frac{H}{H_o} = 0.16x^{0.301273}$	0.26835	-0.16119	0.19783	-17.13290	28.56498	0.28565	0.21374
$T_{ave}$	$\frac{H}{H_o} = 0.16x^{0.4}$	0.210768	-0.08800	0.15922	-4.37856	25.28866	0.25289	0.14862
<b>H-S</b>								
$\Delta T$	$\frac{H}{H_o} = 0.16x^{0.5}$	0.25758	0.02860	0.22721	24.40118	47.30027	0.47300	0.27159



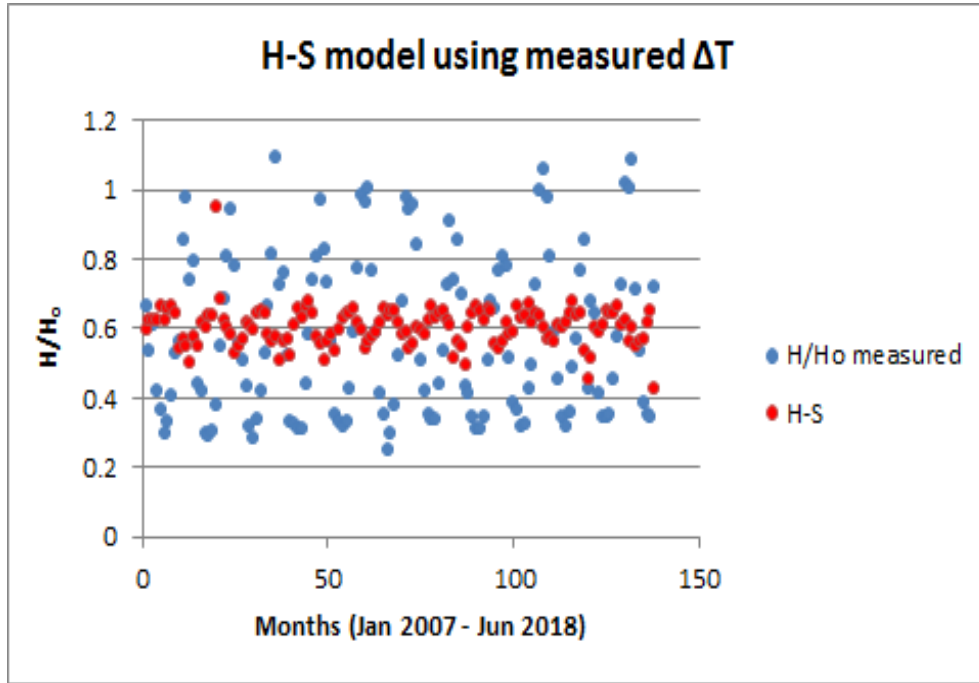


Figure 17: Graph of calculated  $\frac{H}{H_o}$  using the H-S model for Johannesburg

The H-S model for Johannesburg showed a much lower correlation between  $\Delta T$  and  $\frac{H}{H_o}$ . Over and underestimation by the model is also noticed in the high MAPE. From this we proceeded to consider  $T_{max}$  and  $T_{ave}$  for our multivariate analysis.

**Table 13: Regression equations using relative humidity**

Equation	RMSE	MBE	MABE	MPE	MAPE	MARE	$R^2$
$\frac{H}{H_o} = 0.58116 \left(\frac{RH}{100}\right) + 0.09248$	0.25698	-0.14159	0.19326	-13.57680	29.40031	0.29400	0.12890
$\frac{H}{H_o} = -1.10772 \left(\frac{RH}{100}\right)^2 + 2.10221 \left(\frac{RH}{100}\right) - 0.39111$	0.24640	-0.12489	0.18962	-10.74490	30.09811	0.30098	0.13160
$\frac{H}{H_o} = -40.593 \left(\frac{RH}{100}\right)^3 + 71.07095 \left(\frac{RH}{100}\right)^2 - 39.984 \left(\frac{RH}{100}\right) + 7.651299$	0.24074	-0.12098	0.17972	-10.36430	27.92801	0.27928	0.17310
$\frac{H}{H_o} = 0.751864 \left(\frac{RH}{100}\right)^{0.8666676}$	0.24017	-0.10600	0.18742	-6.65555	30.76775	0.30768	0.12840

The analysis of the dependence of RH on GSR suggests that this variable cannot be solely considered in estimation models.

**Table 14: Regression equations using sunshine duration**

Equation	RMSE	MBE	MABE	MPE	MAPE	MARE	R <sup>2</sup>
$\frac{H}{H_o} = 0.27 \left(\frac{S}{S_o}\right) + 0.22$	0.26673	0.14618	0.19688	4.13060	29.87833	0.29878	0.19200
$\frac{H}{H_o} = 1.960243 \left(\frac{S}{S_o}\right)^2 - 2.9172 \left(\frac{S}{S_o}\right) + 1.479157$	0.26913	0.15229	0.19614	15.61894	29.26792	0.29268	0.79588
$\frac{H}{H_o} = 18.82406 \left(\frac{S}{S_o}\right)^3 - 36.3036 \left(\frac{S}{S_o}\right)^2 + 22.10114 \left(\frac{S}{S_o}\right) - 3.70059$	0.25657	0.12317	0.18655	10.08309	29.12540	0.29125	0.81448
$\frac{H}{H_o} = 0.353657 \left(\frac{S}{S_o}\right)^{-0.48832}$	0.26571	0.14598	0.19461	14.26980	29.46137	0.29461	0.80103
<b>A-P:</b> $\frac{H}{H_o} = 0.5 \left(\frac{S}{S_o}\right) + 0.25$	0.22718	-0.03927	0.19365	-23.80130	41.55346	0.41554	0.85455

The A-P model produced the highest correlation coefficient and MAPE for Johannesburg. The above relative sunshine regression relations indicate a high dependence of this variable in the estimation of  $\frac{H}{H_o}$ . Quadratic and cubic relations proved to be more efficient.

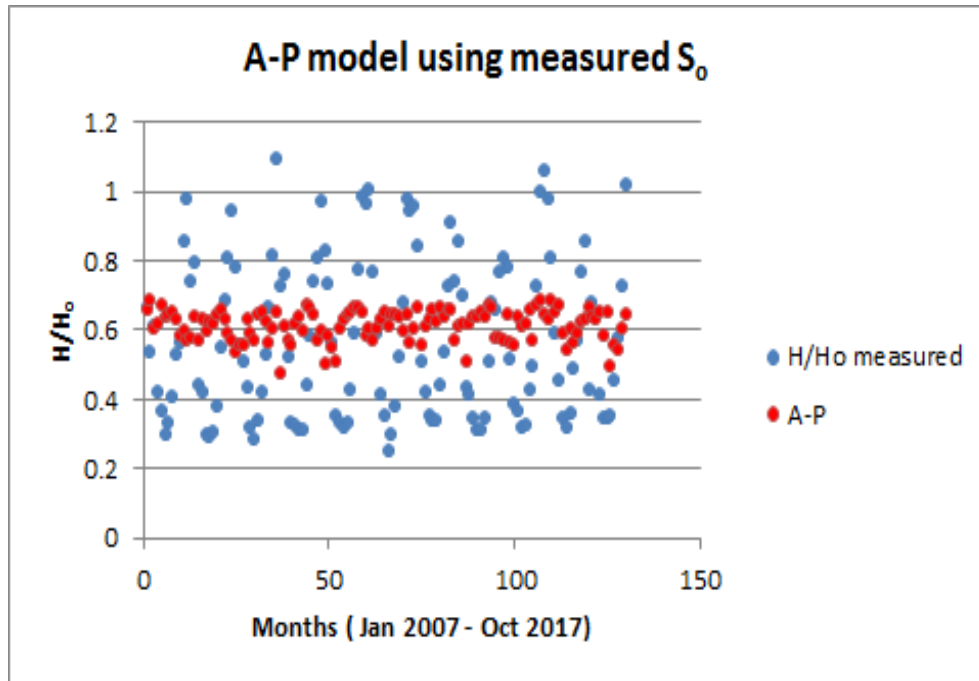


Figure 18: Graph of calculated  $\frac{H}{H_o}$  using the A-P model for Johannesburg

### 5.1.5. Pietermaritzburg (PMB)

Temperature dependent regression equations shown in Table 15 describe a moderate correlation for Pietermaritzburg. Low statistical error indicators suggest that the equations fit the measured data with the exception of the over and underestimations. Higher order equations

show a stronger relationship between temperature variables and  $\frac{H}{H_o}$ .

**Table 15: Regression equations using air temperature**

Variable (x)	Equation	RMSE	MBE	MABE	MPE	MAPE	MARE	R <sup>2</sup>
<b>Linear</b>								
$\Delta T$	$\frac{H}{H_o} = -0.0829x + 1.3609$	0.22252	-0.11564	0.16728	-12.87250	30.48468	0.30485	0.24890
$T_{max}$	$\frac{H}{H_o} = 0.0573x - 0.97001$	0.18421	-0.07093	0.14049	-5.51051	25.78168	0.25782	0.29038
$T_{ave}$	$\frac{H}{H_o} = 0.062105x - 0.65967$	0.14920	$9.48 \times 10^{-6}$	0.12425	7.91552	25.99313	0.25993	0.53450
<b>Quadratic</b>								
$T_{max}$	$\frac{H}{H_o} = -0.00005x^2 + 0.0598x - 0.9907$	0.18051	-0.06066	0.13906	-3.15648	25.95779	0.25958	0.31864
$T_{ave}$	$\frac{H}{H_o} = 0.000701x^2 - 0.035547x - 0.41278$	0.14911	$5.4 \times 10^{-6}$	0.12393	7.96082	25.77662	0.25777	0.53504
<b>Cubic</b>								
$T_{max}$	$\frac{H}{H_o} = -7.91 \times 10^{-4}x^3 + 0.057892x^2 - 1.34235x + 10.2818$	0.16878	$4.16 \times 10^{-6}$	0.14088	10.59041	29.52683	0.29527	0.40428
$T_{ave}$	$\frac{H}{H_o} = -0.00122x^3 + 0.068879x^2 - 1.2122x + 7.087538$	0.14657	$7.45 \times 10^{-5}$	0.11987	7.65499	24.70998	0.24710	0.55077
<b>Power</b>								
$\Delta T$	$\frac{H}{H_o} = 0.16x^{0.319753}$	0.28349	-0.17067	0.21257	-19.09680	34.69122	0.34691	0.26720
$T_{max}$	$\frac{H}{H_o} = 0.16x^{0.26}$	0.26138	-0.15156	0.19522	-15.97860	32.14088	0.32141	0.42866
$T_{ave}$	$\frac{H}{H_o} = 0.16x^{0.31}$	0.24002	-0.12204	0.18143	-9.83200	31.24894	0.31249	0.43020
<b>H-S</b>								
$\Delta T$	$\frac{H}{H_o} = 0.16x^{0.5}$	0.23947	0.02262	0.21062	26.28364	49.62950	0.49629	0.19916

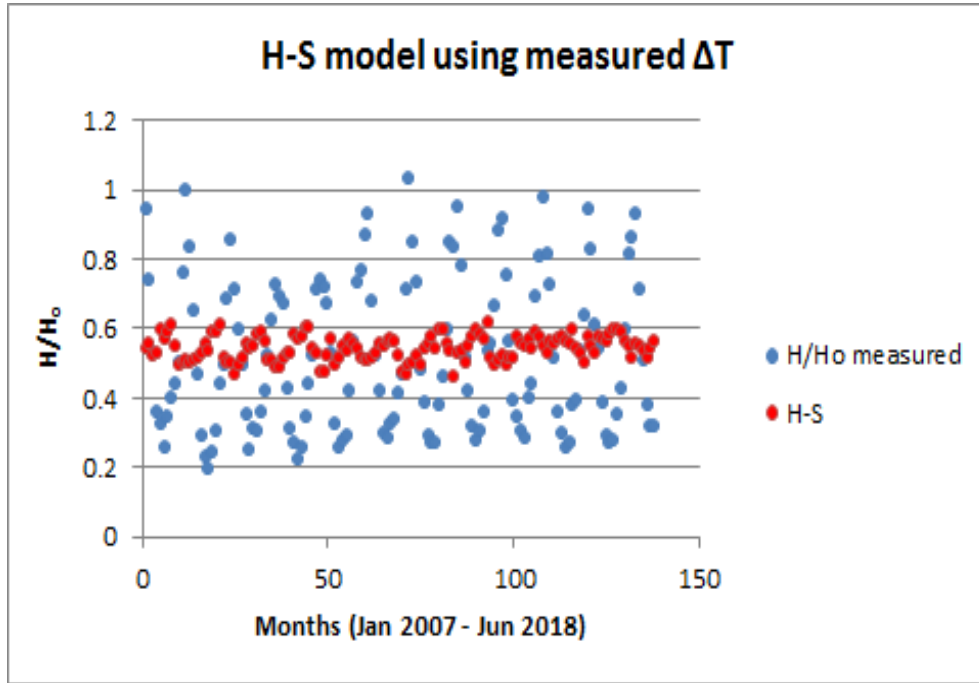


Figure 19: Graph of calculated  $\frac{H}{H_o}$  using the H-S model for Pietermaritzburg

For Pietermaritzburg (interior region -  $K_r = 0.16$ ), the H-S model indicated a weak relationship between  $\Delta T$  and  $\frac{H}{H_o}$ . This could be explained by the high levels of humidity experienced in Pietermaritzburg which contribute largely to the air temperatures experienced. The RH equations in Table 16 show a higher correlation to  $K_T$  as compared to the previous four sites, with the cubic relation having  $R^2 = 0.46440$ .

**Table 16: Regression equations using relative humidity**

Equation	RMSE	MBE	MABE	MPE	MAPE	MARE	$R^2$
$\frac{H}{H_o} = 1.523051 \left( \frac{RH}{100} \right) - 0.49671$	0.17195	-0.00225	0.13144	10.46588	28.48477	0.28485	0.37378
$\frac{H}{H_o} = 7.39351 \left( \frac{RH}{100} \right)^2 - 8.10468 \left( \frac{RH}{100} \right) + 2.511903$	0.17717	-0.06729	0.12671	-0.12796	22.77110	0.22771	0.33525
$\frac{H}{H_o} = -53.311 \left( \frac{RH}{100} \right) + 110.26 \left( \frac{RH}{100} \right)^2 - 73.339 \left( \frac{RH}{100} \right) + 16.157$	0.15903	-0.00018	0.12172	9.23548	25.99783	0.25998	0.46440
$\frac{H}{H_o} = 1.260179 \left( \frac{RH}{100} \right)^{2.258722}$	0.17290	-0.00775	0.12957	8.35968	27.72947	0.27729	0.36686

**Table 17: Regression equations using sunshine duration**

Equation	RMSE	MBE	MABE	MPE	MAPE	MARE	$R^2$
$\frac{H}{H_o} = 0.365666 \left(\frac{S}{S_o}\right) + 0.258202$	0.18357	0.02783	0.13202	-6.78010	27.41389	0.27414	0.0346
$\frac{H}{H_o} = 3.792668 \left(\frac{S}{S_o}\right)^2 - 4.90156 \left(\frac{S}{S_o}\right) + 2.063567$	0.16990	$-3.3 \times 10^{-7}$	0.12297	-11.64720	27.3272	0.27327	0.87343
$\frac{H}{H_o} = -6.28953 \left(\frac{S}{S_o}\right)^3 + 17.17263 \left(\frac{S}{S_o}\right)^2 - 14.0939 \left(\frac{S}{S_o}\right) + 4.108383$	0.16911	$1.64 \times 10^{-7}$	0.12142	-11.52180	27.06397	0.27064	0.87461
$\frac{H}{H_o} = 0.5527 \left(\frac{S}{S_o}\right)^{0.2794}$	0.18545	0.03076	0.13243	-6.30279	27.24884	0.27249	0.84921
<b>A-P:</b> $\frac{H}{H_o} = 0.5 \left(\frac{S}{S_o}\right) + 0.25$	0.18348	-0.02533	0.13490	-18.65210	32.25505	0.32255	0.85239

Equations in Table 17 indicate low overall error values and high correlation coefficients with the exception of the linear model. A graphical description of the A-P model is shown in Figure 20. Despite the strong correlation ( $R^2 = 0.85239$ ), the model does not account for most of the lower values of  $\frac{H}{H_o}$ .

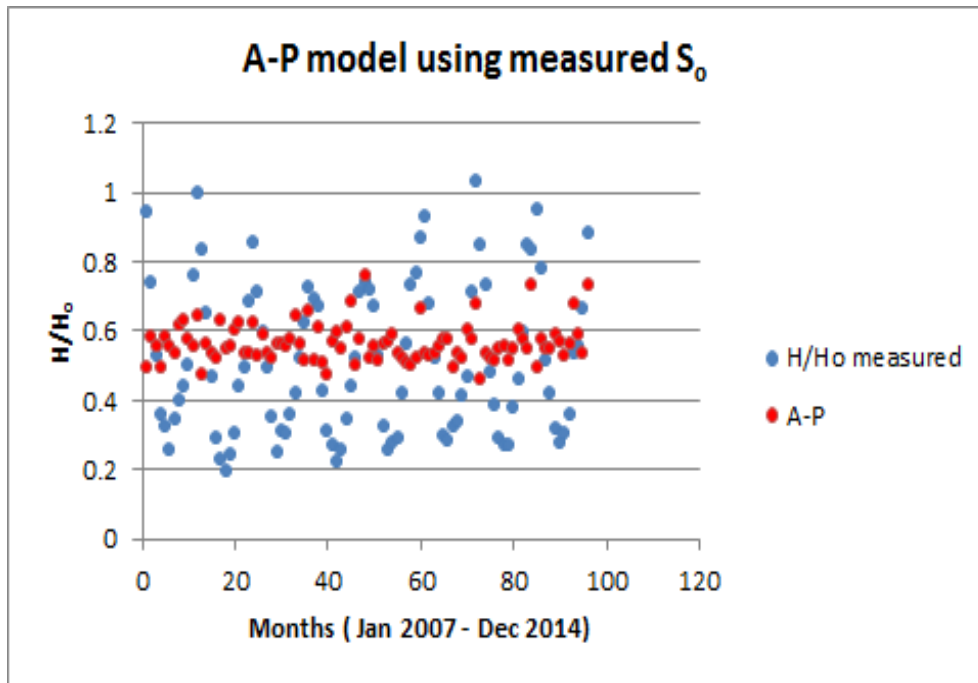


Figure 20: Graph of calculated  $\frac{H}{H_o}$  using the A-P model for Pietermaritzburg

Above we have analyzed the single variable dependence of GSR on air temperature, humidity and relative sunshine. From the regression relations obtained for all five sites,  $\Delta T$  showed a weaker correlation to  $\frac{H}{H_o}$  when compared to  $T_{max}$  and  $T_{ave}$ . While  $R^2$  values indicated

a low to moderate relationship between temperature and GSR, we realized that estimation models which include additional meteorological variables may perform better. Furthermore, higher order relations (quadratic, cubic and power) showed a better fit to the measured values.

Relative humidity indicated the weakest relationship to  $\frac{H}{H_o}$ . No established GSR estimation models for this quantity exist, as it is unable to predict GSR solely and is often used in combination models which do not implicitly account for RH.

Sunshine regression equations demonstrated higher correlation values from all three variables. The A-P model performed considerably well and the large number of outliers which were not included by the model can be explained by the use of the universal A-P coefficients. Since established A-P coefficients for the above cities do not exist, we made use of the universal coefficients;  $a = 0.25$ ,  $b = 0.5$ . These coefficients are general and can be used for any site for which the A-P coefficients are unknown. There is merit in obtaining specific A-P coefficients for each site as this enhances the performance of each model based on the site's observed historic sunshine data.

## 5.2. Multivariate analysis

Following the single variable analysis in the previous section, we analyzed the dependency of  $\frac{H}{H_o}$  on all four variables;  $\Delta T$ ,  $T_{max}$ ,  $RH$  and  $\frac{S}{S_o}$ . We have included the variables for which the multivariate analysis showed a stronger correlation. Tables 18 - 27 below, describe the proposed multivariate equations for each site, as well as their associated error indicators.

### 5.2.1. Bloemfontein (BFN)

**Table 18: Proposed multivariate equations**

No.	Equation
1	$\frac{H}{H_o} = -0.053 (\Delta T) - 0.766 \left(\frac{RH}{100}\right) + 2.597 \left(\frac{S}{S_o}\right) + 1.930$
2	$\frac{H}{H_o} = -0.393 (\sqrt{\Delta T}) - 0.631 \left(\frac{RH}{100}\right) + 2.623 \left(\frac{S}{S_o}\right) + 0.821$
3	$\frac{H}{H_o} = 0.040 (T_{max}) - 0.307 \left(\frac{RH}{100}\right) + 1.151 \left(\frac{S}{S_o}\right) - 0.979$
4	$\frac{H}{H_o} = 0.394 \left(\sqrt{T_{max}}\right) - 0.275 \left(\frac{RH}{100}\right) + 1.214 \left(\frac{S}{S_o}\right) - 1.999$
5	$\frac{H}{H_o} = -0.018 (\Delta T)^2 + 0.552 (\Delta T) - 1.500 \left(\frac{RH}{100}\right)^2 - 0.339 \left(\frac{RH}{100}\right) + 3.752 \left(\frac{S}{S_o}\right)^2 - 3.546 \left(\frac{S}{S_o}\right) - 2.175$
6	$\frac{H}{H_o} = 0.002 (T_{max})^2 - 0.037 (T_{max}) - 8.813 \left(\frac{RH}{100}\right)^2 - 8.107 \left(\frac{RH}{100}\right) + 3.262 \left(\frac{S}{S_o}\right)^2 - 4.315 \left(\frac{S}{S_o}\right) + 0.225$
7	$\frac{H}{H_o} = 0.004 (\Delta T)^3 - 0.24 (\Delta T)^2 + 4.16 (\Delta T) + 57.59 \left(\frac{RH}{100}\right)^3 - 89.82 \left(\frac{RH}{100}\right)^2 + 43.11 \left(\frac{RH}{100}\right) - 2.65 \left(\frac{S}{S_o}\right)^3 + 9.31 \left(\frac{S}{S_o}\right)^2 - 37.29 \left(\frac{S}{S_o}\right) - 27.40$
8	$\frac{H}{H_o} = -9.4 \times 10^{-6} (T_{max})^3 + 0.003 (T_{max})^2 - 0.06 (T_{max}) + 27.58 \left(\frac{RH}{100}\right)^3 - 49.35 \left(\frac{RH}{100}\right)^2 + 27.50 \left(\frac{RH}{100}\right) + 0.14 \left(\frac{S}{S_o}\right)^3 + 2.13 \left(\frac{S}{S_o}\right)^2 - 2.99 \left(\frac{S}{S_o}\right) - 2.99$

**Table 19: Error indicators for proposed equations**

Equation	RMSE	MBE	MABE	MPE	MAPE	MARE	R <sup>2</sup>
1	0.39594	0.05721	0.27450	-9.72644	35.91319	0.35913	0.16348
2	0.39734	0.05721	0.27587	-9.95571	36.22391	0.36224	0.82761
3	0.38825	0.05721	0.26900	-6.70049	33.71226	0.33712	0.83507
4	0.39012	0.05721	0.27177	-6.907291	34.27409	0.34274	0.83348
5	0.3249	0.05721	0.26734	-8.12844	34.65066	0.34651	0.21935
6	0.37720	0.05801	0.25875	-5.83789	32.12539	0.32125	0.24080
7	0.38037	0.05721	0.26825	-7.07460	34.50267	0.34503	0.27990
8	0.37725	0.05721	0.26037	-6.06718	32.31451	0.32315	0.24115

For Bloemfontein, the first order multivariate equations produced a higher correlation as opposed to the second and third order relations. Low RMSE and MPE indicators which fall within the accepted range [-10% ; 10%] are also obtained by the first order relations. Figure 21 below shows the performance of the proposed model (Equation 3) amongst the measured values of  $\frac{H}{H_o}$ . The model performs well in fitting the clearness index values previously measured in Bloemfontein, with the exception of outliers which occur in the last 2 - 3 years (months = 110 - 130). These discrepancies may be a result of the climate change experienced

over the last few years, or possible data recording defects.

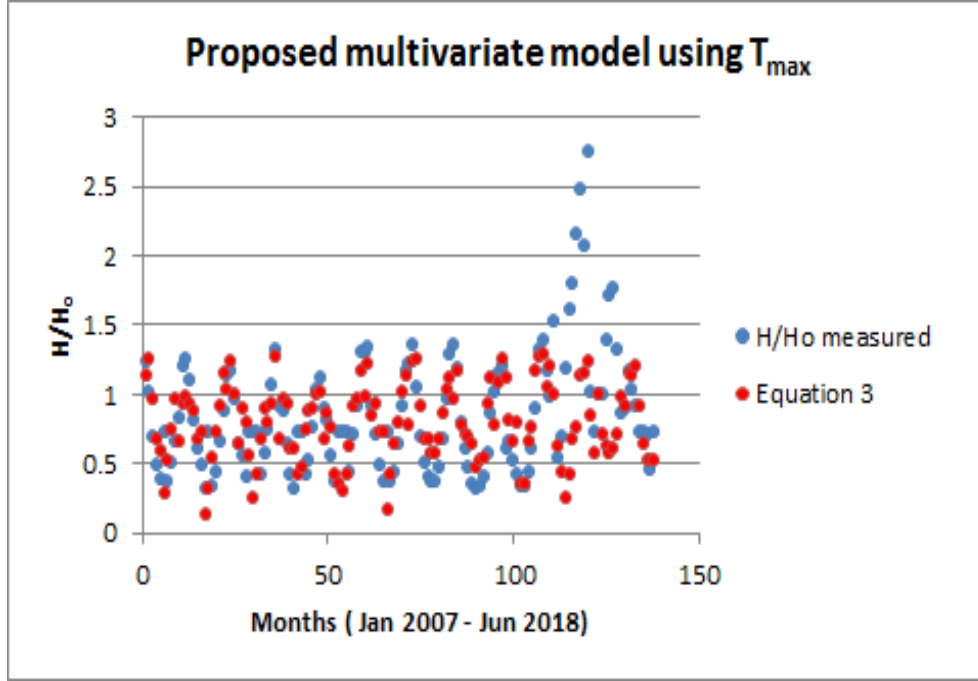


Figure 21: Proposed model for the estimation of  $\frac{H}{H_o}$  for Bloemfontein

### 5.2.2. Cape Town (CT)

Table 20: Proposed multivariate equations

No.	Equation
1	$\frac{H}{H_o} = -0.069 (\Delta T) - 0.179 \left(\frac{RH}{100}\right) + 2.539 \left(\frac{S}{S_o}\right) - 0.433$
2	$\frac{H}{H_o} = -0.395 (\sqrt{\Delta T}) - 0.176 \left(\frac{RH}{100}\right) + 2.540 \left(\frac{S}{S_o}\right) + 0.124$
3	$\frac{H}{H_o} = -0.004 (T_{max}) + 0.165 \left(\frac{RH}{100}\right) + 2.358 \left(\frac{S}{S_o}\right) - 1.042$
4	$\frac{H}{H_o} = -0.034 \left(\sqrt{T_{max}}\right) + 0.165 \left(\frac{RH}{100}\right) + 2.360 \left(\frac{S}{S_o}\right) - 0.962$
5	$\frac{H}{H_o} = -0.014 (\Delta T)^2 + 0.128 (\Delta T) - 3.041 \left(\frac{RH}{100}\right)^2 + 2.340 \left(\frac{RH}{100}\right) + 2.812 \left(\frac{S}{S_o}\right)^2 - 1.305 \left(\frac{S}{S_o}\right) - 0.159$
6	$\frac{H}{H_o} = -0.003 (T_{max})^2 + 0.094 (T_{max}) - 0.965 \left(\frac{RH}{100}\right)^2 + 0.942 \left(\frac{RH}{100}\right) + 3.549 \left(\frac{S}{S_o}\right)^2 - 2.060 \left(\frac{S}{S_o}\right) - 0.597$
7	$\frac{H}{H_o} = -0.002 (\Delta T)^3 - 0.001 (\Delta T)^2 + 0.15 (\Delta T) + 32.35 \left(\frac{RH}{100}\right)^3 - 47.97 \left(\frac{RH}{100}\right)^2 + 17.94 \left(\frac{RH}{100}\right) + 1.23 \left(\frac{S}{S_o}\right)^3 + 0.80 \left(\frac{S}{S_o}\right)^2 - 0.40 \left(\frac{S}{S_o}\right) - 0.69$
8	$\frac{H}{H_o} = 4 \times 10^{-4} (T_{max})^3 - 0.03 (T_{max})^2 + 0.71 (T_{max}) + 13.33 \left(\frac{RH}{100}\right)^3 - 19.66 \left(\frac{RH}{100}\right)^2 + 7.52 \left(\frac{RH}{100}\right) + 2.25 \left(\frac{S}{S_o}\right)^3 - 0.46 \left(\frac{S}{S_o}\right)^2 - 0.37 \left(\frac{S}{S_o}\right) - 5.41$



**Table 21: Error indicators for proposed equations**

Equation	RMSE	MBE	MABE	MPE	MAPE	MARE	$R^2$
1	0.29168	0.06358	0.22174	2.34321	39.68114	0.39681	0.57990
2	0.30012	0.06358	0.22187	2.20763	39.70152	0.39702	0.88447
3	0.29956	0.06358	0.22425	3.95230	39.85326	0.39853	0.88490
4	0.29958	0.06358	0.22424	3.93864	39.86163	0.39862	0.88489
5	0.27006	0.06358	0.19926	3.07052	31.81996	0.31820	0.65884
6	0.26905	0.06358	0.19935	3.57050	31.91099	0.31911	0.90716
7	0.26640	0.06358	0.19182	2.86728	29.20680	0.29207	0.66803
8	0.26336	0.06358	0.19213	3.22039	28.85694	0.28857	0.91104

Tables 20 and 21 show the proposed equations for Cape Town.  $\frac{H}{H_o}$  values show a stronger dependency on  $T_{max}$ , with the quadratic (Equation 6) and cubic (Equation 8) relations having the highest  $R^2$  and lowest RMSE values for this city. MPE indicators are within the accepted range and the MAPEs can be explained by the large number of outliers in the data set. The proposed equation - Equation 8 fits the measured values of GSR well as indicated in Figure 22. A few underestimations are noticeable but overall the model includes most data points.

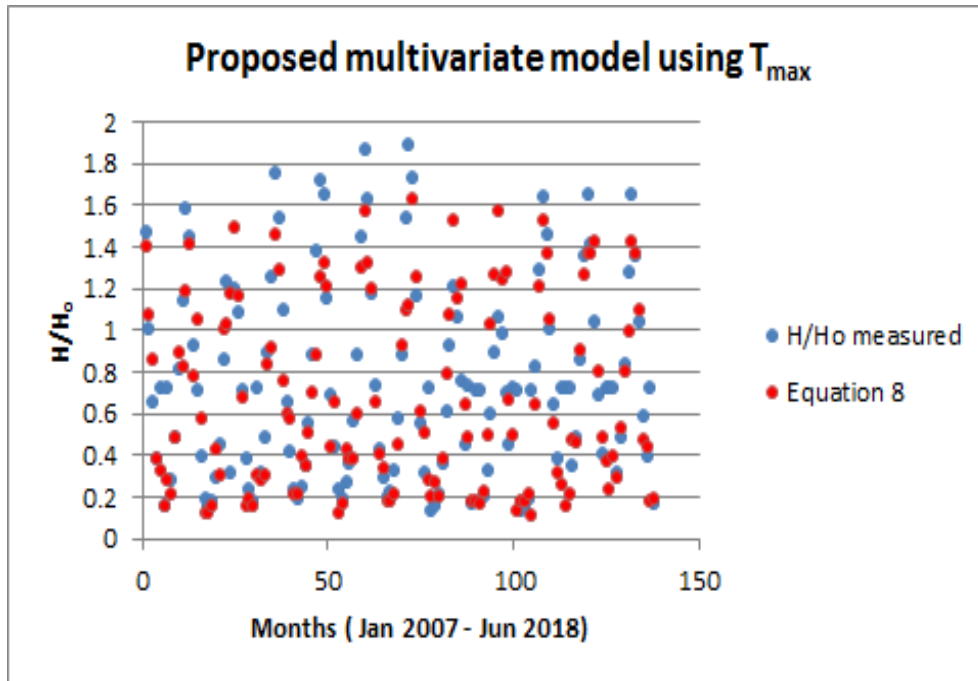


Figure 22: Proposed model for the estimation of  $\frac{H}{H_o}$  for Cape Town

### 5.2.3. Durban (DBN)

**Table 22: Proposed multivariate equations**

No.	Equation
1	$\frac{H}{H_o} = 0.002 (\Delta T) + 2.033 \left(\frac{RH}{100}\right) + 0.365 \left(\frac{S}{S_o}\right) - 1.201$
2	$\frac{H}{H_o} = 0.020 (\sqrt{\Delta T}) + 2.040 \left(\frac{RH}{100}\right) + 0.361 \left(\frac{S}{S_o}\right) - 1.242$
3	$\frac{H}{H_o} = 0.008 (T_{max}) + 1.919 \left(\frac{RH}{100}\right) + 0.413 \left(\frac{S}{S_o}\right) - 1.325$
4	$\frac{H}{H_o} = 0.102 (\sqrt{T_{max}}) + 1.905 \left(\frac{RH}{100}\right) + 0.416 \left(\frac{S}{S_o}\right) - 1.732$
5	$\frac{H}{H_o} = 4.5 \times 10^{-4} (\Delta T)^2 - 0.019 (\Delta T) + 7.039 \left(\frac{RH}{100}\right)^2 - 8.255 \left(\frac{RH}{100}\right) + 0.521 \left(\frac{S}{S_o}\right)^2 - 0.159 \left(\frac{S}{S_o}\right) + 2.844$
6	$\frac{H}{H_o} = -1.4 \times 10^{-3} (T_{max})^2 + 0.108 (T_{max}) + 13.097 \left(\frac{RH}{100}\right)^2 - 16.833 \left(\frac{RH}{100}\right) - 1.180 \left(\frac{S}{S_o}\right)^2 + 1.6025 \left(\frac{S}{S_o}\right) + 3.399$
7	$\frac{H}{H_o} = -9 \times 10^{-5} (\Delta T)^3 + 0.005 (\Delta T)^2 - 0.06 (\Delta T) - 230.5 \left(\frac{RH}{100}\right)^3 + 499.5 \left(\frac{RH}{100}\right)^2 - 355.4 \left(\frac{RH}{100}\right) - 9.27 \left(\frac{S}{S_o}\right)^3 + 13.1 \left(\frac{S}{S_o}\right)^2 - 5.46 \left(\frac{S}{S_o}\right) + 84.15$
8	$\frac{H}{H_o} = 3.6 \times 10^{-5} (T_{max})^3 - 0.005 (T_{max})^2 + 0.23 (T_{max}) - 142.8 \left(\frac{RH}{100}\right)^3 + 320.3 \left(\frac{RH}{100}\right)^2 - 235.9 \left(\frac{RH}{100}\right) - 9.18 \left(\frac{S}{S_o}\right)^3 + 11.78 \left(\frac{S}{S_o}\right)^2 - 4.19 \left(\frac{S}{S_o}\right) - 54.78$

**Table 23: Error indicators for proposed equations**

Equation	RMSE	MBE	MABE	MPE	MAPE	MARE	R <sup>2</sup>
1	0.15789	0.02188	0.13075	-7.18984	29.15333	0.29153	0.42176
2	0.15792	0.02188	0.13082	-7.21693	29.20971	0.29210	0.42153
3	0.15648	0.02188	0.12888	-6.34183	27.92393	0.27924	0.92113
4	0.39039	0.02188	0.12188	3.86583	-31.31340	0.42384	0.30871
5	0.14688	0.02188	0.11608	-6.07546	25.32882	0.25329	0.49962
6	0.12589	0.02188	0.10413	-2.0700	21.34543	0.21345	0.94895
7	0.14598	0.02188	0.11043	-4.05942	22.36994	0.22370	0.50567
8	0.13117	0.02188	0.10559	-1.59414	20.55594	0.20560	0.94458

First, second and third order equations using  $T_{max}$  indicate high correlation coefficients and low RMSEs. This makes these equations well suited. The percentage errors are all within the accepted range. We propose Equation 6 for the city of Durban and this model's performance is depicted in Figure 23. Since sunshine data was not measured from May 2010 - Jun 2018, we excluded these months from our analysis. The shape of the data shown below suggests that the model adequately estimates  $K_T$  for the period available. Since fewer data points were analyzed, this also has an impact on the error indicators reported in the table above.

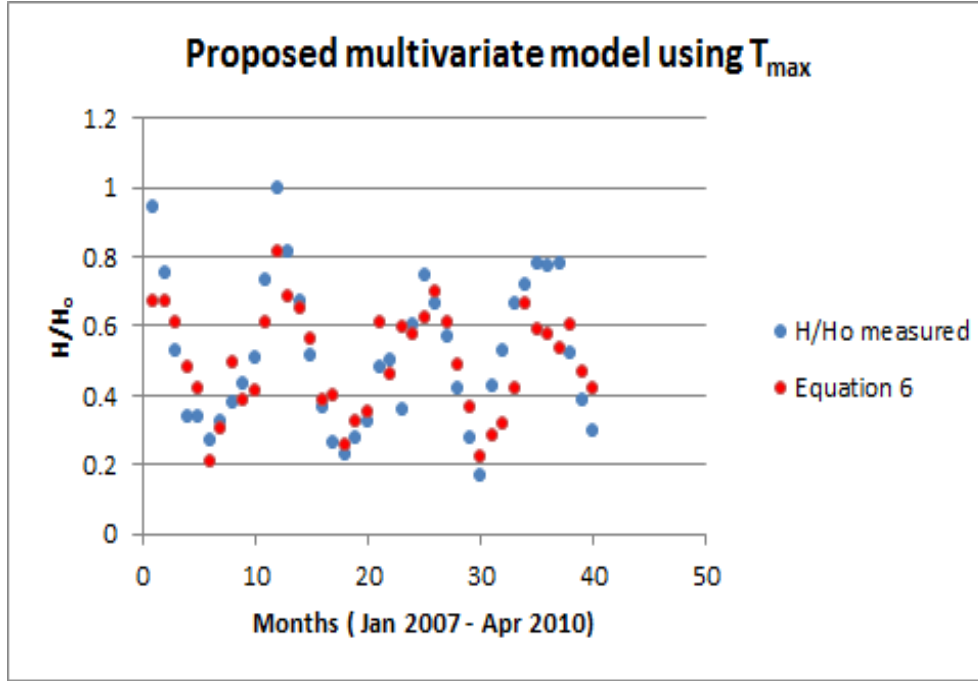


Figure 23: Proposed model for the estimation of  $\frac{H}{H_o}$  for Durban

#### 5.2.4. Johannesburg (JHB)

Table 24: Proposed multivariate equations

No.	Equation
1	$\frac{H}{H_o} = -0.029 (\Delta T) + 0.618 \left(\frac{RH}{100}\right) + 0.3135 \left(\frac{S}{S_o}\right) + 0.178$
2	$\frac{H}{H_o} = -0.232 (\sqrt{\Delta T}) + 0.460 \left(\frac{RH}{100}\right) + 0.624 \left(\frac{S}{S_o}\right) - 0.581$
3	$\frac{H}{H_o} = 0.045 (T_{max}) + 0.474 \left(\frac{RH}{100}\right) + 0.159 \left(\frac{S}{S_o}\right) - 0.887$
4	$\frac{H}{H_o} = 0.433 (\sqrt{T_{max}}) + 0.453 \left(\frac{RH}{100}\right) + 0.169 \left(\frac{S}{S_o}\right) - 1.936$
5	$\frac{H}{H_o} = 1.9 \times 10^{-3} (\Delta T)^2 - 0.110 (\Delta T) - 1.304 \left(\frac{RH}{100}\right)^2 + 1.677 \left(\frac{RH}{100}\right) + 1.044 \left(\frac{S}{S_o}\right)^2 - 0.982 \left(\frac{S}{S_o}\right) + 1.026$
6	$\frac{H}{H_o} = -1.8 \times 10^{-3} (T_{max})^2 + 0.131 (T_{max}) - 1.154 \left(\frac{RH}{100}\right)^2 + 1.757 \left(\frac{RH}{100}\right) - 0.4735 \left(\frac{S}{S_o}\right)^2 + 0.811 \left(\frac{S}{S_o}\right) - 2.436$
7	$\frac{H}{H_o} = 6.7 \times 10^{-4} (\Delta T)^3 - 0.04 (\Delta T)^2 + 0.62 (\Delta T) - 25.60 \left(\frac{RH}{100}\right)^3 + 47.02 \left(\frac{RH}{100}\right)^2 - 28.50 \left(\frac{RH}{100}\right) - 2.57 \left(\frac{S}{S_o}\right)^3 - 1.85 \left(\frac{S}{S_o}\right)^2 - 0.49 \left(\frac{S}{S_o}\right) + 3.83$
8	$\frac{H}{H_o} = 7.5 \times 10^{-4} (T_{max})^3 - 0.06 (T_{max})^2 - 1.27 (T_{max}) - 6.14 \left(\frac{RH}{100}\right)^3 + 11.25 \left(\frac{RH}{100}\right)^2 - 6.43 \left(\frac{RH}{100}\right) - 18.59 \left(\frac{S}{S_o}\right)^3 + 36.74 \left(\frac{S}{S_o}\right)^2 - 23.70 \left(\frac{S}{S_o}\right) + 15.80$

**Table 25: Error indicators for proposed equations**

Equation	RMSE	MBE	MABE	MPE	MAPE	MARE	$R^2$
1	0.25244	0.15038	0.19397	17.47650	30.41315	0.30413	0.19989
2	0.24853	0.14751	0.19093	16.9053	29.76287	0.29763	0.8602
3	0.14144	$-4 \times 10^{-9}$	0.10475	-5.08111	19.6809	0.19368	0.94689
4	0.14166	0.01584	0.10686	-1.73778	19.44057	0.19441	0.94672
5	0.39480	0.34215	0.34764	14.63490	31.40490	0.31405	0.20488
6	0.13838	$6.41 \times 10^{-16}$	0.10853	-4.58710	20.46811	0.20468	<b>0.94916</b>
7	0.18301	$-2.1 \times 10^{-15}$	0.15512	-10.94380	30.67616	0.30676	0.33782
8	0.11753	$-1 \times 10^{-14}$	0.09414	-3.16928	16.61409	0.16614	0.96333

Error analysis for the proposed equations for Johannesburg shows low RMSE and MBE values, which make the above equations suitable. It is evident that  $T_{max}$  equations have a stronger correlation to clearness index values. Equation 8 which is a cubic function of  $T_{max}$  is proposed for Johannesburg and illustrated in Figure 24 below. The proposed model fits the historic data well and there are a few underestimations which result from effects of any of the three variables included in the equation.

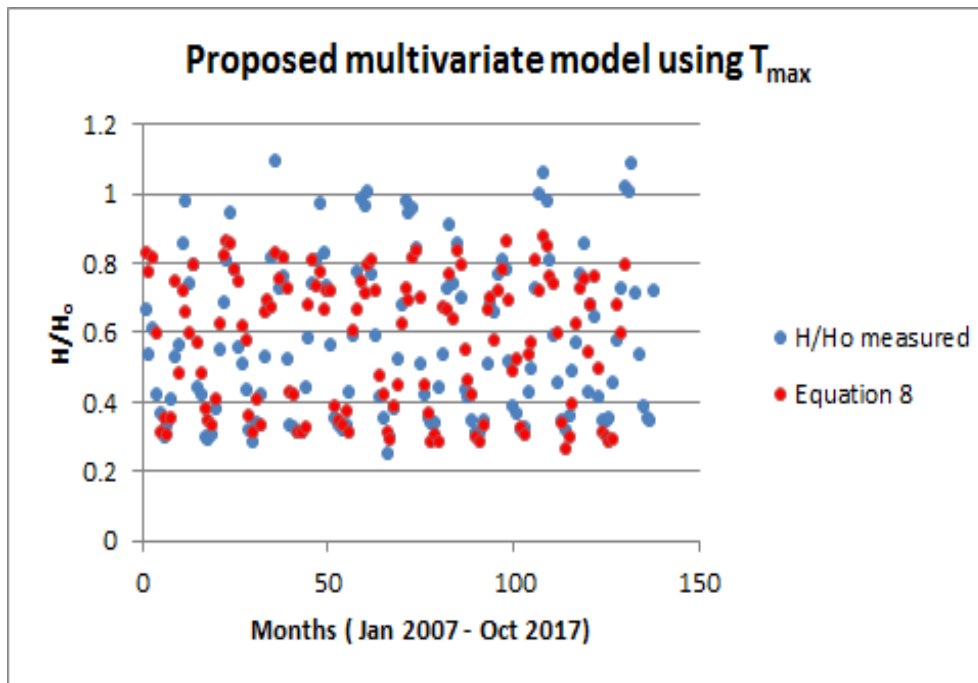


Figure 24: Proposed model for the estimation of  $\frac{H}{H_o}$  for Johannesburg

### 5.2.5. Pietermaritzburg (PMB)

**Table 26: Proposed multivariate equations**

No.	Equation
1	$\frac{H}{H_o} = 0.048 (\Delta T) + 2.633 \left(\frac{RH}{100}\right) + 0.174 \left(\frac{S}{S_o}\right) - 1.876$
2	$\frac{H}{H_o} = 0.310 (\sqrt{\Delta T}) + 2.599 \left(\frac{RH}{100}\right) + 0.885 \left(\frac{S}{S_o}\right) - 2.361$
3	$\frac{H}{H_o} = 0.032 (T_{max}) + 1.462 \left(\frac{RH}{100}\right) + 0.235 \left(\frac{S}{S_o}\right) - 1.390$
4	$\frac{H}{H_o} = 0.319 (\sqrt{T_{max}}) + 1.463 \left(\frac{RH}{100}\right) + 0.231 \left(\frac{S}{S_o}\right) - 2.168$
5	$\frac{H}{H_o} = -0.016 (\Delta T)^2 + 0.475 (\Delta T) + 13.621 \left(\frac{RH}{100}\right)^2 - 13.963 \left(\frac{RH}{100}\right) + 1.237 \left(\frac{S}{S_o}\right)^2 - 1.612 \left(\frac{S}{S_o}\right) + 0.808$
6	$\frac{H}{H_o} = 0.002 (T_{max})^2 - 0.085 (T_{max}) + 7.513 \left(\frac{RH}{100}\right)^2 - 8.183 \left(\frac{RH}{100}\right) - 0.910 \left(\frac{S}{S_o}\right)^2 - 1.110 \left(\frac{S}{S_o}\right) + 3.533$
7	$\frac{H}{H_o} = 0.003 (\Delta T)^3 - 0.12 (\Delta T)^2 + 1.67 (\Delta T) - 9.02 \left(\frac{RH}{100}\right)^3 + 31.06 \left(\frac{RH}{100}\right)^2 - 25.38 \left(\frac{RH}{100}\right) - 8.77 \left(\frac{S}{S_o}\right)^3 + 19.99 \left(\frac{S}{S_o}\right)^2 - 14.53 \left(\frac{S}{S_o}\right) + 2.0$
8	$\frac{H}{H_o} = 8.9 \times 10^{-5} (T_{max})^3 - 0.004 (T_{max})^2 + 0.047 (T_{max}) - 22.51 \left(\frac{RH}{100}\right)^3 + 50.56 \left(\frac{RH}{100}\right)^2 - 35.24 \left(\frac{RH}{100}\right) - 9.17 \left(\frac{S}{S_o}\right)^3 + 20.59 \left(\frac{S}{S_o}\right)^2 - 14.7 \left(\frac{S}{S_o}\right) + 11.3$

**Table 27: Error indicators for proposed equations**

Equation	RMSE	MBE	MABE	MPE	MAPE	MARE	R <sup>2</sup>
1	0.13726	-6.6 × 10 <sup>-16</sup>	0.11001	-6.71925	25.21744	0.25217	0.59623
2	0.13758	-9.6 × 10 <sup>-16</sup>	0.11045	-6.79374	25.39489	0.25395	0.93908
3	0.12468	-1.3 × 10 <sup>-16</sup>	0.10076	-5.39414	22.82711	0.22827	0.94996
4	0.12490	9.4 × 10 <sup>-17</sup>	0.10090	-5.39830	22.89302	0.22893	0.94979
5	0.18160	0.14	0.14929	-20.75960	28.27592	0.28276	0.29317
6	0.11116	1.44 × 10 <sup>-15</sup>	0.08474	-4.43616	17.83656	0.17837	0.96023
7	0.11077	9.7 × 10 <sup>-15</sup>	0.08462	-4.43619	17.68162	0.17682	0.73701
8	0.10744	2.4 × 10 <sup>-15</sup>	0.08199	-4.22186	17.64309	0.17643	0.96285

First order equations using  $\sqrt{\Delta T}$ ,  $T_{max}$  and  $\sqrt{T_{max}}$  indicate high  $R^2$  values with low error indicators shown in Table 27. Equations containing  $T_{max}$  again show a stronger relationship to  $K_T$  values. For Pietermaritzburg, Equation 6 is proposed. The models efficiency is depicted in Figure 25 and indicates a well suited model. Sunshine duration data was unavailable for certain months and hence the analysis was completed only for the period 2007 - 2014.

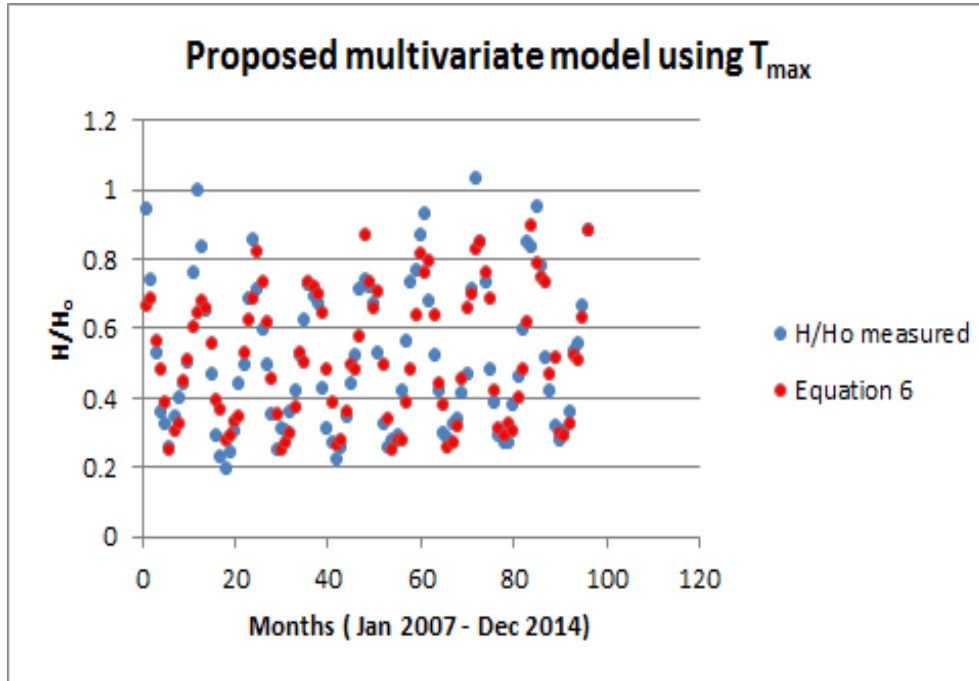


Figure 25: Proposed model for the estimation of  $\frac{H}{H_o}$  for Pietermaritzburg

The above analysis is evidence that multivariate models are more efficient in estimating GSR as opposed to single variable models. Strong  $R^2$  coefficients are detailed for the proposed multivariate equations. Low error indicators (RMSE, MBE and MPE) describe the suitability of these models for GSR prediction over the long-term. MAPE error values can be explained by the rounding and averaging of hourly and daily recordings to obtain monthly average values. We have found that the dependence of  $\frac{H}{H_o}$  on  $T_{max}$  is stronger than that of  $\Delta T$  (derived from the H-S model), while relative sunshine duration  $\frac{S}{S_o}$  is a strong indicator of the GSR experienced across the study sites. Higher order equations (both single and multivariate relationships) prove to be more accurate. The equations which we have suggested for the five study sites demonstrate their suitability for the estimation of GSR over the long-term i.e. forecasting horizon and are summarized in the following;

**Table 28: Summary of multivariate equations for each study site**

Site	Equation
<b>BFN</b>	$\frac{H}{H_o} = 0.040 (T_{max}) - 0.307 \left(\frac{RH}{100}\right) + 1.151 \left(\frac{S}{S_o}\right) - 0.979$
<b>CT</b>	$\frac{H}{H_o} = 4 \times 10^{-4} (T_{max})^3 - 0.03 (T_{max})^2 + 0.71 (T_{max}) + 13.33 \left(\frac{RH}{100}\right)^3 - 19.66 \left(\frac{RH}{100}\right)^2 + 7.52 \left(\frac{RH}{100}\right) + 2.25 \left(\frac{S}{S_o}\right)^3 - 0.46 \left(\frac{S}{S_o}\right)^2 - 0.37 \left(\frac{S}{S_o}\right) - 5.41$
<b>DBN</b>	$\frac{H}{H_o} = -1.4 \times 10^{-3} (T_{max})^2 + 0.108 (T_{max}) + 13.097 \left(\frac{RH}{100}\right)^2 - 16.833 \left(\frac{RH}{100}\right) - 1.180 \left(\frac{S}{S_o}\right)^2 + 1.6025 \left(\frac{S}{S_o}\right) + 3.399$
<b>JHB</b>	$\frac{H}{H_o} = 7.5 \times 10^{-4} (T_{max})^3 - 0.06 (T_{max})^2 - 1.27 (T_{max}) - 6.14 \left(\frac{RH}{100}\right)^3 + 11.25 \left(\frac{RH}{100}\right)^2 - 6.43 \left(\frac{RH}{100}\right) - 18.59 \left(\frac{S}{S_o}\right)^3 + 36.74 \left(\frac{S}{S_o}\right)^2 - 23.70 \left(\frac{S}{S_o}\right) + 15.80$
<b>PMB</b>	$\frac{H}{H_o} = 0.002 (T_{max})^2 - 0.085 (T_{max}) + 7.513 \left(\frac{RH}{100}\right)^2 - 8.183 \left(\frac{RH}{100}\right) - 0.910 \left(\frac{S}{S_o}\right)^2 - 1.110 \left(\frac{S}{S_o}\right) + 3.533$

## Chapter 6: Conclusions

Solar insolation received throughout South Africa has the potential to supplement the state utility supply. This potential has not been fully considered and as such remains idle. Solar technologies such as PV applications remain relevant to private and off-grid utilization as sufficient investment into these technologies is not available on a governmental level. While ESKOM continues to face dire financial restraints, aging infrastructure and growing electricity demands result in regular implementation of scheduled power outages. The economic and social consequences thereof make this country unappealing for foreign investment. South Africa receives ample solar resource for the implementation of CSPs at several sites across the country; the primary limitation for this is the lack of available funding and research. This study aims to provide further insight into the amount of GSR received in major cities of the country while trying to promote the undertaking of research related to solar energy as an alternate resource. While consequences of climate change due to global warming continue to be experienced throughout the country, insufficient attempts are being made to decrease our carbon footprint.

Meteorological parameters used for this research were substantially easy to obtain, with the exception of sunshine data measurements which are not always available as a consequence of the costly equipment required to perform this function. For most regions in South Africa, solar radiation and sunshine duration variables are not measured, thus reiterating the need for reliable solar radiation estimation models. In this study we have analyzed the impact of single variable, linear estimation models on the available GSR within South Africa in comparison to multivariate, non-linear regression models which incorporate variations of meteorological parameters. These are the first non-linear GSR estimation models to be introduced for South Africa. The insights provided in this work show that the estimation of GSR can be accurate and subsequently cost effective. Our suggested models are unique to each city in South Africa and may be incorporated into the design and installation processes



of solar PV technologies which will enhance their efficiency while endorsing their application.

South Africa being one of the most developed countries on the African continent requires sustainable investment and sufficient research to undertake renewable energy technologies. Thus the estimation of solar radiation potential across the country through readily available meteorological variables such as air temperature, relative humidity and sunshine duration is of great significance. In this study we have provided multivariate, non-linear models which are able to effectively estimate the amount of solar radiation incident over five major cities. Our results suggest that models listed in Table 28 perform considerably well in the estimation of GSR for South Africa.

The empirical Hargreaves-Samani (H-S) and Angstrom-Prescott (A-P) models proved to be reliable methods for estimating the amount of GSR in smaller study periods (i.e. one calendar year), but lacked accuracy for long-term estimations as indicated in this study. Our work further indicates that models which make use of a single meteorological variable and most linear models are not able to adequately predict GSR for our selected regions over periods longer than ten calendar years. As a recommendation, we suggest that research be conducted to establish sufficient A-P coefficients for the available historical sunshine data for South Africa to enable GSR estimation for period when measured data is not available. These empirical coefficients may be integrated into the above suggested models for each study site and provide models with higher correlations. Further studies into the impact of aerosols on the amount of GSR incident in a specific area will allow for a correction factor to be introduced to GSR estimation models. This will prove to be a profound contribution towards the existing research in the field. Due to the complexity of aerosols and their composition this is not possible until further innovations have been made.

## References

- [1] [www.worldbank.org](http://www.worldbank.org)
- [2] Fourteenth Session of the United Nations Commission on Sustainable Development. South Africa country report. Department of Environmental Affairs and Tourism. 2005.
- [3] The Rise of Renewable Energy Implementation in South Africa. Jain S., Jain P. K. Applies Energy Symposium and Forum. Science Direct, Energy Procedia 143. 2017. Pp. 721-726
- [4] [www.moneyweb.co.za/news/south-africa/south-africa-signs-first-of-r55-92bn-renewable-energy-deals/](http://www.moneyweb.co.za/news/south-africa/south-africa-signs-first-of-r55-92bn-renewable-energy-deals/)
- [5] Challenges for South Africa's Electricity Supply Industry. Joffe H. Spokesperson for ESKOM Holdings Limited.
- [6] Sustainable Electricity Generation Technologies in South Africa: Initiatives, Challenges and Policy implications. Energy and Environment Research, Vol 1 (1). Dec 2011. Musango J. K., Amigun B., Brent A. C.
- [7] Current energy landscape in the Republic of South Africa. Pollet B. G., Staffell I., Adamson K. International Journal of Hydrogen Energy, 40. 2015. Pp. 16685-16701
- [8] Energy security in South Africa. Trollip H., Butler A., Burton J., Caetano T., Godhino C. Research paper, Issue 17. Mitigation and Action Plans (MAPS) 2014.
- [9] Renewable Energy Scenarios for municipalities in South Africa. South African Local Government Association opportunities in Renewable Energy and Energy Efficiency for Municipalities in South Africa. January 2018.
- [10] Pocket guide to South Africa 2016/17 Energy and Water. National Development Plan.
- [11] The state of Energy Research in South Africa. Academy of Science in South Africa. August 2014. ISBN: 978-0-9922268-1-3
- [12] Utility-scale renewable energy. Market Intelligence Report. Green Cape. 2017.
- [13] <https://solargis.info/imaps-and-gis-data/download/south-africa>
- [14] Renewable Energy Vision 2030 – South Africa, Climate Change and Energy. World e Fund for Nature (WWF) Technical Report. 2014.
- [15] Solar PV Feasibility Assessment – Course Outline. Green Career Training. Terra Firma Academy. [www.terrafirma-academy.com](http://www.terrafirma-academy.com)
- [16] Models for calculating monthly average solar radiation from air temperature in Swaziland. Dlamini M.

- D., Varkey A. J., Mkhonta S. K. *International Journal of Physical Sciences*, Vol 12. 2017.pp. 247-254. DOI: 10.5897/IJPS2017.4679
- [17] Estimation of hourly, daily and monthly global solar radiation on inclined surfaces: Models re-visited. Maleki S. A. M., Hizam H., Gomes C. *Energies*. 2017. DOI: 10.3390/en10010134
- [18] Predicting clear-sky global horizontal irradiance at eight locations in South Africa using four models. Zhandire E. *Journal of Energy in Southern Africa*, Vol 28 (4). 2017. Pp. 77-86.
- [19] Solar radiation models and information for renewable energy applications - E. O. Falayi, A. B. Rabi
- [20] Qiang Fu. *Radiation (Solar)*. University of Washington. Seattle, WA. USA. Elsevier Ltd. 2003
- [21] Solar irradiance since 1874 revisited. S.K. Solanki and M. Fligge. *Geophysical research letters*, vol 25, No.3, pg. 341-344, Feb 1998.
- [22] Sayigh A. A. M. *Solar radiation availability prediction from climatological data*. Academic Press, New York. 1977. pp.61. ISBN: 0-12-620850-6
- [23] Viorel B. *Modeling solar radiation at the earth's surface: Recent advances*. Springer. 2008. ISBN: 3540774548
- [24] Earth System Science Education Alliance (ESSEA), Institute for Global Environmental Strategies (IGES) [Internet]. Image provided by the National Science Digital Library. 2015. Available from: [http://esseacourses.strategies.org/module.php?module\\_id=99](http://esseacourses.strategies.org/module.php?module_id=99)
- [25] Boeker E., Van Grondelle R. *Environmental physics: Sustainable energy and climate change*. 3rd Ed. John Wiley and Sons Ltd. 2011.
- [26] Kennewell J. Mc Donald A. *IPS-Satellite communications and space weather* [Internet]. The Australian Space Weather Agency. 2008. Available from: <http://www.ips.gov.au/Educational/1/3/2>
- [27] Earth's annual global mean energy budget. J.T. Kiehl, K.E. Trenberth. *Bulletin of the American Meteorological Society*, 197-208, Vol.78, No.2, 1997 (Feb).
- [28] Queener B. D. *Intra-hour direct normal irradiance solar forecasting using genetic programming*. [Electronic Masters Thesis]. San Diego, California, USA. 2012. Available from: [http://escholarship\\_uc\\_item3g06n4dp.pdf](http://escholarship_uc_item3g06n4dp.pdf)
- [29] Iqbal Muhammad. *An Introduction to solar radiation*. Elsevier Ltd. 2012.
- [30] Paescu M., Paescu E., Gravila P., Badescu V. *Weather modeling and forecasting of PV systems operation*. Springer Science and Business Media. 2012.
- [31] Boyle G. *Renewable Energy*. OXFORD University Press. 2004.

- [32] Campbell G. S., John M. N. An Introduction to environmental biophysics. 2nd Ed. Springer, New York. 1998.
- [33] Günther, Matthias and Janotte, Nicole and Mezrhab, Ahmed and Pottler, Klaus and Schillings, Christoph and Wilbert, Stefan and Wolfstätter, Fabian. (2011). Solar Radiation. Chapter 2.
- [34] Sproul A. B. Derivation of the solar geometric relationships using vector analysis. Renewable Energy. No. 32. pp.1187-1205. 2007.
- [35] Conradie D. Maximising the Sun. 2010.
- [36] Roderick M. L. Methods for calculating solar position and day length included computer programs and subroutines. Land Management, Western Australian Department of Agriculture. 1992.
- [37] Meinel A. B., Meinel M. P. Applied solar energy. An Introduction. 1976.
- [38] Wayfinding: Modern Methods and Techniques of Non-Instrument Navigation, Based on Pacific Traditions. The Polynesian Voyaging Society. Voyage into the New Millennium. Hana Hou, 41.
- [39] Tijjani B.I. Comparison between first and second order Angstrom type models for sunshine hours in Katsina Nigeria. Bayero Journal of Pure and Applied sciences. Vol 4(2). pp.24-27. Available from: [dx.doi.org/10.4314/bajopas.v4i2.5](http://dx.doi.org/10.4314/bajopas.v4i2.5)
- [40] Ituen Eno E., Esen Nisken U., Nwokolo Samuel C., Uto Ema G. Prediction of Global solar radiation using relative humidity, maximum temperature and sunshine hours in Uyo in the Niger delta Region, Nigeria. Advances in Applied Science Research. Vol. 3(4). 2012. pp.1923-1937. ISSN: 0976-8610
- [41] Srivasta R. C., Pandey H. Estimating Angstrom-PreScott coefficients for India and developing a correlation between sunshine hours and global solar radiation for India. ISRN Renewable Energy. Vol 2013. Hindawi Publishing. Available form: <http://dx.doi.org/10.1155/2013/403742>
- [42] Almorox J., Hontoria C., Benito M. Models for obtaining daily global solar radiation with measured air temperature data in Madrid (Spain). Applied Energy 88. 2011. pp.1703-1709. DOI: 10.1016/j.apenergy.2011.11.003
- [43] Rahimikoob A. Estimating global solar radiation using ANN and air temperature data in semi-arid environment (Iran).Renewable Energy. Vol. 35. 2010. pp.2131-2135. DOI:10.1016/j.renene.2010.01.029
- [44] Gilani S. I. U. H., Dimas F. A. R., Shiraz M. Hourly solar radiation estimation using ambient temperature and relative humidity data. International Journal of Environmental Science and Development, 2(3). pp.

188-193.

- [45] E. B. Babatunde. Solar Radiation, a friendly renewable energy source. INTECH Open Access Publisher. 2012.
- [46] Diabate L., Blanc P., Wald L. Solar Radiation climate in Africa. Solar Energy. No. 76. Elsevier Ltd. pp.733-744. 2004. <hal-00361362>
- [47] Effect of aerosol vertical distribution on aerosol-radiation interaction: A theoretical prospect. Mishra A. K., Koren I., Rudich V. Heliyon (2015).
- [48] Govinda R. T., Lado K., Patrick A. N. A review of solar energy, markets, economies and policies. Policy research working paper. The world bank, development and research group, environment and energy team. 2011. Available from: <http://econ.worldbank.org>
- [49] Dresselhaus M. S., Thomas I. L. Alternative Energy Technologies. Nature, 414 (6861). pp. 332-337. 2001
- [50] Kumar R., Umanand L. Estimation of global radiation using clearness index model for sizing PV systems. Renewable Energy, 30. pp. 2221-2233. 2005.
- [51] Pelland S., Remund J., Kleissl J., Oozeki T., De Brabandere K. Photovoltaic and solar forecasting: State of the art. IEA PVPS. Task 14. 2013.
- [52] Fluri T. P. The potential of Concentrating Solar Power in South Africa. Energy Policy. No. 37. pp.5075-5080. 2009.
- [53] Pitz-Paal. Concentrating Solar Power. Energy: Improved, Sustainable and Clean Options for our planet. Elsevier, Oxford. pp. 171-192. 2008.
- [54] Ulbricht R., Fischer U., Lehner W., Donker H. First steps towards a systematical optimized strategy for solar energy supply forecasting. In proceedings of the European Conference on Machine Learning and Principles and Practice of Knowledge Discovery in Databases (ECMLPKDD). Prague, Czech Republic, Vol. 2327. 2013.
- [55] Neher I., Buchmann T., Crewell S., Evers-Dietze B., Pfeilsticker K., Pospical B., Schirrmeister C., Melinger S. Impact of atmospheric aerosols on PV energy production scenario for the Sahel zone. Energy Procedia 125. 2017. Elsevier. pp. 170-179.
- [56] Green A. M. Photovoltaic Solar Energy Conversion. Brazilian Journal of Physics, Vol 26 (1).1996.

- [57] Khan M. K. A., Paul S., Zobayer A., Hossain S. S. A study on Photovoltaic Conversion. International journal of scientific engineering research. Vol 4(3). 2013.
- [58] Bosshard P. Hermann W., Hung E., Hunt R., Simon A. J. An assessment of solar energy conversion technologies and research opportunities. Global Climate and Energy Project (GCEP) Energy Assessment Analysis. Technical Assessment Report. 2016.
- [59] Kiehl J. T., Hack J. J., Bonan G. B., Boville B. A., Williamson D. L., Rasch P. J. The National Center for Atmospheric Research. Community Climate Model: CCM3\*. Journal of Climate, vol. 11 (6). pp. 1131-1149.
- [60] Zhang J., Hodge B. M., Forita A., Lu S., Hamann H. F., Banunarayanan V. Metrics for evaluating the accuracy of solar power into power systems, London, England.
- [61] Hofmann M., Seckmeyer G. A new model for estimating the diffuse fraction of solar irradiance for Photovoltaic system simulations. Energies. 2017.
- [62] Inanlougani A., Reddy T. A., Katiamula S. Evaluation of time-series, regression and neural network models for solar forecasting. Part 1: One-hour horizon.
- [63] Sendanayake S. Miguntanna N. P., Jayasinghe M. T. R. Estimating incident solar radiation in tropical islands with short term weather data. European Scientific Journal, vol. 10 (3). 2014.
- [64] Abraha M. G., Savage M. J. Comparison of estimates of daily solar radiation from air temperature range for application in crop simulations. Agricultural and Forest Meteorology, 148. pp. 401-416. 2008.
- [65] Prescott J. A. Evaporation from water surface in relation to solar radiation. Transactions of the Royal Society of Australia, 46. pp. 114-118. 1940.
- [66] Da Silva V. J., Da Silva C. R., Almorox J., Junior J. A. Temperature based solar radiation models for use in simulated soybean potential yield. Australian journal of crop science. 2016. Vol 10 (7). pp. 926-932.
- [67] Allen R. G., Pereira L. S., Raes D., Smith M. Crop Evapotranspiration (Guidelines for computing crop water requirements). FAO Irrigation and Drainage Paper No. 56. 2006.
- [68] Meenal R., Boazina P. G., Selvakumar A. I. Temperature based radiation models for the estimation of global solar radiation at horizontal surface in India. Indian journal of science and technology. Vol 9(46). 2016.
- [69] Samani Z. Estimating solar radiation and evapotranspiration using minimum climatological data. Journal of Irrigation and Drainage Engineering. 2000. pp.265-267.

- [70] Allen R.G. Self-calibrating method for estimating global solar radiation from air temperature. *Journal of Hydrologic Engineering*. New York. Vol.2. 1991. pp.56-57. ISSN: 10840699
- [71] Hargreaves G. H., Samani Z. A. Estimating potential evapotranspiration. *Journal of irrigation and drainage engineering*. ASCE. 108(IR3). 1982. pp.223-230.
- [72] Almorox J., Bocco M., Wellington E. Estimation of daily global solar radiation from measured temperatures at Canada de Luque, Corboda, Argentina. *Renewable Energy*, Elsevier, vol. 60(C). pp. 382-387. 2013
- [73] Dlamini M. D., Varkey A. J., Mkhonta S. K. Models for calculating monthly average solar radiation from air temperature in Swaziland. *International journal of physical sciences*. Vol 12. pp. 247-254. 2017.
- [74] Sarkar N.I., Sifat A. I., Paul S., Hossain S., Rahman M. Solar radiation estimation using temperature data for Dhaka, Bangladesh. 2016.
- [75] Ya'u M. J., Gele M. A., Ali Y. Y., Alhaji M. Global solar radiation models: A review. *Journal of photonic materials and technology*. Vol 4(1). pp. 26-32. 2018.
- [76] Maluta E. N., Mulaudzi T. S., Sankaran V. Estimation of the global solar radiation on the horizontal surface from temperature data for the Vhembe District in the Limpopo Province of South Africa. *International Journal of Green Energy*, 11 (5). pp. 454-464. 2014.
- [77] Hargreaves G. H., Allen R. G. History and evaluation of the Hargreaves evapotranspiration equation. *Journal of Irrigation and Drainage Engineering*, 129 (1). pp. 53-63. 2003.
- [78] Razieli T., Pereira L. S. Estimation of ETo with Hargreaves-Samani and FAO-PM temperature methods for a wide range of climates in Iran. *Agricultural Water Management*, 121. pp. 1-18. 2013.
- [79] Gadiwala M. S. Usman A., Akhtar M., Jamil K. Empirical models for the estimation of global solar radiation with sunshine hours on horizontal surface in various cities of Pakistan. *Pakistan Journal of Meteorology*. Vol. 9(18). 2013.
- [80] Angstrom A. Solar and atmospheric radiation. *International commission for solar research on Actinometric Investigations of solar and atmospheric radiation*. *Journal of the Royal Meteorological Society*. pp.121-126. 1923.
- [81] Teke A., Yilidirim H. B. Estimating the monthly global solar radiation for Eastern Mediterranean Region. *Energy Conversion and Management*, 87. pp. 628-635. 2014.
- [82] Salima G., Chavula G. M. S. Determining Angstrom coefficients for estimating solar radiation in Malawi.

International Journal of Geosciences (3). pp. 391-397. 2012.

[83] Falayi E. O., Adepitan J. O., Rablu A. B. Empirical models for the correlation of global solar radiation with meteorological data in Iseyin, Nigeria. International Journal of Physical Sciences, vol. 3 (9). pp. 210-216. 2008

[84] Page J. K. The estimation of monthly mean values of daily total short wave radiation on vertical and inclined surfaces from sunshine records for latitudes 40°N - 40° S. In : Proceedings of UN conference on new sources of energy. pp. 378-390. 1961.

[85] Chegaar M., Chibani A. A simple method for computing global solar radiation. Rev. Energy. Ren. : Chemss. pp. 111-115. 2000.

[86] Waleed I. Empirical Models for the correlation of clearness index with meteorological parameters in Iraq. IOSR. Journal of Engineering, 4 (3). pp. 12-18. 2014.

[87] Adeala A. A., Huan Z., Enweremadu C. C. Evaluation of solar radiation using multiple weather parameters as predictors for South Africa provinces. Thermal science. Vol 19 (2). pp. 495-509.2015

[88] Itodo I. N., Yohanna J. K. Correlation between global solar radiation, ambient air temperature and sunshine hours for Makurdi Nigeria.

[89] Nia M., Chegaar M., Benatallah M. F., Aillerie M. Contribution to the quantification of solar radiation in Algeria. Energy Procedia. Vol 36. pp. 730-737. 2013

[90] van den Besselaar E. J. M., Sanchez-Lorenzo A., Wild M., Tank A. M. G. K., de Laat A. T. J. Relationship between sunshine duration and temperature trends across Europe since the second half of the 20th century. Journal of geophysical research: Atmospheres.

[91] Chen J.L., Li G.S. Estimation of monthly average daily solar radiation from measured meteorological data in Yangtze River Basin in China. International journal of climatology. Vol 33. pp. 487-498. 2013.

[92] Rivington M., Bellocchi G., Matthews K. B., Buchan K. Evaluation of three model estimations of solar radiation at 24 UK stations. Agricultural and Forest Meteorology. Vol 132. pp. 228-243. 2005.

[93] Conradie D. C. U. South Africa's Climatic Zones: Today, Tomorrow. International Green Building Conference and Exhibition. Future Trends and Issues Impacting on the Built Environment. July 25-26, 2012, Sandton, South Africa. CSIR Research Space.

[94] Jury M. R. Climate trends in southern Africa. South African journal of science. Vol 109 (1/2) Article



980, 11 pages. 2013 <http://dx.doi.org/10.1590/sajs.2013/980>

[95] Burton, M.; Cooke, S.; Godfrey, A.; Neville, L.; Pauker, E.; le Roux-Rutledge, E. Africa Talks Climate: The public understanding of climate change in ten countries. Executive Summary. BBC World Service Trust, London, UK (2010) 20 pp.

[96] Lesson 3: Africa's Climate Regions. Available from:

[http://learn.mindset.co.za/sites/default/files/resourcelib/emshare-show-note-asset/771\\_fdoc.pdf](http://learn.mindset.co.za/sites/default/files/resourcelib/emshare-show-note-asset/771_fdoc.pdf)

[97] South Africa Climate and Weather by regions. Available from:

[www.cosechaypostcosecha.org/data/.../ConvenioSudafrica/ClimateAndWeather.pdf](http://www.cosechaypostcosecha.org/data/.../ConvenioSudafrica/ClimateAndWeather.pdf)

[98] Tadross M. and Johnston P. Sub-Saharan African Cities: A five-city network to pioneer climate adaptation through participatory research and local action. ICLEI – Local Governments for Sustainability – Africa. Climate Systems Regional Report: Southern Africa. 2012. ISBN: 978-0-9921794-6-5

[99] [https://upload.wikimedia.org/wikipedia/commons/thumb/e/e0/South\\_Africa\\_K%C3%B6ppen.svg/1024px-South\\_Africa\\_K%C3%B6ppen.svg.png](https://upload.wikimedia.org/wikipedia/commons/thumb/e/e0/South_Africa_K%C3%B6ppen.svg/1024px-South_Africa_K%C3%B6ppen.svg.png)

[100] Climate change (207). Chapter 11. Climate change. 2011. Available from:

[https://www.environment.gov.za/sites/default/files/reports/environmentoutlook\\_chapter11.pdf](https://www.environment.gov.za/sites/default/files/reports/environmentoutlook_chapter11.pdf)

[101] Benhin J. K. A. Climate change and South African agriculture: Impacts and adaptation options. CEEPA Discussion Paper No. 21. Special Series on Climate Change and Agriculture in Africa ISBN 1-920160-01-09 . ISBN: 1-920160-21-3. 2006

[102] Kiker G. A. South African county study on climate change: Synthesis report for the vulnerability and adaptation assessment section. Draft paper. Available from:

[https://unfccc.int/sites/default/files/sem\\_sup5\\_south\\_africa.pdf](https://unfccc.int/sites/default/files/sem_sup5_south_africa.pdf)

[103] Five year integrated human settlements plan. Council annexure 31 May 2017. Mangaung Metropolitan Municipality.

[104] Dinga M. N. V., du Preez P. J. Grassland communities of urban open spaces in Bloemfontein, Free State, South Africa. Koedoe 55 (1), no. 1075, 8 pages. <http://dx.doi.org/10.4102/koedoe.v55i1.1075>

[105] Western Cape IWRM Action Plan: Status Quo Report DEADP. Final draft. 2011. Available from: [https://www.westerncape.gov.za/other/2011/8/final\\_draft\\_exec\\_summary\\_report\\_2011.pdf](https://www.westerncape.gov.za/other/2011/8/final_draft_exec_summary_report_2011.pdf)

[106] Sharing spatial planning and land use management. Lessons learnt in the Ethekwini Municipality.

Municipal Institute of Learning. 2012. Available from:

[http://www.durban.gov.za/Resource\\_Centre/Development\\_Site/Documents/Lessons\\_Learnt\\_Spatial\\_Planning\\_and\\_Land\\_Use\\_March2013\\_3.pdf](http://www.durban.gov.za/Resource_Centre/Development_Site/Documents/Lessons_Learnt_Spatial_Planning_and_Land_Use_March2013_3.pdf)

[107] Climate change adaptation plan. City of Johannesburg. 2009. Available from:

[https://www.preventionweb.net/files/38589\\_38507climatechangeadaptationplancit.pdf](https://www.preventionweb.net/files/38589_38507climatechangeadaptationplancit.pdf)

[108] Johannesburg Population. (2018-06-12). Retrieved 2018-12-12, from <http://worldpopulationreview.com/world-cities/johannesburg/>

[109] <http://www.southafrica.com/maps/>

[110] Sarkar M. N. I., Sifat A. I. Global solar radiation estimation from commonly available meteorological data for Bangladesh. *Renewables* 3(6). 2016. DOI: 10.1186/s40807-0.160027-3

[111] Marwal V.K., Punia R.C., Sengar N., Mahawar S., Dashora P., A comparative study of correlation functions for estimation of monthly mean daily global solar radiation for Jaipur, Rajasthan (India), *Indian J. Sci. Techn.*, 2012, 5(5), 2729-2732.

[112] Robaa S.M. Evaluation of sunshine duration from cloud data in Egypt, *Energy*, 2008, 33(5), 789-795.

## APPENDIX A

### FORTRAN CODE TO CALCULATE $H_o$

```
program HoCalc
!This program allows the user to calculate the  $H_o$  for a given site of latitude (phi) and day (Dn)

implicit none

real:: delta, d, omega
real:: phi, Isc, Ho
real:: pi
real:: E, X, s
real:: y, z, theta

Open (unit=10, file='HoInput', status='old', action='read')
Open (unit=9, file='HoOutput', status='new', action='write')
read (10,*)d

Isc= 1367.0
phi=29.6679
pi= 4.0*atan(1.0)
y= (360.0*(284+d))/365.0
delta= ((23.45*pi/180.0)*sin((y*pi)/180.0))
E= ((24.0*3.6e-3*Isc)/pi)
s=(phi*pi)/180.0
omega = acos(-1*(tan(s))*(tan(delta)))
z= 360.0*(d/365.0)
X= (1+(0.033*(cos((z*pi)/180.0))))
Ho= (E * X *(cos(s)*cos(delta)*sin(omega) + omega*sin(s)*sin(delta)))

write(9,*)Ho
close (unit=9)
```

```
close (unit=10)
end program HoCalc
```

## FORTRAN CODE TO CALCULATE $S_o$

```
program SoCalc
!This program allows the user to calculate  $S_o$  for a given site of latitude (phi)

real:: delta, d, omega
real:: phi, So, s
real:: pi, y
integer:: i

open (unit=10, file='HoInput.txt', status='old', action='read')
open (unit=9, file='SoOutput.txt', status='new', action='write')

do i=1,365

read (10,*)d
phi=29.6270
pi= 4.0*atan(1.0)
y= (360.0*(284+d))/365.0
delta= ((23.45*pi/180.0)*((sin(y*pi)/180.0)))
s=(phi*pi)/180.0
omega = acos(-1*(tan(s))*(tan(delta)))
So = ((2.0/15.0)*(omega*180.0/pi))
write(9,*)So

end do
close(unit=9)
close(unit=10)
end program SoCalc
```

## APPENDIX B

### Research paper (Published in Open Physics)

Govindasamy, Tamara Rosemary and Chetty, Naven. Quantifying the global solar radiation received in Pietermaritzburg, KwaZulu-Natal to motivate the consumption of solar technologies. Open Physics, De Gruyter. Vol 16 (1).2018. pp. 786 - 794. ID: 10.1515/phys-2018-0098.

## Research Article

Tamara Rosemary Govindasamy and Naven Chetty\*

# Quantifying the global solar radiation received in Pietermaritzburg, KwaZulu-Natal to motivate the consumption of solar technologies

<https://doi.org/10.1515/phys-2018-0098>

Received Apr 16, 2018; accepted Aug 13, 2018

**Abstract:** In South Africa, power outages and scheduled load shedding are common practices in a bid to safeguard power resources. With the increase in cost of conventional energy sources, and the depletion of fossil fuels, attempts to use renewable resources to their full potential are underway. South Africa and in particular Pietermaritzburg receives sunshine throughout the year, making it suitable for harnessing solar power. In this work we estimate the amount of Global Solar Radiation (GSR) received in Pietermaritzburg which is the capital of the KwaZulu-Natal province. An air temperature model (Hargreaves-Samani) is used to approximate the GSR received in Bisley in comparison to measured data obtained from the ARC, for a period of one calendar year (July 2014 – June 2015). We proceed to apply the Angstrom-Prescott model to evaluate the competence of the initial prediction method. The primary aim of this study is to validate the efficiency and accuracy of the above-mentioned forecasting models, for areas within close proximity. Our results compare fairly well with the observed data provided by the ARC. Both models prove to sufficiently estimate the amount of GSR incident in Bisley. The deviations from the actual measured values suggest that a model which incorporates both variables may improve the accuracy of GSR estimations. The use of comprehensive prediction and forecasting models will allow for optimal placement of solar technologies for the harnessing of GSR within Pietermaritzburg. Though Pietermaritzburg may not be suitable for large scale solar power plants, the employment of solar panels in both in-

dustrial and residential areas will contribute greatly to a decrease in demand of grid electricity.

**Keywords:** Load shedding, global solar radiation, photovoltaic technologies, air temperature model, Angstrom-Prescott model

**PACS:** 88.40.fc, 88.40.ff, 92.60.Vb, 92.60.Aa

## 1 Introduction

Solar energy is a pure, inexhaustible, and readily available resource. The escalation in price of conventional energy sources, together with the depletion of non-renewable resources and fossil fuels, necessitates a great demand for alternative power sources. Green energy sources which are beneficial to the environment are being studied as alternate resources which could potentially assist in the energy crisis. The cost of these technologies has reduced significantly in the past decade, however it still remains higher than the cost of conventional energy and hence uptake is still relatively slow [1].

Within South Africa, we rely solely on the energy harnessed from coal power stations operated by ESKOM, the state power utility. The increased demand for electricity has resulted in a rise in production costs due to the strain placed on existing power stations, aging infrastructure as well as the depletion of non-renewable resources [2]. Since our country has been alarmed about the security of energy resources for the country's energy demands, load shedding (power outages) have been implemented almost daily over the past few years in an attempt to save energy [2]. The consequences of load shedding have affected the entire country with even more devastating effects on the economy [2, 3]. Though resources have recently been secured to increase energy production, the cause of the crisis cannot be cured. The depletion of non-renewable energy sources remains an issue, and will surely result in greater consequences in the long-term.

\***Corresponding Author: Naven Chetty:** University of KwaZulu-Natal, School of Chemistry and Physics, Private Bag X01, Scottsville 3209, Pietermaritzburg, South Africa  
Email: chetty3@ukzn.ac.za

**Tamara Rosemary Govindasamy:** University of KwaZulu-Natal, School of Chemistry and Physics, Private Bag X01, Scottsville 3209, Pietermaritzburg, South Africa

Growth in solar energy technologies has been noted, together with its theoretical potential to supply the global demand for energy being the major contributing factor [1]. South Africa is well suited for the harnessing of solar radiation because sunshine is available throughout the year including the winter months. Depending on the geographical location certain areas in Africa receive more than double the amount of radiation as compared to countries in the northern hemisphere [3]. Despite this abundance, there are many financial and technical restraints with regards to solar energy technologies, which limit its use to private off-grid connections. These limitations need to be overcome in order to increase the contribution of solar power to the energy supply of the country.

The amount of solar radiation incident at the earth's surface is a measurable quantity. Solar radiation outside of the earth's atmosphere, received at a surface which is normal to the incident radiation is known as the solar constant [4, 5]. This quantity is measured from space through the use of satellite data and has a value of  $1367 \text{ Wm}^{-2}$ , which changes by approximately 0.01% over a period of 30 years [5–8]. The amount of solar radiation received at the earth's surface is largely depleted due to the attenuation processes which occur in the atmosphere [6].

Solar radiation is responsible for many processes which transpire on the earth's surface and its research finds applications in many science and engineering fields [9]. Knowledge and prediction of solar radiation available at a specific location is of great importance for the designing and performance evaluation of solar energy conversion systems [9, 10]. Solar energy can be harnessed and utilized for applications which fall into two main categories; Solar Thermal and Solar Photovoltaic (PV) [1, 9, 10].

In many geographical locations, Global Solar Radiation (GSR) is not measured because it is too expensive to purchase and maintain the apparatus required. If measured data is available, it is not always complete as equipment can fail due to numerous faults [9, 11]. As a result, accurate and efficient forecasting methods are increasingly required. Hence, researchers have employed the use of empirical methods which are able to calculate and predict GSR for a particular location [5, 9, 11–13].

Many of these empirical models require the input of other meteorological variables (which are often more accessible than solar radiation data) or historical weather data. Some of these meteorological parameters include; air temperature, precipitation, relative humidity, sunshine duration, etc. [11–13]. The empirical model is classified according to the climatic variable which it requires [9], e.g. sunshine duration models [10, 13–16], temperature based

methods [9, 17–19], and cloud-based methods which require the use of satellite sky images [6].

Although industries within South Africa are aware of the solar technologies which exist, they are not being implemented to translate their true potential. With accurate prediction and forecasting models for our country, we may be able to enhance the use of these technologies while alleviating the strain placed on existing energy infrastructure.

## 2 Sample site details

The city of Pietermaritzburg (Midlands) is the capital city of the KwaZulu-Natal province in South Africa. This city is found in a hollow which is surrounded by the escarpment (Drakensberg Mountain Range) and is seen as an inland region. Having a geographical location that ideally receives sunshine throughout the year, Pietermaritzburg is one of the warmest cities in the province. Weather stations in the neighboring cities were unable to provide records of daily solar radiation or sunshine duration for Pietermaritzburg. Such data is not readily available for this location, hence making this work significant as a predictor of GSR. A study center in Ukulinga (Bisley, Pietermaritzburg), was able to provide the necessary data required for this work. Temperature, Humidity and Dew point measurements were recorded hourly with the use of a sensor. Table 1 provides the geographical data of the site considered in this study. The land use in Bisley has more of an industrial and commercial setting. Figure 1 is a satellite illustration of Bisley, Pietermaritzburg.

**Table 1:** Geographical details of study sites

	Bisley	Ukulinga
<b>Latitude <math>\Phi</math> (South)</b>	$-29.668^\circ$	$-29.663^\circ$
<b>Longitude (East)</b>	$30.416^\circ$	$30.405^\circ$
<b>Elevation</b>	752m	750m

The main focus of our research was to estimate the amount of GSR received in Pietermaritzburg using meteorological data which is readily and easily available. Since the cost of equipment to measure certain climatic parameters was too high, we decided to use an approach that estimated solar radiation using air temperature and sunshine duration. Records of solar radiation incident in Pietermaritzburg are conducted by the Agricultural Research Council (ARC). The ARC conducts work with the Ukulinga Research Center (based in Bisley), and was able to provide



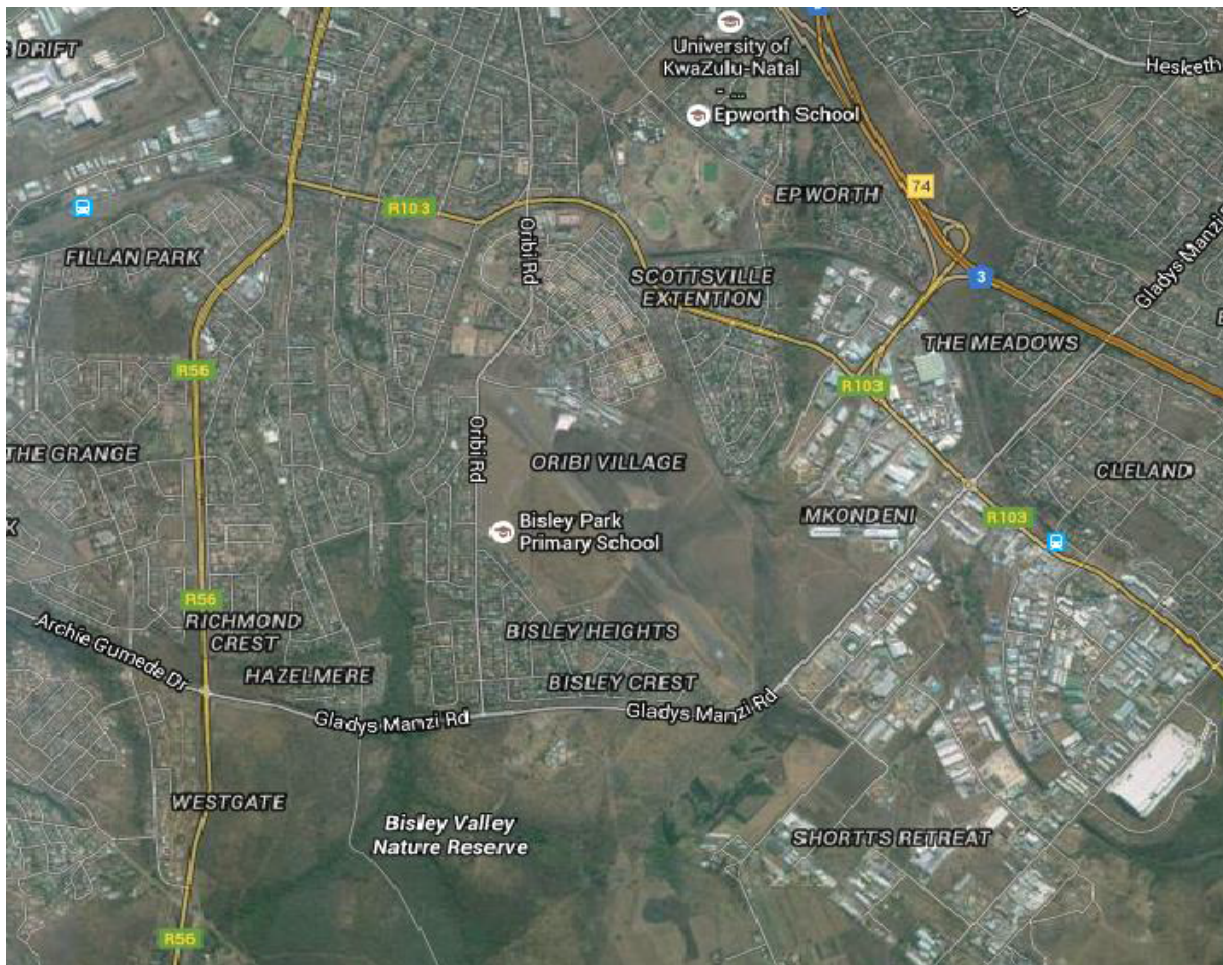


Figure 1: Satellite image of Scottsville, Bisley [Google maps]

the necessary GSR data for this study. This data was used to verify our calculations and interpret our differences. The Hargreaves-Samani equation [19] was applied to calculate the solar radiation incident on a horizontal surface, for Bisley following the approach studied by Maluta *et al.* [20]. Thereafter we proceeded to validate this method using the Angstrom-Prescott model. Due to time and equipment constraints we were only able to yield measurements over a period of one calendar year, however this technique can be further developed to analyze historic data for any location.

### 3 Background theory

In areas where solar radiation information is inaccessible, methods of forecasting are employed. The simplest method involves the use of the air temperature of a given location. Air temperature measurements are easy to con-

duct and can be obtained in regions where there are no weather stations nearby. The Hargreaves-Samani equation [18–20] relates the amount of extraterrestrial radiation ( $H_o$ ) to the difference between the maximum and minimum air temperatures ( $\Delta T = T_{\max} - T_{\min}$ ), in order to calculate the amount of GSR incident on a horizontal surface ( $H$ ), using the equation below [6, 11, 17, 18, 20];

$$H = H_o K_r (\Delta T)^{0.5} \quad (1)$$

where the empirical coefficient  $K_r = 0.16$  for 'interior regions' and  $K_r = 0.19$  for 'coastal regions' [9, 17, 20]. The extraterrestrial radiation  $H_o$ ; is given by [6, 16, 21, 22];

$$H_o = \frac{24 \times 3.6 \times 10^{-3} I_{sc}}{\pi} \left[ 1 + 0.033 \cos \left( \frac{2\pi D_n}{365} \right) \right] \cdot [\cos \phi \cos \delta \sin \omega_s + \omega_s \sin \phi \sin \delta] \quad (2)$$

where  $I_{sc} = 1367 \text{ W/m}^2$  is known as the solar constant [6, 16, 20],  $D_n$  is the Julian calendar day of the year (Jan 1st corresponds to  $D_n = 1$ , Dec 31st corresponds to  $D_n = 365$ ).

The latitude of the site is denoted by  $\phi$ ; and all angles are calculated in radians.  $\delta$ , is the declination angle which is given by [6, 10, 16, 21, 22];

$$\delta = 23.45 \frac{\pi}{180} \sin \left[ \frac{2\pi(D_n + 284)}{365} \right] \quad (3)$$

The sunset hour angle,  $\omega_s$ , is given by [6, 20, 22, 23];

$$\omega_s = \cos^{-1}(-\tan \phi \tan \delta) \quad (4)$$

By calculating the solar angles it is possible to predict the amount of solar irradiance received on a horizontal surface at a given location. The clearness index ( $K_T$ ) describes the atmosphere's transparency and is found by comparing the amount of GSR to the amount of extraterrestrial solar radiation as shown by [6, 20, 21];

$$K_T = \frac{H}{H_o} \quad (5)$$

The Angstrom-Prescott equation can be used to calculate the clearness index from the relative sunshine duration, provided the Angstrom-Prescott coefficients for the area are known [6, 14, 15, 21];

$$K_T = \frac{H}{H_o} = a + b \left( \frac{S}{S_o} \right) \quad (6)$$

where  $a$ ,  $b$  are the Angstrom-Prescott coefficients,  $S$  is the actual hours of sunshine received, and  $S_o$ ; is the maximum possible duration of sunshine for a given day calculated from [15, 16, 21, 23];

$$S_o = \frac{2\omega_s}{15} \quad (7)$$

For areas where the Angstrom coefficients are unknown, it is prescribed to use  $a = 0.25$  and  $b = 0.50$  [23].

The temperature data for Bisley (Commercial/ Industrial area) was studied for the period July 2014 – June 2015. A MT668 Temperature and humidity data logger was used to record hourly maximum and minimum temperatures, relative humidity and dew point for this location. The Hargreaves-Samani equation was applied to calculate the GSR for Bisley which was then related to the measured values for Ukulinga, provided by ARC. The Angstrom-Prescott model was used to validate the Hargreaves-Samani model, using measured sunshine duration data for Bisley. Thereafter, the clearness index was determined using each of the above models. We again verified the efficiency of both models in comparison to the measured quantities.

## 4 Results and discussion

Daily average measurements of temperature, relative humidity and dew point were recorded using data loggers cal-

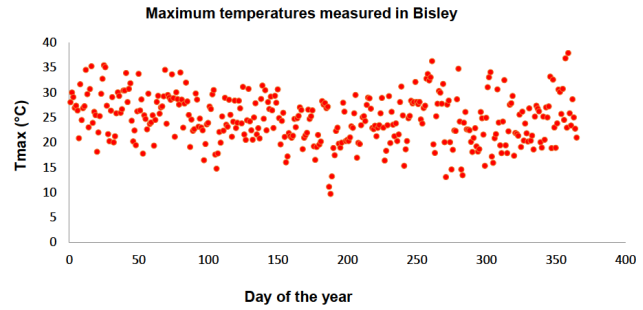


Figure 2: Graph of measured maximum temperatures for Bisley

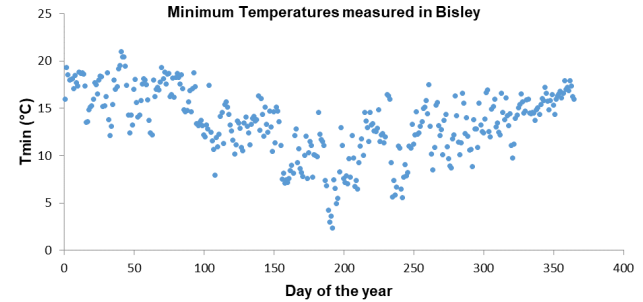


Figure 3: Graph of measured minimum temperatures for Bisley

ibrated in Bisley. Attention to their placement was essential as the sensors had to be installed at a height of 1,5m above the ground and could not be sheltered, as this would alter the recordings drastically. Graphs showing the measured maximum and minimum air temperatures for this suburb are provided in Figures 2 and 3. These measurements were conducted for each day of the time period studied (July 2014 - June 2015). The latitude of Bisley was used to calculate the relevant solar angles using eqs. (3) and (4) which then allowed us to evaluate the extraterrestrial solar radiation ( $H_o$ ) in Eq. (2). The Hargreaves-Samani (H-S) equation (Eq.(1)), together with the measured air temperature values gave results which are averaged in Table 2. The GSR values listed below are the calculated monthly averages based on daily maximum and minimum air temperatures. We then estimated the GSR for Bisley using measured sunshine duration hours and the  $H_o$  within the Angstrom-Prescott (A-P) model. The maximum possible sunshine duration Eq. (7) was calculated using the hour angle Eq. (4). These results are represented in Table 3.

The measured values ( $H_{measured}$ ) listed in Tables 2 and 3, are the actual observed values of GSR for Bisley. The data was supplied by the ARC and enabled us to compare the values calculated by Eqs. (1) and (6) with the measured data. Temperature variations show a similar distribution to the  $H$  (both observed and calculated) values which illustrates the relationship between air temperature and GSR.

**Table 2:** Bisley, Ukulinga results using the Hargreaves-Samani Model (July 2014-June 2015)

Month	$T_{\max}$ (°C)	$T_{\min}$ (°C)	$\Delta T$ (°C)	$H_o$ (MJ/m <sup>2</sup> /day)	$H_{\text{calculated}}$ (MJ/m <sup>2</sup> /day)	$H_{\text{measured}}$ (MJ/m <sup>2</sup> /day)
July	21.84	8.10	13.74	19.98	11.69	12.34
Aug	23.73	11.34	12.38	24.70	13.70	13.71
Sep	27.37	12.54	14.82	31.34	18.98	17.88
Oct	22.51	12.56	9.95	37.63	18.48	15.34
Nov	22.60	14.14	8.47	41.95	19.03	14.94
Dec	26.01	15.96	10.05	43.74	21.61	17.63
Jan	27.46	17.10	10.36	42.94	21.64	19.69
Feb	26.23	16.55	9.68	39.69	19.50	19.45
Mar	27.08	16.76	10.32	34.13	17.32	17.83
Apr	23.86	13.51	10.35	27.31	13.75	14.58
May	25.84	12.99	12.84	21.58	12.25	13.76
Jun	22.11	9.80	12.32	18.87	10.47	12.44
<b>Average</b>	<b>24.72</b>	<b>13.45</b>	<b>11.27</b>	<b>31.99</b>	<b>16.54</b>	<b>15.80</b>

**Table 3:** Bisley, Ukulinga results using the Angstrom-Prescott Model (July 2014-June 2015)

Month	S (hours)	$S_o$ (hours)	$S/S_o$	$H_o$ (MJ/m <sup>2</sup> /day)	$H_{\text{calculated}}$ (MJ/m <sup>2</sup> /day)	$H_{\text{measured}}$ (MJ/m <sup>2</sup> /day)
July	6.80	10.30	0.66	19.98	11.59	12.34
Aug	6.50	10.97	0.59	24.70	13.46	13.71
Sep	6.20	11.85	0.52	31.34	15.98	17.88
Oct	6.00	12.76	0.47	37.63	18.25	15.34
Nov	6.50	13.51	0.48	41.95	20.56	14.94
Dec	6.90	13.88	0.50	43.74	21.87	17.63
Jan	6.30	13.67	0.46	42.94	20.61	19.69
Feb	6.60	13.04	0.51	39.69	20.04	19.45
Mar	6.90	12.18	0.57	34.13	18.26	17.83
Apr	7.40	11.27	0.66	27.31	15.84	14.58
May	7.90	10.51	0.75	21.58	13.49	13.76
Jun	7.60	10.13	0.75	18.87	11.80	12.44
<b>Average</b>	<b>6.8</b>	<b>12.01</b>	<b>0.58</b>	<b>31.99</b>	<b>16.81</b>	<b>15.80</b>

The accuracy of both models was determined based on the error analysis between the predicted and measured values of GSR. Table 4 provides the average annual errors for the Hargreaves-Samani (H-S) and Angstrom-Prescott (A-P) models. The mean bias error (MBE) indicates the average deviance of the calculated values from that of the measured and is used to decide the long-term performance of a model [24]. Positive values of MBE correspond to an over estimation, while a negative MBE indicates an under estimation. The RMSE gives insight into the short-term performance of a correlation. Low values for all statistic error measures are desired [25]. Earlier studies suggest that percentage errors between -10% and 10% are acceptable [26].

Statistical analysis reported in Table 4 was calculated using the below;

**Table 4:** Error analysis

	H-S	A-P
<b>RMSE (MJ/m<sup>2</sup>/day)</b>	2.14	2.34
<b>MPE (%)</b>	3.85	6.15
<b>MAPE (%)</b>	10.62	10.43
<b>MBE (MJ/m<sup>2</sup>/day)</b>	0.74	1.01
<b>MABE (MJ/m<sup>2</sup>/day)</b>	1.65	1.65



**Mean bias error (MBE) and mean absolute bias error (MABE)**

$$MBE = \frac{1}{n} \sum_{i=1}^n (H_c - H_m)$$

$$MABE = \frac{1}{n} \sum_{i=1}^n (|H_c - H_m|)$$

**Mean percentage error (MPE) and mean absolute percentage error (MAPE)**

$$MPE = \frac{1}{n} \sum_{i=1}^n \left( \frac{H_c - H_m}{H_m} \right) \times 100\%$$

$$MAPE = \frac{1}{n} \sum_{i=1}^n \left| \left( \frac{H_c - H_m}{H_m} \right) \right| \times 100\%$$

**Root mean square errors (RMSE)**

$$RMSE = \sqrt{\frac{\sum_{i=1}^n (H_c - H_m)^2}{n}}$$

where  $H_c$  and  $H_m$  are the calculated and measured values of GSR, respectively.

Positive errors indicate that the models under study have overestimated values of GSR for the given period. The MPE falls within the prescribed interval (-10%; 10%), however the MAPE is slightly over the 10% interval (Table 4). This is a minor deviation in comparison to the daily sample size. Averaging and rounding of hourly, daily measurements when calculating monthly average values, would have contributed to the error being over the acceptable range. In this regard, the results are still acceptable. The RMSE, MBE and MABE values are moderate and can be lower to show a stronger correlation. The calculated values of H for Bisley conformed well to the shape of the data observed by the ARC, with the exception of a few outliers. This is represented in Figures 4 and 5. Maximum calculated values for H were observed during October - February (Figures 4 and 5) which are the spring and summer months in South Africa. Both the (H-S) and (A-P) models demonstrated the most deviation from the measured GSR values in these spring/summer months, which may indicate over estimation by the selected methods.

The over prediction may be a consequence of; the accuracy and competence of the equipment used, the effects of wind, or other temperature invasion factors such as pol-

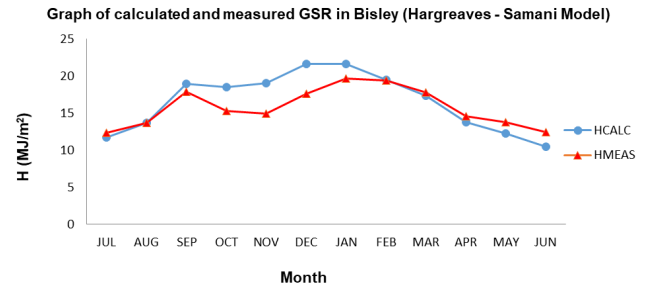


**Figure 4:** Graph comparing the measured and calculated values of H using the H-S Model

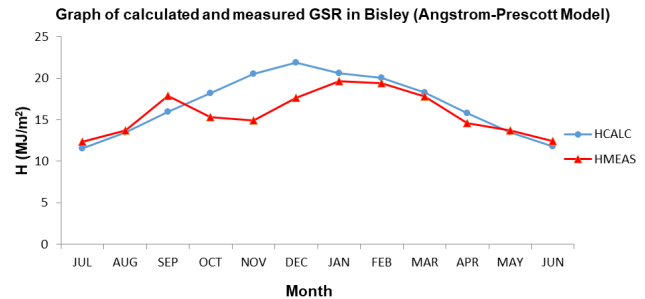


**Figure 5:** Illustration comparing the measured and calculated values of H using the A-P Model

lution. Observed values could be better validated by adjusting the temperature based model (H-S) to account for short wave radiation. The sunshine duration model may be modified by introducing a non-linear relationship between the GSR and sunshine duration ratio. For optimal prediction, this work suggests that a new model be devised to include both sunshine and temperature variables. This is a consequence of both models being able to sufficiently estimate the GSR in Bisley (based on the annual average errors), while each model performed differently when we consider each individual month. Other meteorological factors such as relative humidity, wind speed and air pressure can also be included for improved prediction. During the autumn, winter and parts of spring months, both models performed considerably well in estimating the amount of GSR. Overall, the distribution and monthly variation of the calculated values of GSR show great similarities when compared to the observed values.

The annual average GSR values obtained for Pietermaritzburg, show close similarities to the results presented by Maluta *et al.* [20], for the Limpopo Province in South Africa. In the study conducted by [20], stations which have an altitude close to that of Pietermaritzburg, had an annual average H value in the range: [14.71-17.82] MJ/m<sup>2</sup>, whilst  $H_{calculated}$  for Bisley is in the range: [16.54-16.81] MJ/m<sup>2</sup>. The main contributing difference in these locations is the site's latitude.

The clearness index, being the ratio of GSR to extraterrestrial radiation provides information on the degree of transparency of the atmosphere. Using eq. (5),  $K_T$  values were calculated and interpreted by the following work conducted in [6];

**Table 5:** Clearness index ( $K_T$ ) results using each of the models

Month	$K_T$ (Hmeas)	$K_T$ (H-S)	$K_T$ (A-P)
Jul	0.58	0.62	0.58
Aug	0.55	0.55	0.54
Sep	0.61	0.57	0.51
Oct	0.49	0.41	0.49
Nov	0.45	0.36	0.49
Dec	0.49	0.40	0.50
Jan	0.50	0.46	0.48
Feb	0.49	0.49	0.51
Mar	0.51	0.52	0.54
Apr	0.50	0.53	0.58
May	0.57	0.64	0.63
Jun	0.56	0.66	0.62
<b>Average</b>	<b>0.53</b>	<b>0.520</b>	<b>0.54</b>

**Table 6:** Classification of day by clearness index,  $K_T$

Day Type	$K_T$
Clear	$0.7 \leq K_T < 0.9$
Partially Cloudy	$0.3 \leq K_T < 0.7$
Cloudy	$0.0 \leq K_T < 0.3$

The calculated values of clearness index for each model as shown in our results suggest that Pietermaritzburg experiences a high number of partially cloudy days, with not many days being classified as cloudy according to Table 5. The discrepancies experienced in the calculated H values may be a result of the influence of cloudiness on the air temperature and sunshine duration data. On average, the monthly data gives a clearness index which falls into the partially cloudy category for both prediction models as well as the measured data in question (Table 5).

In this study we have used the prescribed A-P coefficients of  $a = 0.25$  and  $b = 0.5$ . The Angstrom coefficients vary with each geographical location depending on the amount of relative sunshine received. Other factors such as the geographical locations of the site and atmospheric effects may also introduce deviations in the clearness in-

dex. For a more consistent set of Angstrom coefficients, this study should be extended to analyze data over a longer period of time for the chosen location.

The results obtained in this study indicate that the city of Pietermaritzburg receives sufficient GSR for the use of solar powered technologies such as solar panels, solar heating and cooling technologies for industrial, commercial and residential areas. Prediction models may be used to identify which areas are optimal for the harnessing of GSR. Accurate GSR predictions for this city will also enable a better understanding of the climate experienced and its effects. Clear to partially cloudy days are experienced throughout the year, including during the winter months, making GSR easy to acquire. The H-S and A-P models are suitable for the calculation of GSR, however the accuracy of results during the summer season can be improved. Comprehensive models including both meteorological variables can be introduced to account for this.

Evaluation of the A-P coefficients ( $a$  and  $b$ ) as well as the H-S ( $K_T$ ) coefficient can be conducted via the study of historic meteorological data for enhanced prediction models. These coefficients give insight into the transmissivity and transparency of the atmosphere. Prediction of the type of day and clearness index can also be made, provided the Angstrom coefficients are well-established. Though solar radiation data in the city of Pietermaritzburg is not readily available, the amount of GSR incident in this city can be sufficiently estimated using the Hargreaves-Samani and Angstrom-Prescott models. This study has shown the suitability of this interior region to contribute to the decrease in demand of grid energy by making use of the incident GSR in Pietermaritzburg. Furthermore, the forecasting method described above can be easily implemented for GSR prediction within any location of the world where air temperature and sunshine duration are measurable quantities.

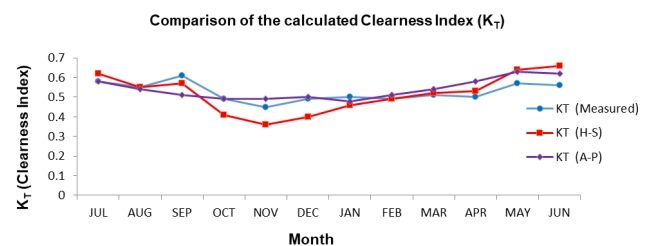


**Figure 6:** Graph comparing calculated and measured values of  $K_T$

## 5 Conclusions

The use of the H-S and A-P equations prove to be adequate methods of estimating the amount of GSR in locations where solar radiation data is not readily available. Our results show that these models have compared considerably well to the measured values of GSR for one suburb in the city of Pietermaritzburg. However, the accuracy of this model can be improved by modifying the equation to account for; more than one meteorological parameter (air temperature, sunshine duration, and relative humidity), shorter forecasting horizons and the inclusion of short wave radiation [23]. A second and third order prediction model may also be identified which could verify an increase in efficacy.

The results herein, show the degree of simplicity such models have, based on the use of one weather parameter alone. The H-S equation is viable for use in any geographical location since its dependency is mainly on the location and air temperature of a given site. While the A-P model performs considerably well without having an established, reliable set of Angstrom-PreScott coefficients. For better understanding and realization of a reliable set of A-P coefficients in Pietermaritzburg, it is suggested that we analyze the data for this city over a longer period ( $\pm 10$  calendar years prior to current data). However, the results which we have obtained in just one calendar year show close proximity to the actual measured GSR values using the prescribed A-P coefficients for locations where this information is unknown.

KwaZulu-Natal is said to be unsuitable for the construction of large scale solar power plantations, primarily due to the low amount of Direct Normal Irradiation (DNI) incident in this province as opposed to the other eight provinces in South Africa [27]. Despite this, our province still receives ample sunshine duration and GSR for the utilization of solar technologies such as photovoltaic cells (both in Industry and for household consumption). With the implementation of accurate and efficient GSR prediction models, we will be able to identify which regions of Pietermaritzburg are suitable for optimal capture of solar radiation.

**Acknowledgement:** The authors would like to acknowledge the assistance of Mr. Richard Kunz of the University of KwaZulu-Natal Research center in Ukulinga, Bisley; The ARC (Cedara) who provided data to the Ukulinga Research Farm. The financial assistance of the National Research Foundation (DAAD-NRF) towards this research is hereby acknowledged. Opinions expressed and conclusions ar-

rived at, are those of the author and are not necessarily to be attributed to the DAAD-NRF.

## References

- [1] Govinda R.T., Lado K., Patrick A. N., A review of solar energy, markets, economics and policies (Policy research working paper), The world bank, development and research group, environment and energy team, October 2011, <http://econ.worldbank.org>
- [2] Eskom web page, [http://www.eskom.co.za/AboutElectricity/ElectricityTechnologies/Pages/Coal\\_Power.aspx](http://www.eskom.co.za/AboutElectricity/ElectricityTechnologies/Pages/Coal_Power.aspx)
- [3] Renewable Energy, Department: Energy, Republic of South Africa, [http://www.energy.co.za/files/esources/renewables/r\\_solar.html](http://www.energy.co.za/files/esources/renewables/r_solar.html)
- [4] Qiang Fu., Radiation (Solar), 2003, University of Washington, Seattle, WA, USA, Elsevier Ltd.
- [5] Sayigh A.A.M., Solar radiation availability prediction from climatological data, 1977, Academic Press, New York, 61.
- [6] Viorel B., Modeling solar radiation at the earth's surface: Recent advances, Springer, 2008.
- [7] Boeker E., Van Grondelle R., Environmental physics: Sustainable energy and climate change, 2011, 3rd Edition, John Wiley and Sons Ltd.
- [8] Kennewell J., McDonald A., IPS-Satellite communications and space weather, The Australian Space Weather Agency, 2008, <http://www.ips.gov.au/Educational/1/3/2>
- [9] Almorox J., Hontoria C., Benito M., Models for obtaining daily global solar radiation with measured air temperature data in Madrid (Spain), Applied Energy, 88, 2011, 1703-1709.
- [10] Tijjani B.I., Comparison between first and second order Angstrom type models for sunshine hours in Katsina Nigeria, Bayero, J. Pure Appl. Sci., 4(2), 24-27.
- [11] Rahimikoob A., Estimating global solar radiation using ANN and air temperature data in semi-arid environment (Iran), Renewable Energy, 2010, 35, 2131-2135.
- [12] Al Riza D.F., Gilani S.I., Aris M.S., Hourly solar radiation estimation using ambient temperature and relative humidity data, Int. J. Envir. Sci. Develop., 2011, 2(3), June.
- [13] Gadiwala M.S. Usman A., Akhtar M., Jamil K., Empirical models for the estimation of global solar radiation with sunshine hours on horizontal surface in various cities of Pakistan, Pakistan J. Meteorol., 2013, 9(18), Jan.
- [14] Angstrom A., Solar and atmospheric radiation. International commission for solar research on Actinometric Investigations of solar and atmospheric radiation, J. Royal Meteorol. Soc., 1923, 121-126.
- [15] Srivasta R.C., Pandey H., Estimating Angstrom-PreScott coefficients for India and developing a correlation between sunshine hours and global solar radiation for India, ISRN Renewable Energy, 2013, Hindawi Publishing, <http://dx.doi.org/10.1155/2013/403742>
- [16] Ituen Eno E., Esen Nisken U., Nwokolo Samuel C., Uto Ema G., Prediction of Global solar radiation using relative humidity, maximum temperature and sunshine hours in Uyo in the Niger delta Region, Nigeria, Advances in Applied Science Research, 2012, 3(4), 1923-1937.

- [17] Samani Z., Estimating solar radiation and evapotranspiration using minimum climatological data, *J. Irrig. Drain. Eng.*, 2000, 265-267.
- [18] Allen R.G., Self-calibrating method for estimating global solar radiation from air temperature, *J. Hydrol. Eng.*, 1991, 2, 56-57.
- [19] Hargreaves G.H., Samani Z.A., Estimating potential evapotranspiration, *J. Irrig. Drain. Eng.*, ASCE, 108(IR3), 1982, 223-230.
- [20] Maluta E.N., Maludzi T.S., Sankaran V., Estimation of the global solar radiation on the horizontal surface from temperature data for the Vhembe district in the Limpopo province of South Africa, *International journal of green energy*, 2013, 11(5), 454-464.
- [21] Salima G., Chavula G.M.S., Determining Angstrom coefficients for estimating solar radiation in Malawi, *Int. J. Geosciences*, 2012, (3), 391-397.
- [22] Teke A., Yildirim H.B., Estimating the monthly global solar radiation for Eastern Mediterranean Region, *Energy Conv. Management* 2014, 87, 628-635.
- [23] Allen R.G., Pereira S.L., Raes D., Smith M., Crop evapotranspiration (Guidelines for computing crop water requirements), *FAO Irrigation and Drainage*, 1977, 56.
- [24] Almorox J., Bocco M., Wellington E., Estimation of daily global solar radiation from measured temperatures at Cañada de Luque, Córdoba, Argentina, *Renew. Ener.*, 2013, 60, 382-387.
- [25] Marwal V.K., Punia R.C., Sengar N., Mahawar S., Dashora P., A comparative study of correlation functions for estimation of monthly mean daily global solar radiation for Jaipur, Rajasthan (India), *Indian J. Sci. Techn.*, 2012, 5(5), 2729-2732.
- [26] Robaa S.M., Evaluation of sunshine duration from cloud data in Egypt, *Energy*, 2008, 33(5), 789-795.
- [27] Fluri T.P., The potential of concentrating solar power in South Africa, *Energy Policy* 2009, 37, 5075-5080.

## APPENDIX C

Monthly average measurements for the period January 2007 - June  
2018

Measured data was sourced from the SAWS and ARC



**Table 1: Monthly averages for Bloemfontein, Free State (January 2007 - June 2018)**

Month	H/Ho	$\Delta T$ (°C)	$T_{max}$ (°C)	$T_{ave}$ (°C)	RH/100	S/So
Jan	1.24306	16.74000	32.07000	23.70000	0.52920	0.86666
Feb	1.01967	18.11000	32.83000	23.77500	0.46050	0.92500
Mar	0.69877	17.56000	29.29000	20.51000	0.51940	0.80834
Apr	0.48348	15.19000	25.08000	17.48500	0.60820	0.72499
May	0.38765	20.12000	21.67000	11.61000	0.49630	0.75001
Jun	0.73042	16.62000	17.06000	8.75000	0.60845	0.67499
Jul	0.37269	19.47000	18.25000	8.51500	0.49760	0.80835
Aug	0.51177	21.60000	22.39000	11.59000	0.42310	0.83333
Sep	0.65999	21.23000	28.86000	18.24500	0.37965	0.78334
Oct	0.83609	14.99000	25.63000	18.13500	0.61850	0.69166
Nov	1.20514	18.13000	28.99000	19.92500	0.53510	0.80001
Dec	1.26042	16.19000	30.19000	22.09500	0.59605	0.80832
Jan	1.09395	15.49000	31.01000	23.26500	0.61080	0.74999
Feb	0.81498	15.60000	30.90000	23.10000	0.60870	0.70000
Mar	0.60418	14.98000	27.54000	20.05000	0.65490	0.65000
Apr	0.48619	19.86000	25.17000	15.24000	0.58015	0.75833
May	0.31157	15.35000	16.10000	8.42500	0.62100	0.56667
Jun	0.73070	17.08000	19.04000	10.50000	0.59040	0.61666
Jul	0.34493	19.92000	19.70000	9.74000	0.50490	0.77502
Aug	0.43610	19.61000	23.26000	13.45500	0.40715	0.78333
Sep	0.65731	21.70000	25.54000	14.69000	0.35635	0.85834
Oct	0.87554	20.00000	31.01000	21.01000	0.40440	0.88333
Nov	1.12813	17.22000	30.83000	22.22000	0.52345	0.80834
Dec	1.17325	18.22000	34.08000	24.97000	0.46925	0.86665
Jan	0.96900	16.27000	32.44000	24.30500	0.55575	0.73333
Feb	0.64795	12.80000	28.89000	22.49000	0.65425	0.58333
Mar	0.55501	17.05000	29.36000	20.83500	0.57850	0.75834
Apr	0.40827	18.12000	27.46000	18.40000	0.53185	0.72499
May	0.72931	16.74000	22.28000	13.91000	0.60255	0.71668
Jun	0.71933	15.76000	18.31000	10.43000	0.62200	0.59166
Jul	0.72877	19.91000	18.06000	8.10500	0.51290	0.72501
Aug	0.41949	19.76000	22.25000	12.37000	0.42900	0.77500
Sep	0.57891	21.06000	27.24000	16.71000	0.35895	0.77500
Oct	0.74965	16.41000	27.74000	19.53500	0.55880	0.72499
Nov	1.07343	17.00000	28.73000	20.23000	0.54000	0.80001
Dec	1.32617	19.71000	34.28000	24.42500	0.49575	0.89998
Jan	0.91155	13.36000	29.85000	23.17000	0.64860	0.57500
Feb	0.87966	15.68000	31.33000	23.49000	0.59800	0.75833
Mar	0.63895	16.73000	30.22000	21.85500	0.60015	0.77500
Apr	0.41341	15.64000	25.31000	17.49000	0.64120	0.66666
May	0.32258	18.11000	23.18000	14.12500	0.59320	0.72501
Jun	0.72966	20.19000	19.33000	9.23500	0.54995	0.69166
Jul	0.73003	19.11000	20.73000	11.17500	0.50095	0.66668
Aug	0.41659	21.62000	23.06000	12.25000	0.44375	0.81667
Sep	0.52435	21.66000	28.58000	17.75000	0.38290	0.71667
Oct	0.76041	19.52000	29.13000	19.37000	0.43640	0.73333

Month	H/Ho	$\Delta T$ (°C)	$T_{max}$ (°C)	$T_{ave}$ (°C)	RH/100	S/So
Nov	1.02485	17.74000	30.62000	21.75000	0.53530	0.80001
Dec	1.12260	17.04000	30.75000	22.23000	0.56210	0.80832
Jan	0.89285	12.64000	29.07000	22.75000	0.65250	0.60000
Feb	0.81003	14.30000	29.89000	22.74000	0.63315	0.72500
Mar	0.55751	15.67000	29.43000	21.59500	0.63380	0.65000
Apr	0.37039	14.82000	23.09000	15.68000	0.67120	0.59166
May	0.72873	16.09000	20.56000	12.51500	0.63645	0.60834
Jun	0.72753	18.03000	17.64000	8.62500	0.59790	0.65832
Jul	0.72954	20.50000	18.48000	8.23000	0.54485	0.71668
Aug	0.43504	20.44000	22.12000	11.90000	0.49300	0.75833
Sep	0.70768	21.61000	26.90000	16.09500	0.40135	0.81667
Oct	0.91966	20.06000	28.40000	18.37000	0.39200	0.79999
Nov	1.31104	20.88000	30.90000	20.46000	0.40400	0.90001
Dec	1.31254	16.69000	30.63000	22.28500	0.54545	0.78332
Jan	1.33015	18.43000	34.41000	25.19500	0.50615	0.84166
Feb	0.91238	15.58000	31.11000	23.32000	0.57790	0.65833
Mar	0.70190	17.81000	30.70000	21.79500	0.51860	0.73334
Apr	0.48484	18.74000	25.37000	16.00000	0.52025	0.74166
May	0.37639	20.68000	24.84000	14.50000	0.45095	0.74168
Jun	0.72968	16.53000	18.27000	10.00500	0.55370	0.50833
Jul	0.36600	20.24000	19.23000	9.11000	0.50325	0.67501
Aug	0.43003	19.60000	23.37000	13.57000	0.40675	0.70833
Sep	0.64031	20.07000	24.59000	14.55500	0.42750	0.80000
Oct	0.90639	18.39000	28.50000	19.30500	0.44400	0.85833
Nov	1.16182	18.80000	31.81000	22.41000	0.44160	0.84168
Dec	1.22682	14.78000	28.98000	21.59000	0.60895	0.67499
Jan	1.35843	17.43000	33.49000	24.77500	0.51740	0.89166
Feb	1.05315	19.17000	33.73000	24.14500	0.50260	0.90000
Mar	0.69971	16.98000	30.80000	22.31000	0.54240	0.71667
Apr	0.50242	17.36000	25.29000	16.61000	0.58220	0.71666
May	0.40992	20.28000	23.69000	13.55000	0.49645	0.75001
Jun	0.36429	21.47000	20.42000	9.68500	0.46000	0.75832
Jul	0.36203	19.79000	21.29000	11.39500	0.47825	0.74168
Aug	0.47828	20.19000	21.24000	11.14500	0.42795	0.80833
Sep	0.67251	21.42000	26.00000	15.29000	0.29435	0.77500
Oct	0.96486	19.89000	28.97000	19.02500	0.38820	0.84166
Nov	1.28829	18.30000	30.82000	21.67000	0.44300	0.86668
Dec	1.35832	15.33000	29.89000	22.22500	0.55310	0.79165
Jan	1.18423	17.19000	34.34000	25.74500	0.47565	0.79999
Feb	0.80204	13.33000	30.02000	23.35500	0.61715	0.64167
Mar	0.61483	14.88000	28.01000	20.57000	0.62250	0.65834
Apr	0.48051	18.30000	25.62000	16.47000	0.54675	0.69999
May	0.35962	19.47000	23.66000	13.92500	0.53085	0.72501
Jun	0.32030	20.73000	19.70000	9.33500	0.49095	0.69999
Jul	0.34345	20.82000	18.96000	8.55000	0.46680	0.77502
Aug	0.39655	17.96000	21.92000	12.94000	0.44545	0.68333
Sep	0.57652	21.72000	28.90000	18.04000	0.31985	0.73334

Month	H/Ho	$\Delta T$ (°C)	$T_{max}$ (°C)	$T_{ave}$ (°C)	RH/100	S/So
Oct	0.86048	20.00000	30.56000	20.56000	0.40225	0.85833
Nov	1.00910	14.29000	27.07000	19.92500	0.53835	0.73334
Dec	1.14841	14.61000	31.31000	24.00500	0.50515	0.83332
Jan	1.19974	18.21000	34.16000	25.05500	0.48395	0.88333
Feb	0.60876	10.37000	30.06000	24.87500	0.31735	0.86667
Mar	0.65336	15.07000	28.97000	21.43500	0.57980	0.70834
Apr	0.52975	18.44000	25.84000	16.62000	0.53860	0.67499
May	0.41868	21.69000	25.89000	15.04500	0.46415	0.76668
Jun	0.34403	17.97000	19.04000	10.05500	0.56380	0.64999
Jul	0.33626	17.36000	19.54000	10.86000	0.51400	0.60835
Aug	0.44506	21.46000	25.57000	14.84000	0.36290	0.63333
Sep	0.60126	19.10000	27.35000	17.80000	0.44445	0.67500
Oct	0.89993	20.27000	33.01000	22.87500	0.37410	0.81666
Nov	1.32111	20.09000	31.32000	21.27500	0.35805	0.95834
Dec	1.39387	19.56000	36.26000	26.48000	0.36710	0.80832
Jan	1.17283	15.34000	33.38000	25.71000	0.49945	0.74166
Feb	0.97668	17.14000	34.08000	25.51000	0.46020	0.82500
Mar	1.51876	16.60000	31.16000	22.86000	0.47910	0.75834
Apr	0.53218	15.39000	25.83000	18.13500	0.59740	0.65833
May	0.68596	15.49000	21.63000	13.88500	0.61090	0.64168
Jun	1.17839	17.04000	19.64000	11.12000	0.57380	0.54166
Jul	1.61192	17.48000	18.31000	9.57000	0.52095	0.72501
Aug	1.79897	19.39000	22.59000	12.89500	0.46420	0.77500
Sep	2.14690	19.52000	26.43000	16.67000	0.39610	0.70000
Oct	2.47778	20.17000	29.98000	19.89500	0.36410	0.88333
Nov	2.07334	17.08000	32.04000	23.50000	0.47870	0.86668
Dec	2.74585	17.92000	34.52000	25.56000	0.44945	0.84165
Jan	1.02099	14.82000	30.28000	22.87000	0.58510	0.68333
Feb	0.72074	11.82000	28.23000	22.32000	0.67960	0.55000
Mar	0.99632	19.03000	30.74000	21.22500	0.53370	0.79167
Apr	1.00214	17.54000	26.66000	17.89000	0.54615	0.68333
May	1.38893	20.10000	23.92000	13.87000	0.51680	0.70001
Jun	1.71371	21.02000	21.25000	10.74000	0.47955	0.73332
Jul	1.75391	21.61000	22.02000	11.21500	0.41680	0.72501
Aug	1.31568	20.42000	22.74000	12.53000	0.37520	0.78333
Sep	0.85644	20.88000	29.07000	18.63000	0.34250	0.78334
Oct	0.90352	18.02000	27.22000	18.21000	0.44710	0.81666
Nov	1.16751	19.82000	31.60000	21.69000	0.38710	0.85834
Dec	1.02470	18.25000	32.65000	23.52500	0.44975	0.82499
Jan	0.91884	17.87000	33.63000	24.69500	0.44060	0.84999
Feb	0.72876	15.23000	30.95000	23.33500	0.58490	0.72500
Mar	0.72249	15.19000	28.52000	20.92500	0.61315	0.58334
Apr	0.71199	14.28000	25.09000	17.95000	0.64985	0.60000
May	0.45647	18.58000	22.23000	12.94000	0.58420	0.69168
Jun	0.73047	21.31000	21.04000	10.38500	0.51950	0.71666

**Table 2: Monthly averages for Cape Town, Western Cape (January 2007 - June 2018)**

Month	H/Ho	$\Delta T$ (°C)	$T_{max}$ (°C)	$T_{ave}$ (°C)	RH/100	S/So
Jan	1.46576	9.36000	26.63000	21.95000	0.68835	0.97150
Feb	0.99994	8.40000	25.08000	20.88000	0.71390	0.89369
Mar	0.65483	9.90000	25.25000	20.30000	0.69005	0.84649
Apr	0.38226	9.42000	22.90000	18.19000	0.72821	0.66639
May	0.72389	8.95000	20.92000	16.44500	0.74614	0.60027
Jun	0.15965	7.03000	18.10000	14.58500	0.72002	0.45808
Jul	0.72014	9.09000	17.74000	13.19500	0.70728	0.55786
Aug	0.27895	7.27000	17.56000	13.92500	0.71996	0.51530
Sep	0.48747	7.69000	18.86000	15.01500	0.72115	0.65756
Oct	0.81316	8.39000	21.61000	17.41500	0.69891	0.80913
Nov	1.14148	6.93000	20.41000	16.94500	0.74416	0.78058
Dec	1.58273	8.43000	24.70000	20.48500	0.71672	0.91311
Jan	1.45041	8.20000	24.85000	20.75000	0.72658	0.95753
Feb	0.92286	8.09000	25.28000	21.23500	0.74009	0.82854
Mar	0.70851	9.78000	25.39000	20.50000	0.70069	0.89275
Apr	0.39225	9.16000	23.19000	18.61000	0.70271	0.73916
May	0.19434	6.26000	20.62000	17.49000	0.76066	0.42664
Jun	0.15627	5.53000	17.32000	14.55500	0.74939	0.42306
Jul	0.18068	6.97000	17.02000	13.53500	0.74216	0.47233
Aug	0.29500	7.45000	17.90000	14.17500	0.71635	0.63871
Sep	0.44807	7.21000	17.11000	13.50500	0.68299	0.57277
Oct	0.85482	7.84000	20.49000	16.57000	0.71330	0.83065
Nov	1.23690	8.31000	22.36000	18.20500	0.70988	0.85222
Dec	0.31505	8.09000	24.44000	20.39500	0.71378	0.90800
Jan	1.20118	8.01000	25.01000	21.00500	0.71969	0.97259
Feb	1.08126	9.59000	26.70000	21.90500	0.67762	0.92704
Mar	0.70585	9.98000	26.20000	21.21000	0.63090	0.79894
Apr	0.38642	8.89000	23.55000	19.10500	0.72330	0.56552
May	0.23361	8.14000	20.18000	16.11000	0.73613	0.50216
Jun	0.18304	6.34000	18.42000	15.25000	0.72107	0.44720
Jul	0.72233	8.25000	19.28000	15.15500	0.69009	0.56592
Aug	0.31773	7.59000	18.06000	14.26500	0.71837	0.55296
Sep	0.48278	6.45000	17.94000	14.71500	0.75366	0.56859
Oct	0.88823	7.85000	21.54000	17.61500	0.70626	0.79488
Nov	1.24995	8.02000	22.46000	18.45000	0.68851	0.82447
Dec	1.75145	8.48000	23.88000	19.64000	0.69210	0.95378
Jan	1.54143	8.48000	25.44000	21.20000	0.69977	0.94006
Feb	1.09524	8.98000	26.42000	21.93000	0.70433	0.83922
Mar	0.65750	8.81000	25.48000	21.07500	0.72619	0.78388

Month	H/Ho	$\Delta T$ (°C)	$T_{max}$ (°C)	$T_{ave}$ (°C)	RH/100	S/So
Apr	0.41666	8.72000	22.40000	18.04000	0.72491	0.72580
May	0.23861	7.50000	19.81000	16.06000	0.73848	0.50945
Jun	0.19510	7.34000	18.72000	15.05000	0.70539	0.49857
Jul	0.25232	8.53000	18.35000	14.08500	0.68371	0.60920
Aug	0.35063	8.34000	19.04000	14.87000	0.70951	0.59384
Sep	0.55095	7.99000	19.46000	15.46500	0.70226	0.66810
Oct	0.88115	7.55000	20.32000	16.54500	0.71809	0.74580
Nov	1.37751	7.80000	21.83000	17.93000	0.70886	0.81081
Dec	1.71816	8.04000	24.25000	20.23000	0.71285	0.92001
Jan	1.64673	9.23000	26.10000	21.48500	0.70569	0.95240
Feb	1.14691	9.36000	27.22000	22.54000	0.73423	0.94405
Mar	0.68517	9.47000	26.05000	21.31500	0.70562	0.74437
Apr	0.44246	8.76000	21.47000	17.09000	0.69681	0.73751
May	0.23936	8.08000	20.50000	16.46000	0.72473	0.44194
Jun	0.18931	6.23000	17.53000	14.41500	0.75745	0.46526
Jul	0.26807	7.73000	18.60000	14.73500	0.68344	0.63011
Aug	0.35545	8.20000	18.06000	13.96000	0.66862	0.60349
Sep	0.55970	7.55000	18.53000	14.75500	0.73254	0.61386
Oct	0.88626	7.35000	20.25000	16.57500	0.68955	0.70808
Nov	1.44279	7.66000	21.19000	17.36000	0.68938	0.89949
Dec	1.86220	7.78000	23.34000	19.45000	0.70689	0.97014
Jan	1.62768	8.62000	26.64000	22.33000	0.71691	0.95858
Feb	1.17486	8.83000	25.44000	21.02500	0.68295	0.92057
Mar	0.73752	8.53000	25.35000	21.08500	0.71172	0.79894
Apr	0.42304	8.39000	22.38000	18.18500	0.70192	0.66083
May	0.28738	8.05000	19.31000	15.28500	0.75005	0.58630
Jun	0.19992	6.65000	17.43000	14.10500	0.76442	0.47222
Jul	0.22548	6.75000	16.70000	13.32500	0.72884	0.50600
Aug	0.32576	6.47000	15.92000	12.68500	0.69915	0.55106
Sep	0.57440	7.78000	18.43000	14.54000	0.71439	0.64425
Oct	0.87998	6.73000	19.21000	15.84500	0.70812	0.80378
Nov	1.53871	8.82000	22.82000	18.41000	0.69464	0.87167
Dec	1.88745	8.73000	26.09000	21.72500	0.70797	0.91399
Jan	1.73192	8.32000	25.25000	21.09000	0.69025	0.99649
Feb	1.16724	10.41000	26.02000	20.81500	0.62739	0.92644
Mar	0.55414	7.87000	24.13000	20.19500	0.65711	0.75298
Apr	0.31291	9.27000	22.21000	17.57500	0.69503	0.69917
May	0.71928	8.29000	20.78000	16.63500	0.72901	0.57586
Jun	0.13625	6.67000	17.37000	14.03500	0.72455	0.50696
Jul	0.16074	6.50000	17.56000	14.31000	0.74850	0.55241

Month	H/Ho	$\Delta T$ (°C)	$T_{max}$ (°C)	$T_{ave}$ (°C)	RH/100	S/So
Aug	0.21129	6.88000	16.88000	13.44000	0.72169	0.51640
Sep	0.35677	6.49000	16.62000	13.37500	0.73350	0.63281
Oct	0.60407	7.29000	20.17000	16.52500	0.73348	0.77044
Nov	0.93056	7.63000	22.20000	18.38500	0.73567	0.86166
Dec	1.21201	8.58000	25.42000	21.13000	0.68733	0.98116
Jan	1.06466	8.36000	25.57000	21.39000	0.73645	0.91449
Feb	0.76065	9.36000	26.86000	22.18000	0.72146	0.94314
Mar	0.44945	7.54000	22.67000	18.90000	0.75686	0.75055
Apr	0.73029	9.69000	25.40000	20.55500	0.67271	0.74414
May	0.16833	7.24000	19.85000	16.23000	0.74257	0.47528
Jun	0.71208	7.51000	17.59000	13.83500	0.69951	0.47502
Jul	0.71356	6.94000	17.00000	13.53000	0.73790	0.47985
Aug	0.20487	6.74000	18.52000	15.15000	0.73508	0.51210
Sep	0.33176	7.83000	19.72000	15.80500	0.69437	0.66359
Oct	0.60172	9.26000	22.99000	18.36000	0.70749	0.85862
Nov	0.88737	8.08000	22.95000	18.91000	0.70577	0.90807
Dec	1.05821	8.06000	24.00000	19.97000	0.71593	0.97636
Jan	0.98211	9.19000	26.23000	21.63500	0.70547	0.93895
Feb	0.70136	8.50000	24.69000	20.44000	0.68606	0.92799
Mar	0.44945	9.26000	25.81000	21.18000	0.69911	0.80727
Apr	0.72716	9.45000	23.13000	18.40500	0.69319	0.71094
May	0.71368	7.42000	20.79000	17.08000	0.72967	0.45513
Jun	0.13047	6.44000	17.32000	14.10000	0.75264	0.47724
Jul	0.14474	5.83000	15.97000	13.05500	0.74594	0.53171
Aug	0.18481	6.64000	17.93000	14.61000	0.76216	0.49220
Sep	0.71123	8.50000	19.95000	15.70000	0.00000	0.58029
Oct	0.82967	10.00000	23.61000	18.61000	0.66005	0.75781
Nov	1.28410	9.55000	23.21000	18.43500	0.62350	0.88304
Dec	1.63897	9.90000	26.73000	21.78000	0.64920	0.98763
Jan	1.45994	9.81000	28.11000	23.20500	0.66855	0.97661
Feb	1.00503	10.11000	27.25000	22.19500	0.65040	0.90448
Mar	0.63950	9.52000	24.95000	20.19000	0.66910	0.75537
Apr	0.38420	9.44000	23.27000	18.55000	0.68245	0.63478
May	0.72591	9.54000	21.69000	16.92000	0.70725	0.57659
Jun	0.71751	7.61000	18.20000	14.39500	0.67965	0.42972
Jul	0.72100	8.23000	18.45000	14.33500	0.66240	0.47663
Aug	0.35090	9.15000	20.33000	15.75500	0.65585	0.64840
Sep	0.48904	8.32000	19.57000	15.41000	0.65430	0.63612
Oct	0.85404	9.57000	22.26000	17.47500	0.62105	0.79762
Nov	1.35240	9.42000	23.88000	19.17000	0.62080	0.90223

Month	H/Ho	$\Delta T$ (°C)	$T_{max}$ (°C)	$T_{ave}$ (°C)	RH/100	S/So
Dec	1.65389	10.09000	25.99000	20.94500	0.64650	0.95270
Jan	1.41549	9.38000	25.68000	20.99000	0.63350	0.94570
Feb	1.04272	10.28000	26.69000	21.55000	0.62930	0.96466
Mar	0.68551	10.90000	26.42000	20.97000	0.62175	0.83010
Apr	0.40251	11.14000	26.06000	20.49000	0.61035	0.72828
May	0.72649	10.39000	22.95000	17.75500	0.63460	0.63227
Jun	0.71770	8.05000	18.13000	14.10500	0.64930	0.48138
Jul	0.72326	8.42000	18.26000	14.05000	0.66615	0.60674
Aug	0.31453	7.17000	18.00000	14.41500	0.66235	0.53981
Sep	0.48528	8.65000	20.41000	16.08500	0.64090	0.66190
Oct	0.84067	9.05000	20.92000	16.39500	0.61505	0.75294
Nov	1.27808	9.35000	22.91000	18.23500	0.63240	0.83555
Dec	1.64700	9.60000	24.97000	20.17000	0.61795	0.94379
Jan	1.35252	9.32000	26.65000	21.99000	0.64545	0.95943
Feb	1.03848	10.79000	27.16000	21.76500	0.61510	0.90412
Mar	0.58481	9.14000	24.31000	19.74000	0.65355	0.71369
Apr	0.38920	9.58000	23.31000	18.52000	0.65455	0.67839
May	0.72178	8.13000	21.39000	17.32500	0.66810	0.49301
Jun	0.16350	7.13000	18.68000	15.11500	0.65950	0.71666

**Table 3: Monthly averages for Durban, KwaZulu-Natal (January 2007 - June 2018)**

Month	H/Ho	$\Delta T$ (°C)	$T_{max}$ (°C)	$T_{ave}$ (°C)	RH/100	S/So
Jan	0.94319	10.83000	28.08000	22.66500	0.76815	0.67310
Feb	0.75562	11.59000	29.27000	23.47500	0.75805	0.72054
Mar	0.52721	10.30000	26.36000	21.21000	0.76895	0.57771
Apr	0.34105	11.52000	25.33000	19.57000	0.74310	0.54140
May	0.34141	17.31000	25.67000	17.01500	0.58945	0.74330
Jun	0.26752	15.51000	21.61000	13.85500	0.63435	0.62055
Jul	0.32535	17.04000	22.64000	14.12000	0.58705	0.71534
Aug	0.38039	21.18000	28.77000	18.18000	0.61385	0.63682
Sep	0.43212	11.57000	24.26000	18.47500	0.72940	0.48525
Oct	0.50719	9.48000	22.65000	17.91000	0.78055	0.38792
Nov	0.73548	9.18000	23.84000	19.25000	0.80585	0.46025
Dec	0.99921	9.66000	25.21000	20.38000	0.82765	0.60508
Jan	0.81531	9.31000	26.68000	22.02500	0.79535	0.48922
Feb	0.67205	9.61000	27.59000	22.78500	0.76685	0.62652
Mar	0.51424	10.44000	26.43000	21.21000	0.75315	0.58173
Apr	0.36305	11.31000	23.53000	17.87500	0.72535	0.59360
May	0.26688	14.95000	25.54000	18.06500	0.68005	0.66774
Jun	0.22687	15.29000	22.16000	14.51500	0.68585	0.58499
Jul	0.27611	18.48000	23.73000	14.49000	0.60900	0.70459
Aug	0.32544	16.34000	24.93000	16.76000	0.64965	0.59169
Sep	0.48376	32.54000	41.05000	24.78000	0.63160	0.60028
Oct	0.50137	38.53000	51.62000	32.35500	0.75490	0.39060
Nov	0.35768	11.92000	28.66000	22.70000	0.77590	0.36475
Dec	0.60103	10.37000	27.60000	22.41500	0.77575	0.37472
Jan	0.74764	10.55000	27.60000	22.32500	0.79955	0.32527
Feb	0.66354	10.01000	27.23000	22.22500	0.79490	0.47736
Mar	0.57117	11.67000	27.38000	21.54500	0.75640	0.63360
Apr	0.41872	13.50000	26.14000	19.39000	0.72390	0.61389
May	0.27613	14.75000	24.52000	17.14500	0.68530	0.62932
Jun	0.16821	14.85000	22.04000	14.61500	0.65700	0.56279
Jul	0.42481	18.08000	22.47000	13.43000	0.59455	0.69624
Aug	0.52753	16.37000	23.94000	15.75500	0.64745	0.64221
Sep	0.66394	18.03000	27.26000	18.24500	0.61740	0.51670
Oct	0.71990	8.73000	22.70000	18.33500	0.83800	0.38332
Nov	0.78089	10.10000	25.76000	20.71000	0.79615	0.38004
Dec	0.77331	11.18000	28.40000	22.81000	0.77660	0.33954
Jan	0.77961	12.79000	30.56000	24.16500	0.72710	0.40243
Feb	0.52151	12.31000	28.65000	22.49500	0.73860	0.71278
Mar	0.38504	13.77000	27.46000	20.57500	0.68970	0.61292



Month	H/Ho	$\Delta T$ (°C)	$T_{max}$ (°C)	$T_{ave}$ (°C)	RH/100	S/So
Apr	0.30064	16.40000	26.68000	18.48000	0.65200	0.62863
May	0.23807	16.36000	22.53000	14.35000	0.62590	#N/A
Jun	0.26696	17.29000	23.49000	14.84500	0.60905	#N/A
Jul	0.37141	18.21000	25.38000	16.27500	0.58405	#N/A
Aug	0.46214	15.47000	27.46000	19.72500	0.64400	#N/A
Sep	0.50101	11.91000	25.86000	19.90500	0.73235	#N/A
Oct	0.69390	10.55000	25.10000	19.82500	0.77145	#N/A
Nov	0.72943	9.58000	25.39000	20.60000	0.80375	#N/A
Dec	0.81438	9.46000	26.98000	22.25000	0.79250	#N/A
Jan	0.77071	11.20000	28.47000	22.87000	0.74245	#N/A
Feb	0.54112	13.37000	30.76000	24.07500	0.70880	#N/A
Mar	0.33807	11.27000	23.98000	18.34500	0.74795	#N/A
Apr	0.26037	12.88000	22.83000	16.39000	0.70280	#N/A
May	0.23515	15.06000	20.71000	13.18000	0.66045	#N/A
Jun	0.35714	14.73000	24.82000	17.45500	0.56405	#N/A
Jul	0.44503	14.96000	25.45000	17.97000	0.63505	#N/A
Aug	0.59197	19.68000	29.48000	19.64000	0.63160	#N/A
Sep	0.82385	14.33000	29.85000	22.68500	0.22890	#N/A
Oct	0.91659	18.40000	28.00000	18.80000	0.56495	#N/A
Nov	0.64110	11.40000	29.33000	23.63000	0.36870	#N/A
Dec	0.47281	12.51000	28.29000	22.03500	0.63920	#N/A
Jan	0.36712	14.74000	25.91000	18.54000	0.72545	#N/A
Feb	0.26162	15.65000	25.86000	18.03500	0.70035	#N/A
Mar	0.23904	17.62000	23.42000	14.61000	0.69790	#N/A
Apr	0.27908	17.36000	22.99000	14.31000	0.66855	#N/A
May	0.30933	14.86000	23.83000	16.40000	0.67635	#N/A
Jun	0.39458	11.27000	21.90000	16.26500	0.73210	#N/A
Jul	0.42351	9.61000	22.86000	18.05500	0.80080	#N/A
Aug	0.61968	10.63000	24.36000	19.04500	0.85090	#N/A
Sep	0.86982	10.93000	27.78000	22.31500	0.84565	#N/A
Oct	0.75184	10.64000	27.78000	22.46000	0.85210	#N/A
Nov	0.65270	11.79000	28.72000	22.82500	0.69925	#N/A
Dec	0.45826	10.39000	26.73000	21.53500	0.71675	#N/A
Jan	0.36468	13.80000	26.07000	19.17000	0.74520	#N/A
Feb	0.27663	15.34000	24.49000	16.82000	0.68410	#N/A
Mar	0.23831	17.77000	23.35000	14.46500	0.65895	#N/A
Apr	0.23306	14.44000	22.27000	15.05000	0.61215	#N/A
May	0.34420	17.84000	24.76000	15.84000	0.68970	#N/A
Jun	0.43962	16.33000	25.87000	17.70500	0.61170	#N/A
Jul	0.56068	13.82000	25.75000	18.84000	0.64855	#N/A

Month	H/Ho	$\Delta T$ (°C)	$T_{max}$ (°C)	$T_{ave}$ (°C)	RH/100	S/So
Aug	0.75828	12.38000	26.98000	20.79000	0.70245	#N/A
Sep	0.74641	10.22000	26.15000	21.04000	0.72795	#N/A
Oct	0.89652	11.46000	29.56000	23.83000	0.76745	#N/A
Nov	0.63607	10.65000	27.74000	22.41500	0.73045	#N/A
Dec	0.48261	12.11000	28.80000	22.74500	0.70305	#N/A
Jan	0.37282	14.75000	27.38000	20.00500	0.72675	#N/A
Feb	0.27038	16.64000	26.71000	18.39000	0.65725	#N/A
Mar	0.22979	18.60000	24.51000	15.21000	0.62810	#N/A
Apr	0.26349	18.25000	23.77000	14.64500	0.57980	#N/A
May	0.31937	15.59000	25.02000	17.22500	0.55825	#N/A
Jun	0.46845	16.61000	27.64000	19.33500	0.60775	#N/A
Jul	0.49300	11.19000	23.92000	18.32500	0.64615	#N/A
Aug	0.57170	4.41000	23.36000	21.15500	0.72860	#N/A
Sep	0.60937	10.79000	27.78000	22.38500	0.89900	#N/A
Oct	0.45668	12.42000	28.82000	22.61000	0.77000	#N/A
Nov	0.31852	12.08000	25.08000	19.04000	0.72310	#N/A
Dec	0.24061	16.48000	27.14000	18.90000	0.73155	#N/A
Jan	0.21665	16.79000	23.61000	15.21500	0.64175	#N/A
Feb	0.21401	14.91000	22.63000	15.17500	0.60490	#N/A
Mar	0.31356	15.41000	25.67000	17.96500	0.67280	#N/A
Apr	0.35945	12.47000	25.15000	18.91500	0.62525	#N/A
May	0.59233	13.95000	28.46000	21.48500	0.71840	#N/A
Jun	0.69077	12.01000	26.11000	20.10500	0.69830	#N/A
Jul	0.87781	10.86000	29.01000	23.58000	0.72985	#N/A
Aug	0.75044	10.85000	28.69000	23.26500	0.75985	#N/A
Sep	0.67089	12.57000	30.01000	23.72500	0.76975	#N/A
Oct	0.46712	11.54000	28.82000	23.05000	0.68565	#N/A
Nov	0.30684	13.01000	27.50000	20.99500	1.00000	#N/A
Dec	0.26412	15.17000	25.11000	17.52500	0.69860	#N/A
Jan	0.22273	15.98000	23.56000	15.57000	0.63680	#N/A
Feb	0.23405	14.77000	21.28000	13.89500	0.63475	#N/A
Mar	0.35741	16.95000	25.01000	16.53500	0.62275	#N/A
Apr	0.37296	11.14000	23.42000	17.85000	0.56350	#N/A
May	0.49919	10.45000	23.16000	17.93500	0.68955	#N/A
Jun	0.56960	9.29000	24.37000	19.72500	0.71685	#N/A
Jul	0.93277	11.92000	28.80000	22.84000	0.74555	#N/A
Aug	0.78078	11.36000	28.31000	22.63000	0.67815	#N/A
Sep	0.57571	10.70000	28.64000	23.29000	0.69765	#N/A
Oct	0.51677	12.99000	29.43000	22.93500	0.71555	#N/A
Nov	0.36468	13.05000	26.64000	20.11500	0.66160	#N/A

Month	H/Ho	$\Delta T$ (°C)	$T_{max}$ (°C)	$T_{ave}$ (°C)	RH/100	S/So
Dec	0.26512	14.60000	25.37000	18.07000	0.66135	#N/A
Jan	0.24805	16.72000	24.10000	15.74000	0.63960	#N/A
Feb	0.24741	16.39000	23.67000	15.47500	0.58875	#N/A
Mar	0.33205	15.15000	23.78000	16.20500	0.59925	#N/A
Apr	0.42221	14.49000	26.22000	18.97500	0.58770	#N/A
May	0.59488	12.33000	24.28000	18.11500	0.63840	#N/A
Jun	0.78868	11.89000	25.46000	19.51500	0.68185	#N/A
Jul	0.83984	10.26000	25.58000	20.45000	0.68265	#N/A
Aug	0.90072	12.38000	29.33000	23.14000	0.71060	#N/A
Sep	0.67630	11.19000	28.72000	23.12500	0.67210	#N/A
Oct	0.45984	11.02000	27.33000	21.82000	0.69885	#N/A
Nov	0.31363	11.12000	26.24000	20.68000	0.71830	#N/A
Dec	0.25862	13.57000	24.07000	17.28500	0.69910	#N/A
Jan	0.25511	16.33000	23.48000	15.31500	0.64550	#N/A
Feb	1.03848	10.79000	27.16000	21.76500	0.60030	#N/A
Mar	0.58481	9.14000	24.31000	19.74000	0.65355	#N/A
Apr	0.38920	9.58000	23.31000	18.52000	0.65455	#N/A
May	0.21785	8.13000	21.39000	17.32500	0.66810	#N/A
Jun	0.71635	7.13000	18.68000	15.11500	0.65950	#N/A

\*#N/A - Data was not measured during this month

**Table 4: Monthly averages for Johannesburg, Gauteng (January 2007 - June 2018)**

Month	H/Ho	$\Delta T$ (°C)	$T_{max}$ (°C)	$T_{ave}$ (°C)	RH/100	S/So
Jan	0.66154	13.74000	27.38000	20.51000	0.65565	0.81747
Feb	0.53609	15.18000	28.56000	20.97000	0.60785	0.87501
Mar	0.60664	15.20000	27.27000	19.67000	0.61100	0.69974
Apr	0.42142	15.05000	23.93000	16.40500	0.62910	0.72873
May	0.36781	17.19000	21.12000	12.52500	0.45985	0.84545
Jun	0.29999	15.16000	17.54000	9.96000	0.59690	0.77758
Jul	0.33048	16.74000	17.86000	9.49000	0.50325	0.78765
Aug	0.40463	17.14000	21.10000	12.53000	0.46000	0.79785
Sep	0.52816	16.13000	26.60000	18.53500	0.48655	0.76527
Oct	0.56457	11.38000	22.10000	16.41000	0.74425	0.66518
Nov	0.85667	12.52000	25.58000	19.32000	0.66720	0.68845
Dec	0.97805	11.81000	24.91000	19.00500	0.71390	0.63654
Jan	0.73872	9.75000	23.90000	19.02500	0.78660	0.64735
Feb	0.79204	12.91000	26.20000	19.74500	0.69575	0.77439
Mar	0.44191	11.83000	23.63000	17.71500	0.74010	0.63796
Apr	0.42088	14.75000	22.23000	14.85500	0.62970	0.76692
May	0.29952	14.10000	20.34000	13.29000	0.65695	0.69251
Jun	0.28915	15.71000	18.36000	10.50500	0.62085	0.75220
Jul	0.30130	15.69000	17.94000	10.09500	0.57340	0.73345
Aug	0.37734	35.27000	35.32000	17.68500	0.49625	0.78467
Sep	0.55002	18.33000	25.27000	16.10500	0.49305	0.82056
Oct	0.68119	15.27000	27.33000	19.69500	0.58860	0.76343
Nov	0.80675	14.20000	28.29000	21.19000	0.64495	0.67243
Dec	0.94208	13.17000	28.04000	21.45500	0.68770	0.64113
Jan	0.77646	10.90000	26.87000	21.42000	0.75865	0.56526
Feb	0.55775	11.71000	26.14000	20.28500	0.76065	0.61125
Mar	0.50635	12.76000	24.45000	18.07000	0.72125	0.60995
Apr	0.43561	14.95000	23.42000	15.94500	0.64960	0.75970
May	0.31810	14.50000	19.87000	12.62000	0.65775	0.68413
Jun	0.28373	13.78000	17.76000	10.87000	0.62045	0.64108
Jul	0.33971	16.18000	16.14000	8.05000	0.56060	0.78201
Aug	0.41644	16.42000	19.92000	11.71000	0.58695	0.80754
Sep	0.53137	16.08000	25.24000	17.20000	0.51430	0.75369
Oct	0.66507	13.33000	25.61000	18.94500	0.66470	0.62848
Nov	0.81371	12.30000	24.54000	18.39000	0.72940	0.71107
Dec	1.09227	12.88000	26.78000	20.34000	0.73765	0.79695
Jan	0.72473	9.95000	25.20000	20.22500	0.80100	0.44970
Feb	0.75919	12.34000	26.44000	20.27000	0.73365	0.72526
Mar	0.52458	12.52000	25.66000	19.40000	0.74255	0.64334

Month	H/Ho	$\Delta T$ (°C)	$T_{max}$ (°C)	$T_{ave}$ (°C)	RH/100	S/So
Apr	0.32905	10.58000	21.68000	16.39000	0.78355	0.61034
May	0.32162	14.60000	20.86000	13.56000	0.67315	0.72775
Jun	0.31428	16.94000	17.89000	9.42000	0.51290	0.76860
Jul	0.31402	15.37000	17.67000	9.98500	0.55680	0.68793
Aug	0.43796	17.37000	21.35000	12.66500	0.46375	0.84328
Sep	0.58063	17.82000	26.15000	17.24000	0.45180	0.82750
Oct	0.74190	16.35000	27.83000	19.65500	0.50530	0.79220
Nov	0.80880	13.11000	26.31000	19.75500	0.62955	0.63705
Dec	0.97131	12.16000	26.34000	20.26000	0.64875	0.69862
Jan	0.82905	10.01000	24.93000	19.92500	0.71030	0.49769
Feb	0.73392	12.28000	25.71000	19.57000	0.65990	0.66579
Mar	0.56227	13.20000	26.30000	19.70000	0.64025	0.60331
Apr	0.34993	11.09000	21.06000	15.51500	0.69955	0.52069
May	0.33292	13.75000	19.86000	12.98500	0.59835	0.70807
Jun	0.31822	15.41000	17.19000	9.48500	0.51440	0.75612
Jul	0.33322	16.11000	16.36000	8.30500	0.50205	0.78139
Aug	0.42379	16.10000	20.06000	12.01000	0.48695	0.79945
Sep	0.58733	17.04000	24.98000	16.46000	0.42870	0.82224
Oct	0.77243	14.71000	25.77000	18.41500	0.51645	0.82340
Nov	0.98267	13.80000	26.49000	19.59000	0.57235	0.80472
Dec	0.96141	11.39000	25.72000	20.02500	0.66065	0.66094
Jan	1.00419	12.32000	26.62000	20.46000	0.65535	0.69973
Feb	0.76893	12.82000	27.56000	21.15000	0.63045	0.63662
Mar	0.58658	13.70000	25.88000	19.03000	0.60340	0.70108
Apr	0.41579	14.75000	22.39000	15.01500	0.57980	0.76053
May	0.35476	16.74000	22.25000	13.88000	0.48945	0.79786
Jun	0.24753	15.80000	17.76000	9.86000	0.51955	0.72354
Jul	0.29805	16.64000	19.07000	10.75000	0.46045	0.78846
Aug	0.38076	16.38000	21.45000	13.26000	0.41280	0.78253
Sep	0.52262	14.83000	22.21000	14.79500	0.55290	0.76786
Oct	0.67947	13.14000	24.61000	18.04000	0.59105	0.69408
Nov	0.97490	13.50000	25.93000	19.18000	0.59530	0.78582
Dec	0.94388	11.45000	25.70000	19.97500	0.65030	0.62251
Jan	0.95330	12.13000	26.89000	20.82500	0.65345	0.71032
Feb	0.84005	14.36000	27.94000	20.76000	0.61980	0.82335
Mar	0.51091	13.84000	26.04000	19.12000	0.62230	0.60807
Apr	0.41713	13.29000	21.93000	15.28500	0.61270	0.71378
May	0.35501	15.34000	21.01000	13.34000	0.50725	0.75403
Jun	0.33792	17.28000	19.61000	10.97000	0.49180	0.81806
Jul	0.33721	15.48000	18.80000	11.06000	0.49690	0.75322

Month	H/Ho	$\Delta T$ (°C)	$T_{max}$ (°C)	$T_{ave}$ (°C)	RH/100	S/So
Aug	0.44163	16.08000	19.87000	11.83000	0.47765	0.82338
Sep	0.53807	16.51000	25.47000	17.21500	0.41220	0.76811
Oct	0.72509	15.23000	25.55000	17.93500	0.55875	0.81946
Nov	0.90617	14.52000	26.88000	19.62000	0.56505	0.81089
Dec	0.73837	10.47000	24.66000	19.42500	0.69245	0.63946
Jan	0.85237	12.31000	27.45000	21.29500	0.61995	0.72279
Feb	0.69565	11.86000	26.51000	20.58000	0.65755	0.73055
Mar	0.43219	9.58000	23.41000	18.62000	0.74935	0.51216
Apr	0.41204	14.24000	22.13000	15.01000	0.60075	0.73275
May	0.34246	16.31000	21.94000	13.78500	0.51680	0.77233
Jun	0.31132	17.19000	18.87000	10.27500	0.45395	0.77195
Jul	0.31177	16.49000	17.94000	9.69500	0.45280	0.80728
Aug	0.34822	15.21000	20.34000	12.73500	0.43895	0.77607
Sep	0.50747	17.01000	26.07000	17.56500	0.39625	0.84307
Oct	0.67947	16.49000	26.32000	18.07500	0.50815	0.82662
Nov	0.66030	12.00000	24.12000	18.12000	0.63000	0.65096
Dec	0.76311	11.46000	25.84000	20.11000	0.66985	0.64937
Jan	0.80445	12.26000	27.04000	20.91000	0.63700	0.64112
Feb	0.78121	14.71000	28.32000	20.96500	0.59610	0.78569
Mar	0.51638	13.17000	25.85000	19.26500	0.62855	0.62138
Apr	0.38393	13.46000	23.24000	16.51000	0.60345	0.61614
May	0.36731	17.24000	23.58000	14.96000	0.46090	0.77688
Jun	0.31575	15.39000	17.47000	9.77500	0.53745	0.72387
Jul	0.32474	15.74000	18.57000	10.70000	0.51075	0.73979
Aug	0.42694	17.70000	23.86000	15.01000	0.39690	0.81210
Sep	0.49144	14.99000	24.71000	17.21500	0.50765	0.64211
Oct	0.72509	16.36000	28.91000	20.73000	0.45390	0.83815
Nov	0.99822	15.80000	28.00000	20.10000	0.43035	0.86964
Dec	1.06034	14.06000	29.77000	22.74000	0.54405	0.79197
Jan	0.97365	12.58000	27.76000	21.47000	0.61005	0.76011
Feb	0.80720	12.85000	28.14000	21.71500	0.61670	0.87554
Mar	0.59206	12.30000	26.02000	19.87000	0.62535	0.80630
Apr	0.45542	14.48000	24.79000	17.55000	0.59455	0.84388
May	0.34221	14.14000	19.78000	12.71000	0.61865	0.68559
Jun	0.31477	14.81000	18.32000	10.91500	0.56955	0.58833
Jul	0.35617	16.06000	17.98000	9.95000	0.50435	0.70537
Aug	0.48572	17.88000	22.18000	13.24000	0.38530	0.62213
Sep	0.57072	15.83000	25.28000	17.36500	0.46570	0.67844
Oct	0.76797	16.36000	26.30000	18.12000	0.49665	0.74750
Nov	0.85257	11.32000	26.19000	20.53000	0.60000	0.75618

Month	H/Ho	$\Delta T$ (°C)	$T_{max}$ (°C)	$T_{ave}$ (°C)	RH/100	S/So
Dec	0.42873	8.00000	23.17000	19.17000	0.70605	0.82392
Jan	0.68049	10.39000	25.12000	19.92500	0.60810	0.77499
Feb	0.64160	14.15000	26.11000	19.03500	0.62370	0.76610
Mar	0.41472	13.57000	23.07000	16.28500	0.54965	0.80386
Apr	0.34221	14.64000	20.31000	12.99000	0.53195	0.66613
May	0.34482	16.42000	19.41000	11.20000	0.49670	0.80242
Jun	0.35442	16.24000	19.75000	11.63000	0.45820	0.48431
Jul	0.45554	16.30000	20.78000	12.63000	0.44630	0.60890
Aug	0.57422	17.06000	26.22000	17.69000	0.56155	0.58085
Sep	0.72235	14.51000	24.59000	17.33500	0.52255	0.70829
Oct	1.01908	15.09000	26.63000	19.08500	0.62925	0.78404
Nov	1.00368	12.34000	26.13000	19.96000	0.57185	#N/A
Dec	1.08646	14.06000	27.70000	20.67000	0.67045	#N/A
Jan	0.71370	11.70000	25.72000	19.87000	0.67535	#N/A
Feb	0.53796	12.47000	24.91000	18.67500	0.65265	#N/A
Mar	0.38848	12.78000	23.04000	16.65000	0.55630	#N/A
Apr	0.35175	14.90000	20.47000	13.02000	0.49530	#N/A
May	0.34580	16.37000	19.00000	10.81500	#N/A	#N/A
Jun	0.71635	7.13000	18.68000	15.11500	#N/A	#N/A

\*#N/A - Data was not measured during this month

**Table 5: Monthly averages for Pietermaritzburg, KwaZulu-Natal (January 2007 - June 2018)**

Month	H/Ho	$\Delta T$ (°C)	$T_{max}$ (°C)	$T_{ave}$ (°C)	RH/100	S/So
Jan	0.94200	11.58000	28.30000	22.51000	0.68570	0.49166
Feb	0.73764	11.93000	29.30000	23.33500	0.67240	0.66288
Mar	0.52554	10.57000	25.97000	20.68500	0.69565	0.61250
Apr	0.35743	10.77000	24.59000	19.20500	0.67390	0.49339
May	0.32392	14.00000	24.89000	17.89000	0.47780	0.66840
Jun	0.25641	12.66000	20.98000	14.65000	0.53805	0.61378
Jul	0.34570	13.52000	22.00000	15.24000	0.47510	0.57501
Aug	0.40009	14.39000	23.64000	16.44500	0.52790	0.73046
Sep	0.43797	11.85000	24.87000	18.94500	0.64525	0.76667
Oct	0.50255	9.66000	22.23000	17.40000	0.72045	0.65833
Nov	0.75690	9.86000	23.54000	18.61000	0.74285	0.60584
Dec	0.99460	10.01000	24.70000	19.69500	0.73440	0.79165
Jan	0.83501	9.82000	26.35000	21.44000	0.72610	0.45000
Feb	0.64886	10.10000	27.06000	22.01000	0.71430	0.62500
Mar	0.46427	10.47000	25.84000	20.60500	0.69275	0.56380
Apr	0.29203	10.85000	23.04000	17.61500	0.65465	0.53750
May	0.22987	12.13000	23.92000	17.85500	0.60780	0.75501
Jun	0.19480	11.19000	20.27000	14.67500	0.61530	0.60366
Jul	0.24078	13.49000	22.04000	15.29500	0.48790	0.61668
Aug	0.30740	13.63000	23.85000	17.03500	0.56675	0.70833
Sep	0.44157	14.68000	24.23000	16.89000	0.55040	0.74167
Oct	0.49420	10.41000	22.85000	17.64500	0.72265	0.57499
Nov	0.68157	9.74000	24.17000	19.30000	0.74300	0.57501
Dec	0.85508	9.91000	26.16000	21.20500	0.73315	0.74165
Jan	0.70894	8.50000	24.72000	20.47000	0.79595	0.55833
Feb	0.59946	9.67000	25.95000	21.11500	0.75540	0.67500
Mar	0.49270	10.22000	25.54000	20.43000	0.72265	0.56667
Apr	0.35499	12.01000	25.10000	19.09500	0.65360	0.55000
May	0.25038	11.35000	22.81000	17.13500	0.63510	0.62501
Jun	0.31266	11.68000	20.88000	15.04000	0.56215	0.62499
Jul	0.30265	13.27000	20.97000	14.33500	0.49380	0.60835
Aug	0.35731	13.59000	22.72000	15.92500	0.57500	0.65833
Sep	0.41697	12.43000	23.02000	16.80500	0.62750	0.79167
Oct	0.52470	10.00000	22.77000	17.77000	0.72515	0.62499
Nov	0.62406	10.01000	23.68000	18.67500	0.70055	0.52501
Dec	0.72652	9.26000	24.25000	19.62000	0.76375	0.81665
Jan	0.69406	9.38000	25.95000	21.26000	0.75110	0.53333
Feb	0.67202	10.48000	28.04000	22.80000	0.70785	0.72500
Mar	0.42543	10.88000	27.12000	21.68000	0.70350	0.51667



Month	H/Ho	$\Delta T$ (°C)	$T_{max}$ (°C)	$T_{ave}$ (°C)	RH/100	S/So
Apr	0.30913	10.89000	25.36000	19.91500	0.65105	0.44166
May	0.27165	13.31000	25.69000	19.03500	0.56805	0.63334
Jun	0.22183	12.63000	21.29000	14.97500	0.53900	0.69166
Jul	0.25489	12.97000	22.29000	15.80500	0.52125	0.59168
Aug	0.34305	14.29000	24.15000	17.00500	0.48905	0.71667
Sep	0.43737	14.16000	26.63000	19.55000	0.57850	0.87500
Oct	0.52216	11.49000	24.47000	18.72500	0.67910	0.50833
Nov	0.71054	10.77000	25.04000	19.65500	0.71390	0.65001
Dec	0.73649	8.76000	23.94000	19.56000	0.77215	1.02498
Jan	0.71964	8.70000	25.51000	21.16000	0.76200	0.54166
Feb	0.67434	10.63000	27.74000	22.42500	0.70030	0.61667
Mar	0.52681	12.58000	30.03000	23.74000	0.65830	0.52500
Apr	0.32161	9.55000	22.64000	17.86500	0.71155	0.62499
May	0.25414	10.37000	21.74000	16.55500	0.64390	0.64168
Jun	0.27832	11.71000	19.87000	14.01500	0.58160	0.67499
Jul	0.28953	11.14000	17.80000	12.23000	0.63200	0.56668
Aug	0.41647	12.52000	21.37000	15.11000	0.58835	0.54167
Sep	0.56126	12.20000	23.83000	17.73000	0.63685	0.51667
Oct	0.73313	11.34000	23.99000	18.32000	0.68540	0.50000
Nov	0.76492	10.37000	24.21000	19.02500	0.74565	0.54167
Dec	0.86953	9.97000	26.15000	21.16500	0.76595	0.82499
Jan	0.92618	10.11000	27.96000	22.90500	0.73470	0.56666
Feb	0.67743	10.47000	28.69000	23.45500	0.73340	0.55833
Mar	0.52175	10.93000	27.29000	21.82500	0.70030	0.57500
Apr	0.42311	12.13000	24.49000	18.42500	0.66170	0.61666
May	0.29716	11.91000	24.40000	18.44500	0.62110	0.65834
Jun	0.28271	12.24000	21.48000	15.36000	0.55385	0.64999
Jul	0.32442	12.57000	21.49000	15.20500	0.55625	0.49168
Aug	0.33592	12.35000	23.44000	17.26500	0.58595	0.57500
Sep	0.41547	10.74000	21.61000	16.24000	0.70365	0.55000
Oct	0.46697	8.69000	22.18000	17.83500	0.76885	0.69999
Nov	0.70965	8.50000	22.63000	18.38000	0.77880	0.65834
Dec	1.03198	9.43000	26.43000	21.71500	0.76295	0.85832
Jan	0.85036	9.73000	26.81000	21.94500	0.77065	0.42500
Feb	0.73340	10.67000	27.55000	22.21500	0.74135	0.57500
Mar	0.48196	9.59000	25.78000	20.98500	0.74285	0.54167
Apr	0.38322	11.56000	25.16000	19.38000	0.62955	0.52500
May	0.29216	11.94000	23.32000	17.35000	0.58580	0.60001
Jun	0.27224	13.01000	22.53000	16.02500	0.50935	0.61666
Jul	0.27270	11.37000	21.26000	15.57500	0.63535	0.52501

Month	H/Ho	$\Delta T$ (°C)	$T_{max}$ (°C)	$T_{ave}$ (°C)	RH/100	S/So
Aug	0.37897	13.78000	23.48000	16.59000	0.54655	0.59167
Sep	0.45837	13.98000	25.13000	18.14000	0.60965	0.70000
Oct	0.59624	12.14000	24.47000	18.40000	0.68225	0.65833
Nov	0.84650	11.06000	25.64000	20.11000	0.72260	0.59167
Dec	0.83615	8.29000	23.92000	19.77500	0.79350	0.95832
Jan	0.95177	10.78000	28.59000	23.20000	0.72920	0.48333
Feb	0.78242	11.10000	28.98000	23.43000	0.70950	0.65000
Mar	0.51481	9.93000	26.67000	21.70500	0.74720	0.59167
Apr	0.42013	11.73000	24.97000	19.10500	0.66750	0.60000
May	0.31467	12.98000	24.93000	18.44000	0.68920	0.67501
Jun	0.27686	14.00000	23.06000	16.06000	0.51875	0.63332
Jul	0.30710	13.41000	21.83000	15.12500	0.48565	0.55834
Aug	0.36154	12.77000	24.01000	17.62500	0.54440	0.62500
Sep	0.53637	14.82000	27.18000	19.77000	0.59795	0.85834
Oct	0.55702	10.31000	22.67000	17.51500	0.71630	0.67499
Nov	0.66596	9.51000	23.43000	18.67500	0.75185	0.56667
Dec	0.87850	10.08000	26.04000	21.00000	0.76685	0.96665
Jan	0.91595	10.66000	27.76000	22.43000	0.75290	#N/A
Feb	0.75038	9.67000	26.22000	21.38500	0.77645	#N/A
Mar	0.56313	10.32000	27.08000	21.92000	0.72415	#N/A
Apr	0.39570	10.35000	23.86000	18.68500	0.72045	#N/A
May	0.34418	13.00000	25.81000	19.31000	0.58920	#N/A
Jun	0.30292	12.11000	21.87000	15.81500	0.53405	#N/A
Jul	0.28433	11.81000	21.36000	15.45500	0.62320	#N/A
Aug	0.39798	12.63000	24.96000	18.64500	0.55570	#N/A
Sep	0.43677	11.38000	24.47000	18.78000	0.68440	#N/A
Oct	0.68883	13.45000	27.90000	21.17500	0.67680	#N/A
Nov	0.80682	12.94000	26.55000	20.08000	0.47335	#N/A
Dec	0.97517	11.87000	29.29000	23.35500	0.51060	#N/A
Jan	0.81268	10.97000	28.38000	22.89500	0.81850	#N/A
Feb	0.72722	12.24000	29.40000	23.28000	0.81005	#N/A
Mar	0.51449	11.95000	28.95000	22.97500	0.80045	#N/A
Apr	0.35879	12.75000	27.47000	21.09500	0.75020	#N/A
May	0.29891	13.09000	24.39000	17.84500	0.73545	#N/A
Jun	0.25495	12.48000	22.96000	16.72000	0.71430	#N/A
Jul	0.26850	12.10000	20.72000	14.67000	0.66110	#N/A
Aug	0.37817	13.94000	24.56000	17.59000	0.53640	#N/A
Sep	0.39357	11.59000	23.50000	17.70500	0.72815	#N/A
Oct	0.53305	10.82000	23.09000	17.68000	0.75765	#N/A
Nov	0.63610	9.78000	24.18000	19.29000	0.79040	#N/A

Month	H/Ho	$\Delta T$ (°C)	$T_{max}$ (°C)	$T_{ave}$ (°C)	RH/100	S/So
Dec	0.94477	13.04000	29.26000	22.74000	0.71400	#N/A
Jan	0.82989	11.67000	28.05000	22.21500	0.74650	#N/A
Feb	0.61104	10.88000	28.29000	22.85000	0.75780	#N/A
Mar	0.54323	13.00000	29.30000	22.80000	0.69385	#N/A
Apr	0.38756	12.72000	26.59000	20.23000	0.67325	#N/A
May	0.29016	12.34000	24.50000	18.33000	0.64130	#N/A
Jun	0.27272	13.38000	23.23000	16.54000	0.57645	#N/A
Jul	0.27840	13.75000	23.18000	16.30500	0.57495	#N/A
Aug	0.34965	13.94000	23.64000	16.67000	0.60340	#N/A
Sep	0.42327	13.49000	25.73000	18.98500	0.65655	#N/A
Oct	0.59551	12.33000	24.19000	18.02500	0.72075	#N/A
Nov	0.81084	11.67000	24.98000	19.14500	0.72800	#N/A
Dec	0.86405	10.24000	24.94000	19.82000	0.76715	#N/A
Jan	0.92944	12.15000	28.54000	22.46500	0.73415	#N/A
Feb	0.71255	11.69000	28.55000	22.70500	0.74765	#N/A
Mar	0.50659	11.21000	27.14000	21.53500	0.76120	#N/A
Apr	0.37942	10.36000	25.58000	20.40000	0.75215	#N/A
May	0.31642	11.53000	23.03000	17.26500	0.66720	#N/A
Jun	0.31802	12.47000	22.16000	15.92500	0.60525	#N/A

\*#N/A - Data was not measured during this month

## APPENDIX D

### **Research paper 2 (Published in South African Journal of Energy)**

Govindasamy, Tamara Rosemary and Chetty, Naven. Non-linear multivariate models for the estimation of global solar radiation received across five cities in South Africa. Journal of Energy in South Africa. Vol 30 (2). May 2019. pp. 38 - 51.

## Non-linear multivariate models for estimating global solar radiation received across five cities in South Africa

Tamara Rosemary Govindasamy<sup>1</sup>, Naven Chetty<sup>1,2\*</sup>

1. Department of Physics, School of Chemistry and Physics, University of KwaZulu-Natal (Pietermaritzburg), South Africa. <https://orcid.org/0000-0002-9809-4230>

2. College of Agriculture, Engineering and Science, University of KwaZulu-Natal (Pietermaritzburg), South Africa. <https://orcid.org/0000-0002-0916-578X>

### Abstract

South Africa continues to lag globally in the adoption of renewable energy systems despite a notable decrease in the cost of applicable renewable energy technologies over the past five years. Most applications of potential solar renewable energy systems are currently in various stages of investigation, leaving this readily accessible resource capacity idle. The present study proposes linear and non-linear analysis of multivariate models for estimating global solar radiation (GSR) received across five cities in South Africa. The significance of this study is to provide effective GSR estimation in the application of solar technologies, while increasing their implementation. The dependency of GSR on meteorological variables such as air temperature, relative humidity and relative sunshine duration was evaluated for January 2007 to June 2018 to realise estimation models for each of the study sites. The Hargreaves-Samani and Angstrom-Prescott empirical models served as the basis for single variable analysis of GSR reliance on each meteorological parameter and their relative variations. The results indicated that the proposed non-linear, multivariate equations perform better than the empirical models as well as linear, single variable regression equations. The suggested models are site-specific and demonstrate a strong correlation to historic GSR values with low, acceptable error indicators. It was also recognised that second- and third-order relationships between the clearness index and multiple meteorological variables provide a more accurate description of GSR for most of the cities under study. These methods are cost-effective, easily accessible and appropriate for the evaluation of the feasibility of solar photovoltaic technologies in South Africa.

**Keywords:** renewable energy systems; solar energy; photovoltaic technologies; estimation models

### Highlights:

- Unique non-linear, multivariate estimation models for cities in South Africa
- Estimation models which can be used in photovoltaic technology implementation

---

Journal of Energy in Southern Africa 30(2): 38–51  
DOI: <https://dx.doi.org/10.17159/2413-3051/2019/v30i2a6076>

Published by the Energy Research Centre, University of Cape Town ISSN: 2413-3051  
This work is licensed under a Creative Commons Attribution-ShareAlike 4.0 International Licence  
<https://journals.assaf.org.za/jesa>

Sponsored by the Department of Science and Technology

---

Corresponding author: +27(0)33 260 5660  
Email: [chettn3@ukzn.ac.za](mailto:chettn3@ukzn.ac.za)

## 1. Introduction

South Africa, as one of the world's most coal-dependent countries, has long needed to assess the status of available resources and whether renewables would be a sustainable option for future energy sourcing. The country still trails behind when it comes to discovering and exploring the potential of alternative energy resources, while the world is moving towards greener energy sources to reduce carbon footprint and alleviate the effects of global warming on climatic and environmental conditions.

African countries such as Namibia, Angola and South Africa (especially the Northern Cape) often receive more than double the amount of radiation than countries in the northern hemisphere, e.g. United Kingdom [1]. South Africa is well suited for the harnessing of solar radiation with sunshine being available throughout the year. Disregarding this potential, there are various financial and technical limitations associated with solar energy technologies, which restrict its use to private, off-grid networks. These boundaries need to be resolved to increase the impact and contribution of solar power to the country's energy supply. The present study aims to indicate the amount of underutilised solar potential available in South Africa and to contribute to the knowledge and implementation of solar technologies. With solar radiation data often not being available for most regions locally, most research involves the use of meteorological variables and mathematical relations to investigate the solar potential for sites of interest [2,3]. The cost of equipment associated with the measurement of ground solar radiation levels is relatively high, and although it is often the remote locations that receive high levels of solar radiation, there is no solar radiation data for them. Various international studies over the past two decades have led to the development of solar radiation estimation models and time-series weather prediction models using available, measured meteorological factors [2-4]. It is important to obtain accurate models for locations, making it a field of large interest.

This study analysed and enhanced the existing linear models for five major cities in South Africa. Based on the available meteorological conditions provided by local weather stations, it introduced non-linear regression models for these cities and evaluated their efficiency and accuracy over at least ten years. The study also proposed a multivariate model for each of these cities and tested its performance in accordance to single variable models, as well as non-linear variations of them. These proposed models aim to encourage the use of solar radiation estimation models in the procurement of large-scale solar energy technologies. These cost-effective methods and skills are easily accessible and can be included in the assessment of the feasibility

of solar photovoltaic (PV) technologies in South Africa.

## 2. Background theory

Physical models that depend on meteorological parameters are viable for estimating solar radiation in regions where solar radiation data is not measured as they have lower computational costs and input data requirements [5]. Although solar radiation data is not extensively measured, the majority of physical models require it for validating and calibrating estimation models. Air temperature, relative humidity and, in most cases, sunshine-duration measurements are easy to conduct and can be obtained from weather stations. The Hargreaves-Samani (H-S) equation (Equation 1) [4, 6, 7] relates the amount of extra-terrestrial radiation ( $ETR = H_0$ ) to the difference between the maximum ( $T_{max}$ ) and minimum ( $T_{min}$ ) air temperatures ( $\Delta T = T_{max} - T_{min}$ ), in order to calculate the amount of global solar radiation (GSR =  $H$ ) incident on a horizontal surface ( $H$ ) [8-14]. The main assumption of this model is that the GSR at a site is responsible for the temperature range [15].

$$H = H_0 K_r (\Delta T)^{0.5} \quad (1)$$

where the empirical coefficient ( $K_r$ ) = 0.16 for 'interior regions' and  $K_r = 0.19$  for 'coastal regions' [3, 7, 16], and  $H_0$  is given by Equation 2 [2, 17, 18, 19];

$$H_0 = \frac{24 \times 3.6 \times 10^{-3} I_{sc}}{\pi} \left[ 1 + 0.033 \cos\left(\frac{2\pi D_n}{365}\right) \right] [\cos\phi \cos\delta \sin\omega_s + \omega_s \sin\phi \sin\delta] \quad (2)$$

where  $I_{sc} = 1367 \text{ W/m}^2$  is known as the solar constant [2, 7, 17],  $D_n$  is the calendar day (1 January (Jan):  $D_n = 1$ ; 31 December (Dec):  $D_n = 365$ ). The latitude of the site is denoted by  $\phi$  (all angles expressed in radians), and  $\delta$  is the declination angle given by Equation 3 [20, 21, 22, 23].

$$\delta = 23.45 \frac{\pi}{180} \sin\left[\frac{2\pi(D_n + 284)}{365}\right] \quad (3)$$

The hour angle  $\omega_s$  is given by Equation 4 [20, 23, 24].

$$\omega_s = \cos^{-1}(-\tan\phi \tan\delta) \quad (4)$$

The ratio of the GSR to ETR ( $\frac{H}{H_0}$ ) gives a description of the atmosphere's transparency and is called the clearness index, which is described by Equation 5 [25].

$$K_T = \frac{H}{H_0} \quad (5)$$

The Angstrom-Prescott (A-P) equation (Equation 6) can be used to calculate the clearness index from the relative sunshine duration, provided the A-P coefficients for the area are known [20, 22, 26-29].

$$K_T = \frac{H}{H_o} = a + b \left( \frac{S}{S_o} \right) \quad (6)$$

where a and b are the A-P coefficients, S is the actual hours of sunshine received; and the day length ( $S_o$ ) is used to translate time (in hours) between sunrise and sunset [20, 21, 23, 30, 31], calculated from Equation 7.

$$S_o = \frac{2\omega_s}{15} \quad (7)$$

For areas where the A-P coefficients are unknown, using a = 0.25 and b = 0.50 [32] is prescribed.

### Statistical error analysis

Understanding of the accuracy of analysis and proposed models is quantified in terms of the statistical error analysis. The mean bias error (MBE), Equation 8, specifies the average deviance of the calculated values from observed values and is an indicator of a model's long-term performance [12, 33]. Positive MBE calculations correspond to an over-estimation, while negative MBEs indicate under-estimation. The root mean square error (RMSE), Equation 13, gives insight into the short-term performance of a correlation. The coefficient of determination ( $R^2$ ), Equation 14, is a measure of the correlation between the dependent variables that are predicted from the independent variables. Low values for all statistical error measures are desired [34]. Previous studies propose that percentage errors between -10% and 10% are acceptable [34, 35]. Statistical analysis reported in the present study was calculated using the error-types given by Equations 8–14.

*Mean bias error (MBE) and mean absolute bias error (MABE)*

$$MBE = \frac{1}{n} \sum_{i=1}^n (H_{c,i} - H_{m,i}) \quad (8)$$

$$MABE = \frac{1}{n} \sum_{i=1}^n (|H_{c,i} - H_{m,i}|) \quad (9)$$

*Mean percentage error (MPE) and mean absolute percentage error (MAPE)*

$$MPE = \frac{1}{n} \sum_{i=1}^n \left( \frac{H_{c,i} - H_{m,i}}{H_{m,i}} \right) \times 100\% \quad (10)$$

$$MAPE = \frac{1}{n} \sum_{i=1}^n \left( \left| \frac{H_{c,i} - H_{m,i}}{H_{m,i}} \right| \right) \times 100\% \quad (11)$$

*Mean absolute relative error (MARE)*

$$MARE = \frac{1}{n} \sum_{i=1}^n \left| \left( \frac{H_{m,i} - H_{c,i}}{H_{m,i}} \right) \right| \quad (12)$$

*Root mean square errors (RMSE)*

$$RMSE = \sqrt{\frac{\sum_{i=1}^n (H_{c,i} - H_{m,i})^2}{n}} \quad (13)$$

*Coefficient of determination ( $R^2$ )*

$$R^2 = 1 - \frac{\sum_{i=1}^n (H_{m,i} - H_{c,i})^2}{\sum_{i=1}^n (H_{m,i} - H_{m_{ave}})^2} \quad (14)$$

where  $H_{c,i}$  and  $H_{m,i}$  are the  $i^{th}$  calculated and measured values of GSR, respectively, and  $H_{m_{ave}}$  is the average of the measured H values.

Further research on the estimation of GSR in South Africa through multiple meteorological variables was completed by Adeala et al., which proposed linear models for the nine provinces in South Africa in terms of relative sunshine, air temperature, wind speed and relative humidity. Following a similar approach, the present study focuses on the regression analysis of these meteorological factors and extends to the non-linear impact of multivariate models which include variations of these parameters. Extensive studies were published to detail the non-linear analysis of GSR estimation models across various countries in the world [37-42].

### 3. Experimental technique

Historic meteorological data was obtained from the South African Weather Service (SAWS) and Agricultural Research Council (ARC) for the study sites. Records of sunshine duration (S), air temperature ( $\Delta T, T_{max}$ ), relative humidity (RH) and solar radiation for January 2007–June 2018 was provided by these independent sources. Analysis of the average monthly GSR incident at each site for the specified period was based on dependence on a single meteorological variable and dependence on multiple meteorological variables, using the H-S and A-P Equations 1 and 6 as the foundation models. Sunshine duration and solar radiation measurements are not undertaken for many locations across South Africa because of the cost of equipment and its maintenance. Historic data from the SAWS and ARC was limited for certain regions, e.g., Pietermaritzburg and Durban, as sunshine duration was not measured for the full period. Measurements were recorded for a few months and then stopped, leading to the study being restricted to the available monthly averages. Values for ETR ( $H_o$ ) and  $S_o$  were calculated based on the  $\phi$  of each site, using Fortran programs [Operating system: Linux 3.4.6-2.10-desktop x86\_64,

System: OpenSUSE 12.2(x86\_64), GNU Fortran Compiler, Version: 4.7-2.1.1-86\_64].

South Africa's climate is diverse, because of the wide-ranging landscape and oceanic influence [43–45], and is best described by noting the climate experienced in various regions (climate zones). The eastern coastline experiences a semi-arid and mild, sub-tropical climate, while the south-western region is Mediterranean in type. The north-eastern part experiences sub-tropical conditions, while a small region in the north-west is a desert climate zone [44].

Air temperature and rainfall patterns across the various climate zones are influenced by the region's topography, terrain and sea proximity [43, 44]. Sunshine is received throughout the year, including the winter months (April to September), despite much of the country's rainfall occurring during summer (October to March) [43,44]. Average air temperatures range between 15 and 30 °C during summer and often exceed 38 °C [43]. Table 1 shows the geographical specifics for each study site at five cities across various climate zones.

**Table 1: Geographical details of study sites.**

Site	Province	Latitude (° south)	Longitude (° east)	Elevation (m)
Bloemfontein	Free State	29.1030	26.3263	1400
Cape Town	Western Cape	33.9630	18.4194	670
Durban	KwaZulu-Natal	29.9650	30.4849	670
Johannesburg	Gauteng	26.1430	28.3971	1800
Pietermaritzburg	KwaZulu-Natal	29.6270	30.4062	750

#### 4. Results and discussion

Following a full analysis of single variable dependency of GSR for each of the four variables,  $\Delta T$ ,  $T_{max}$ ,  $RH$  and  $\frac{S}{S_o}$  (relative sunshine duration =  $S$  is the actual hours of sunshine received / the day length  $S_o$ ), the dependency of  $\frac{H}{H_o}$  on multivariate models was further investigated.

##### 4.1. Single variable analysis

Figures 1–10 illustrate the single variable dependence of GSR on air temperature and relative sunshine duration with regard to the H-S and A-P empirical models for each study site.

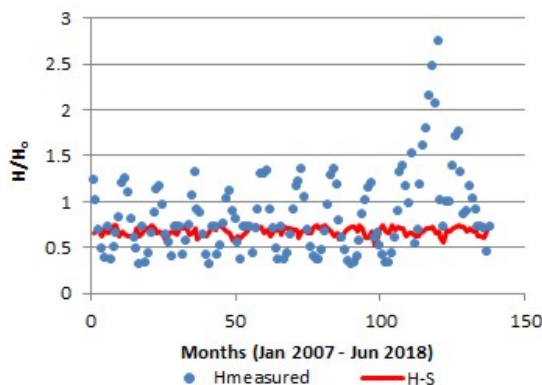


**Figure 1: Calculated extra-terrestrial radiation-global solar radiation ratio ( $\frac{H}{H_o}$ ) using the H-S model for Bloemfontein.  $H_{measured}$  represents the observed values of global solar radiation for the period.**

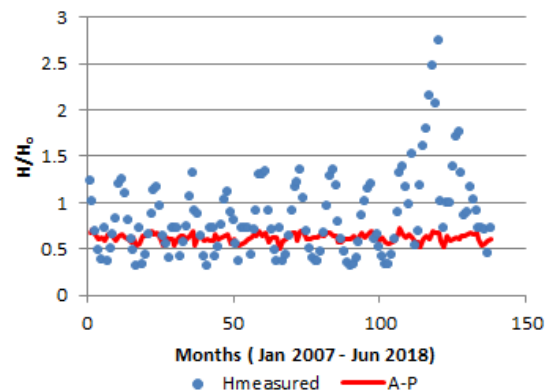


**Figure 2: Calculated extra-terrestrial radiation-global solar radiation ratio ( $\frac{H}{H_o}$ ) using the A-P model for Bloemfontein.  $H_{measured}$  represents the observed values of global solar radiation for the period.**



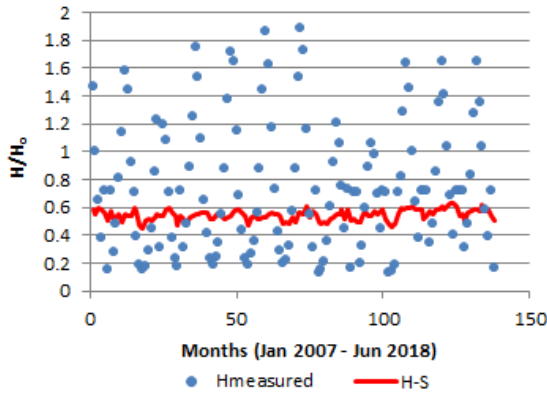


Figure 3: Calculated extra-terrestrial radiation-global solar radiation ratio ( $\frac{H}{H_0}$ ) using the H-S model for Cape Town. Hmeasured represents the observed values of global solar radiation for the period.

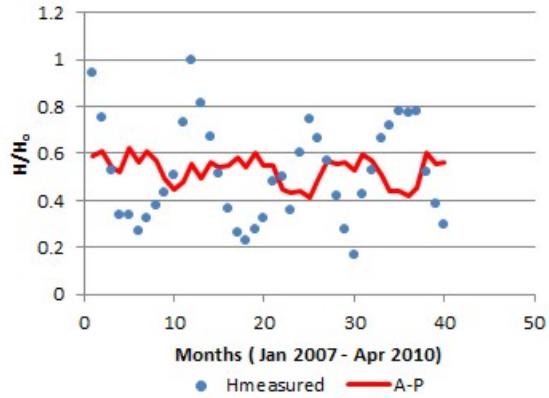


Figure 6: Calculated extra-terrestrial radiation-global solar radiation ratio ( $\frac{H}{H_0}$ ) using the A-P model for Durban. Hmeasured represents the observed values of global solar radiation for the period.

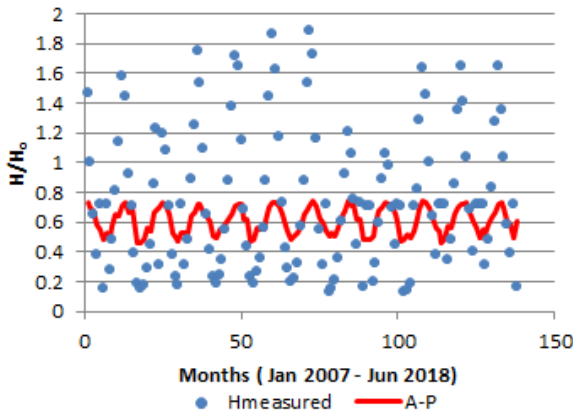


Figure 4: Calculated extra-terrestrial radiation-global solar radiation ratio ( $\frac{H}{H_0}$ ) using the A-P model for Cape Town. Hmeasured represents the observed values of global solar radiation for the period.

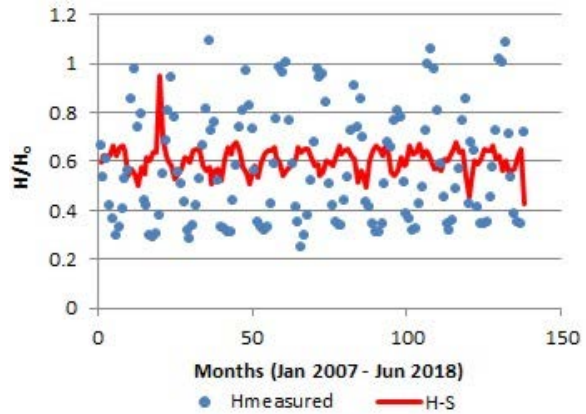


Figure 7: Calculated extra-terrestrial radiation-global solar radiation ratio ( $\frac{H}{H_0}$ ) using the H-S model for Johannesburg. Hmeasured represents the observed values of global solar radiation for the period.

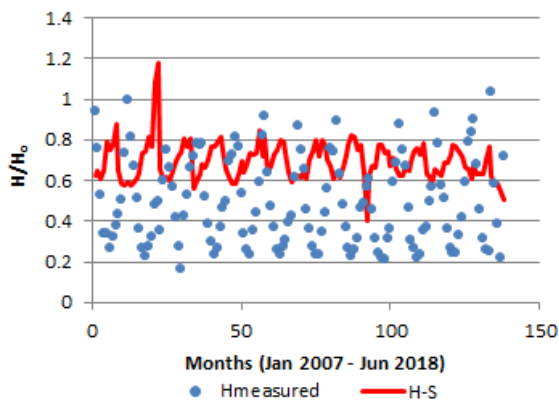


Figure 5: Calculated extra-terrestrial radiation-global solar radiation ratio ( $\frac{H}{H_0}$ ) using the H-S model for Durban. Hmeasured represents the observed values of global solar radiation for the period.

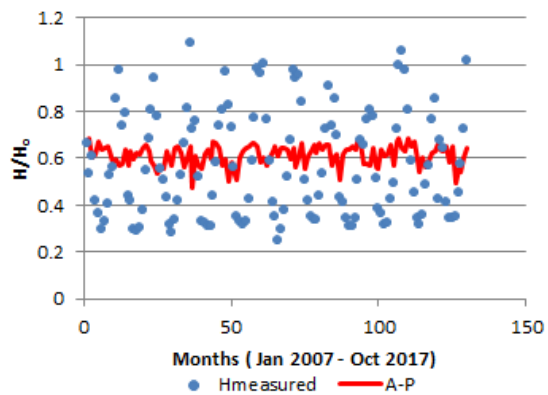
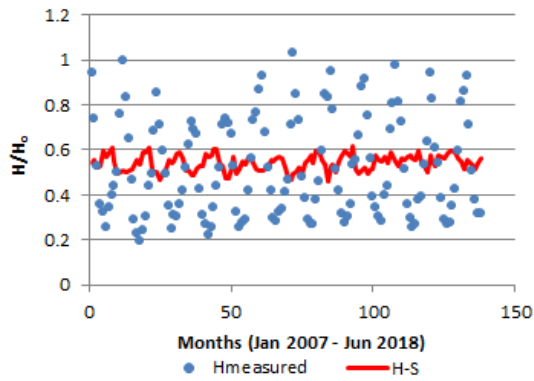
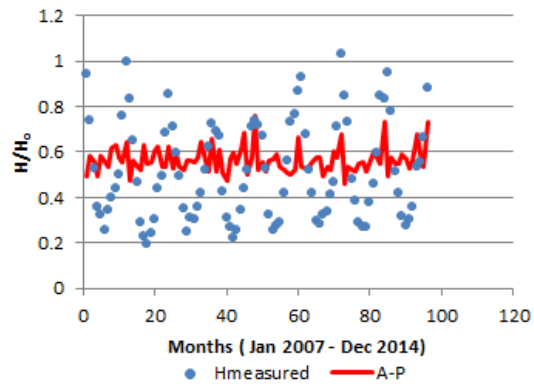


Figure 8: Calculated extra-terrestrial radiation-global solar radiation ratio ( $\frac{H}{H_0}$ ) using the A-P model for Johannesburg. Hmeasured represents the observed values of global solar radiation for the period.



**Figure 9: Calculated extra-terrestrial radiation-global solar radiation ratio ( $\frac{H}{H_o}$ ) using the H-S model for Pietermaritzburg. Hmeasured represents the observed values of global solar radiation for the period.**



**Figure 10: Calculated extra-terrestrial radiation-global solar radiation ratio ( $\frac{H}{H_o}$ ) using the A-P model for Pietermaritzburg. Hmeasured represents the observed values of global solar radiation for the period.**

From the regression relations obtained for all five sites,  $\Delta T$  indicated a weaker correlation to  $\frac{H}{H_o}$  compared with  $T_{max}$  and  $T_{ave}$ . While  $R^2$  values indicated a low to moderate relationship between temperature and GSR, it was found that estimation models that include additional meteorological variables may perform better. Furthermore, higher order relations (quadratic, cubic and power) showed a better fit to the measured values. The single dependency of measured relative humidity (RH) to GSR was also examined. Relative humidity indicated the weakest relationship to  $\frac{H}{H_o}$ . No established GSR estimation

models for this quantity exist, as relative humidity is unable to solely predict GSR. This variable is often used in combination models that do not implicitly account for RH. Sunshine regression equations demonstrated higher correlation values from all three variables. The A-P model performed considerably well and the large number of outliers that were not included by the model can be explained using the universal A-P coefficients. Since established A-P coefficients for the above cities do not exist, the universal coefficients were used:  $a = 0.25$ ;  $b = 0.50$ . These coefficients are general and can be used for any site for which the A-P coefficients are unknown. There is merit in obtaining specific A-P coefficients for each site as this enhances the performance of each model based on the site's observed historic sunshine data.

#### 4.2. Multivariate analysis

Section 4.1 provided the basis to proceed to include only the variables for which the multivariate analysis showed a stronger correlation. Tables 2–11 describe the proposed multivariate equations for each site, as well as their associated error indicators.

**Table 2: Proposed multivariate equations.**

No.	Equation
1	$\frac{H}{H_o} = -0.053(\Delta T) - 0.766\left(\frac{RH}{100}\right) + 2.507\left(\frac{S}{S_o}\right) + 1.930$
2	$\frac{H}{H_o} = -0.393(\sqrt{\Delta T}) - 0.631\left(\frac{RH}{100}\right) + 2.623\left(\frac{S}{S_o}\right) + 0.821$
3	$\frac{H}{H_o} = 0.040(T_{max}) - 0.307\left(\frac{RH}{100}\right) + 1.151\left(\frac{S}{S_o}\right) - 0.979$
4	$\frac{H}{H_o} = 0.394(\sqrt{T_{max}}) - 0.275\left(\frac{RH}{100}\right) + 1.214\left(\frac{S}{S_o}\right) - 1.999$
5	$\frac{H}{H_o} = -0.018(\Delta T)^2 + 0.552(\Delta T) - 1.500\left(\frac{RH}{100}\right)^2 - 0.339\left(\frac{RH}{100}\right) + 3.752\left(\frac{S}{S_o}\right)^2 - 3.546\left(\frac{S}{S_o}\right) - 2.175$
6	$\frac{H}{H_o} = 0.002(T_{max})^2 - 0.037(T_{max}) - 8.813\left(\frac{RH}{100}\right)^2 - 8.107\left(\frac{RH}{100}\right) + 3.262\left(\frac{S}{S_o}\right)^2 - 4.315\left(\frac{S}{S_o}\right) + 0.225$
7	$\frac{H}{H_o} = 0.004(\Delta T)^3 - 0.24(\Delta T)^2 + 4.16(\Delta T) + 57.59\left(\frac{RH}{100}\right)^3 - 89.92\left(\frac{RH}{100}\right)^2 + 43.11\left(\frac{RH}{100}\right) - 2.65\left(\frac{S}{S_o}\right)^3 + 9.31\left(\frac{S}{S_o}\right)^2 - 37.29\left(\frac{S}{S_o}\right) - 27.40$
8	$\frac{H}{H_o} = -9.4 \times 10^{-6}(T_{max})^3 + 0.003(T_{max})^2 - 0.06(T_{max}) + 27.58\left(\frac{RH}{100}\right)^3 - 49.35\left(\frac{RH}{100}\right)^2 + 27.5\left(\frac{RH}{100}\right) + 0.14\left(\frac{S}{S_o}\right)^3 + 2.13\left(\frac{S}{S_o}\right)^2 - 2.99\left(\frac{S}{S_o}\right) - 2.99$

No. = number,  $\frac{H}{H_o}$  = extra-terrestrial radiation-global solar radiation ratio, RH = relative humidity,  $T_{max}$  = maximum temperature,  $\frac{S}{S_o}$  = relative sunshine duration,  $\Delta T$  = temperature difference.

**Table 3: Error indicators for proposed equations.**

Equation	RMSE	MBE	MABE	MPE	MAPE	MARE	R <sup>2</sup>
1	0.39594	0.05721	0.27450	-9.72644	35.91319	0.35913	0.16348
2	0.39734	0.05721	0.27587	-9.95571	36.22391	0.36224	0.82761
3	0.38825	0.05721	0.26900	-6.70049	33.71226	0.33712	0.83507
4	0.39012	0.05721	0.27177	-6.907291	34.27409	0.34274	0.83348
5	0.3249	0.05721	0.26734	-8.12844	34.65066	0.34651	0.21935
6	0.37720	0.05801	0.25875	-5.83789	32.12539	0.32125	0.24080
7	0.38037	0.05721	0.26825	-7.07460	34.50267	0.34503	0.27990
8	0.37725	0.05721	0.26037	-6.06718	32.31451	0.32315	0.24115

RMSE = root mean square error, MBE = mean bias error, MABE = mean absolute bias error, MPE = mean percentage error, MAPE = mean absolute percentage error, MARE = mean absolute relative error, R<sup>2</sup> = coefficient of determination

**Table 4: Proposed multivariate equations.**

No.	Equation
1	$\frac{H}{H_o} = -0.69(\Delta T) - 0.179\left(\frac{RH}{100}\right) + 2.539\left(\frac{S}{S_o}\right) - 0.433$
2	$\frac{H}{H_o} = -0.395(\sqrt{\Delta T}) - 0.176\left(\frac{RH}{100}\right) + 2.540\left(\frac{S}{S_o}\right) + 0.124$
3	$\frac{H}{H_o} = -0.004(T_{max}) - 0.165\left(\frac{RH}{100}\right) + 2.358\left(\frac{S}{S_o}\right) - 1.042$
4	$\frac{H}{H_o} = -0.394(\sqrt{T_{max}}) + 0.165\left(\frac{RH}{100}\right) + 2.360\left(\frac{S}{S_o}\right) - 0.962$
5	$\frac{H}{H_o} = -0.014(\Delta T)^2 + 0.128(\Delta T) - 3.041\left(\frac{RH}{100}\right)^2 + 2.340\left(\frac{RH}{100}\right) + 2.812\left(\frac{S}{S_o}\right)^2 - 1.305\left(\frac{S}{S_o}\right) - 0.159$
6	$\frac{H}{H_o} = -0.003(T_{max})^2 + 0.094(T_{max}) - 0.965\left(\frac{RH}{100}\right)^2 + 0.942\left(\frac{RH}{100}\right) + 3.549\left(\frac{S}{S_o}\right)^2 - 2.060\left(\frac{S}{S_o}\right) - 0.597$
7	$\frac{H}{H_o} = -0.002(\Delta T)^3 - 0.001(\Delta T)^2 + 0.15(\Delta T) + 32.35\left(\frac{RH}{100}\right)^3 - 47.97\left(\frac{RH}{100}\right)^2 + 17.94\left(\frac{RH}{100}\right) + 1.23\left(\frac{S}{S_o}\right)^3 + 0.80\left(\frac{S}{S_o}\right)^2 - 0.40\left(\frac{S}{S_o}\right) - 0.69$
8	$\frac{H}{H_o} = 4 \times 10^{-4}(T_{max})^3 - 0.03(T_{max})^2 + 0.71(T_{max}) + 13.33\left(\frac{RH}{100}\right)^3 - 19.66\left(\frac{RH}{100}\right)^2 + 7.52\left(\frac{RH}{100}\right) + 2.25\left(\frac{S}{S_o}\right)^3 - 0.46\left(\frac{S}{S_o}\right)^2 - 0.368\left(\frac{S}{S_o}\right) - 5.41$

No. = number,  $\frac{H}{H_o}$  = extra-terrestrial radiation-global solar radiation ratio, RH = relative humidity, T<sub>max</sub> = maximum temperature,  $\frac{S}{S_o}$  = relative sunshine duration, ΔT = temperature difference.

For Bloemfontein, the first order multivariate equations produced a higher correlation in contrast with the second and third order relations. Low RMSE and MPE indicators, which fall within the accepted range (-10%; 10%) were also obtained by the first order relations. Figure 11 shows the performance of the proposed model (Equation 3) amongst the measured values of  $\frac{H}{H_o}$ . The model is adequate in fitting the clearness index values previously measured in Bloemfontein, except for outliers in the last two to three years (months = 110 - 130). These discrepancies may be a result of the climate change experienced in recent years, or possible data-recording defects.

Tables 4 and 5 show the proposed equations for Cape Town. The  $\frac{H}{H_o}$  values show a stronger dependency on T<sub>max</sub>, with the quadratic (Equation 6) and cubic (Equation 8) relations having the highest R<sup>2</sup> and lowest RMSE values. The MPE indicators are within the accepted range and the MAPEs can be explained by the large number of outliers in the data set. The proposed Equation 8 provides a strong coefficient of determination and low error indicators

and hence fits the measured values of GSR well, as indicated in Figure 12. A few underestimations are noticeable but overall the model includes most data points.

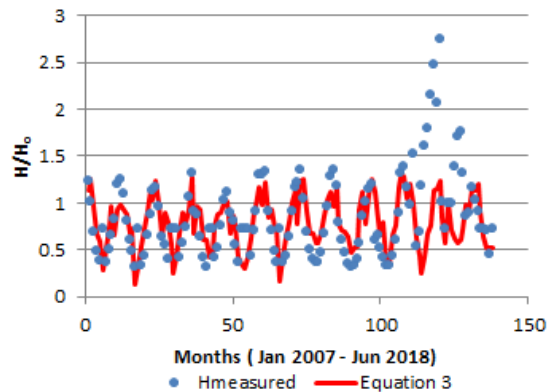


**Figure 11: Proposed multivariate model using T<sub>max</sub> to estimate  $\frac{H}{H_o}$  for Bloemfontein, where T<sub>max</sub>, H<sub>measured</sub> and  $\frac{H}{H_o}$  represent the maximum temperature, observed values of global solar radiation and the extra-terrestrial radiation-global solar radiation ratio respectively.**

**Table 5: Error indicators for proposed equations.**

Equation	RMSE	MBE	MABE	MPE	MAPE	MARE	R <sup>2</sup>
1	0.29168	0.06358	0.22174	2.34321	39.68114	0.39681	0.57990
2	0.30012	0.06358	0.22187	2.20763	39.70152	0.39702	0.88447
3	0.29956	0.06358	0.22425	3.95230	39.85326	0.39853	0.88490
4	0.29958	0.06358	0.22424	3.93864	39.86163	0.39862	0.88489
5	0.27006	0.06358	0.19926	3.07052	31.81996	0.31820	0.65884
6	0.26905	0.06358	0.19935	3.57050	31.91099	0.31911	0.90716
7	0.26640	0.06358	0.19182	2.86728	29.20680	0.29207	0.66803
8	0.26336	0.06358	0.19213	3.22039	28.85694	0.28857	0.91104

RMSE = root mean square error, MBE = mean bias error, MABE = mean absolute bias error, MPE = mean percentage error, MAPE = mean absolute percentage error, MARE = mean absolute relative error, R<sup>2</sup> = coefficient of determination.

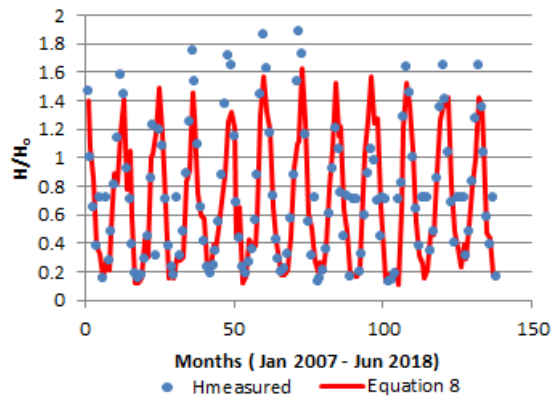


**Figure 12: Proposed multivariate model using T<sub>max</sub> to estimate  $\frac{H}{H_0}$  for Cape Town, where T<sub>max</sub>, H<sub>measured</sub> and  $\frac{H}{H_0}$  represent the maximum temperature, observed values of global solar radiation and the extra-terrestrial radiation-global solar radiation ratio respectively.**

**Table 6: Proposed multivariate equations.**

No.	Equation
1	$\frac{H}{H_0} = 0.002(\Delta T) + 2.033\left(\frac{RH}{100}\right) + 0.365\left(\frac{S}{S_0}\right) - 1.201$
2	$\frac{H}{H_0} = 0.020(\sqrt{\Delta T}) + 2.040\left(\frac{RH}{100}\right) + 0.361\left(\frac{S}{S_0}\right) + 1.242$
3	$\frac{H}{H_0} = 0.008(T_{max}) + 1.919\left(\frac{RH}{100}\right) + 0.413\left(\frac{S}{S_0}\right) - 1.325$
4	$\frac{H}{H_0} = 0.102(\sqrt{T_{max}}) + 1.905\left(\frac{RH}{100}\right) + 0.416\left(\frac{S}{S_0}\right) - 1.732$
5	$\frac{H}{H_0} = 4.5 \times 10^{-4}(\Delta T)^2 - 0.019(\Delta T) + 7.039\left(\frac{RH}{100}\right)^2 - 8.255\left(\frac{RH}{100}\right) + 0.521\left(\frac{S}{S_0}\right)^2 - 0.159\left(\frac{S}{S_0}\right) - 2.844$
6	$\frac{H}{H_0} = -1.4 \times 10^{-3}(T_{max})^2 + 0.108(T_{max}) + 13.097\left(\frac{RH}{100}\right)^2 - 16.833\left(\frac{RH}{100}\right) - 1.180\left(\frac{S}{S_0}\right)^2 + 1.6025\left(\frac{S}{S_0}\right) + 3.399$
7	$\frac{H}{H_0} = -9 \times 10^{-5}(\Delta T)^3 + 0.005(\Delta T)^2 - 0.06(\Delta T) - 230.5\left(\frac{RH}{100}\right)^3 + 499.5\left(\frac{RH}{100}\right)^2 - 355.4\left(\frac{RH}{100}\right) - 9.27\left(\frac{S}{S_0}\right)^3 + 13.1\left(\frac{S}{S_0}\right)^2 - 5.46\left(\frac{S}{S_0}\right) + 84.15$
8	$\frac{H}{H_0} = 3.6 \times 10^{-5}(T_{max})^3 - 0.005(T_{max})^2 + 0.23(T_{max}) - 142.8\left(\frac{RH}{100}\right)^3 + 320.3\left(\frac{RH}{100}\right)^2 - 235.9\left(\frac{RH}{100}\right) - 9.18\left(\frac{S}{S_0}\right)^3 + 11.78\left(\frac{S}{S_0}\right)^2 - 4.19\left(\frac{S}{S_0}\right) - 54.78$

No. = number,  $\frac{H}{H_0}$  = extra-terrestrial radiation-global solar radiation ratio, RH = relative humidity, T<sub>max</sub> = maximum temperature,  $\frac{S}{S_0}$  = relative sunshine duration, ΔT = temperature difference.

**Table 7: Error indicators for proposed equations.**

Equation	RMSE	MBE	MABE	MPE	MAPE	MARE	R <sup>2</sup>
1	0.15789	0.02188	0.13075	-7.18984	29.15333	0.29153	0.42176
2	0.15792	0.02188	0.13082	-7.21693	29.20971	0.29210	0.42153
3	0.15648	0.02188	0.12888	-6.34183	27.92393	0.27924	0.92113
4	0.39039	0.02188	0.12188	3.86583	-31.31340	0.42384	0.30871
5	0.14688	0.02188	0.11608	-6.07546	25.32882	0.25329	0.49962
6	0.12589	0.02188	0.10413	-2.0700	21.34543	0.21345	0.94895
7	0.14598	0.02188	0.11043	-4.05942	22.36994	0.22370	0.50567
8	0.13117	0.02188	0.10559	-1.59414	20.55594	0.20560	0.94458

RMSE = root mean square error, MBE = mean bias error, MABE = mean absolute bias error, MPE = mean percentage error, MAPE = mean absolute percentage error, MARE = mean absolute relative error, R<sup>2</sup> = coefficient of determination.

First, second and third order equations using  $T_{max}$  indicate high correlation coefficients and low RMSEs. This makes these equations well suited for the estimation of clearness index. The percentage errors are all within the accepted range of -10% – 10%. This study proposes Equation 6 for Durban and this model's performance is depicted in Figure 13. The sunshine data was not measured from May

2010 to Jun 2018, due to technical limitations at the ARC, so this period was excluded from the analysis. The shape of the data shown in Figure 13 suggests that the model adequately estimates  $K_T$  for the period available. Since fewer data points were analysed, this also had an impact on the error indicators reported in Table 7.

**Table 8: Proposed multivariate equations.**

No.	Equation
1	$\frac{H}{H_o} = -0.029(\Delta T) + 0.618\left(\frac{RH}{100}\right) + 0.3135\left(\frac{S}{S_o}\right) + 0.178$
2	$\frac{H}{H_o} = -0.232(\sqrt{\Delta T}) + 0.460\left(\frac{RH}{100}\right) + 0.624\left(\frac{S}{S_o}\right) - 0.581$
3	$\frac{H}{H_o} = 0.045(T_{max}) + 0.474\left(\frac{RH}{100}\right) + 0.159\left(\frac{S}{S_o}\right) - 0.887$
4	$\frac{H}{H_o} = 0.433(\sqrt{T_{max}}) + 0.453\left(\frac{RH}{100}\right) + 0.169\left(\frac{S}{S_o}\right) - 1.936$
5	$\frac{H}{H_o} = 1.9 \times 10^{-3}(\Delta T)^2 - 0.110(\Delta T) - 1.304\left(\frac{RH}{100}\right)^2 + 1.677\left(\frac{RH}{100}\right) + 1.044\left(\frac{S}{S_o}\right)^2 - 0.982\left(\frac{S}{S_o}\right) + 1.026$
6	$\frac{H}{H_o} = -1.8 \times 10^{-3}(T_{max})^2 + 0.131(T_{max}) - 1.154\left(\frac{RH}{100}\right)^2 + 1.757\left(\frac{RH}{100}\right) - 0.4735\left(\frac{S}{S_o}\right)^2 + 0.811\left(\frac{S}{S_o}\right) - 2.436$
7	$\frac{H}{H_o} = 6.7 \times 10^{-4}(\Delta T)^3 - 0.04(\Delta T)^2 + 0.615(\Delta T) - 25.6\left(\frac{RH}{100}\right)^3 + 47.02\left(\frac{RH}{100}\right)^2 - 28.5\left(\frac{RH}{100}\right) - 2.57\left(\frac{S}{S_o}\right)^3 - 1.85\left(\frac{S}{S_o}\right)^2 - 0.49\left(\frac{S}{S_o}\right) + 3.83$
8	$\frac{H}{H_o} = 7.5 \times 10^{-4}(T_{max})^3 - 0.06(T_{max})^2 - 1.27(T_{max}) - 6.143\left(\frac{RH}{100}\right)^3 + 11.25\left(\frac{RH}{100}\right)^2 - 6.43\left(\frac{RH}{100}\right) - 18.59\left(\frac{S}{S_o}\right)^3 + 36.74\left(\frac{S}{S_o}\right)^2 - 23.7\left(\frac{S}{S_o}\right) + 15.8$

No. = number,  $\frac{H}{H_o}$  = extra-terrestrial radiation-global solar radiation ratio, RH = relative humidity,  $T_{max}$  = maximum temperature,  $\frac{S}{S_o}$  = relative sunshine duration,  $\Delta T$  = temperature difference.

**Table 9: Error indicators for proposed equations.**

Equation	RMSE	MBE	MABE	MPE	MAPE	MARE	R2
1	0.25244	0.15038	0.19397	17.47650	30.41315	0.30413	0.19989
2	0.24853	0.14751	0.19093	16.9053	29.76287	0.29763	0.8602
3	0.14144	-4x10 <sup>-9</sup>	0.10475	-5.08111	19.6809	0.19368	0.94689
4	0.14166	0.01584	0.10686	-1.73778	19.44057	0.19441	0.94672
5	0.39480	0.34215	0.34764	14.63490	31.40490	0.31405	0.20488
6	0.13838	6.41x10 <sup>-16</sup>	0.10853	-4.58710	20.46811	0.20468	0.94916
7	0.18301	-2.1x10 <sup>-15</sup>	0.15512	-10.94380	30.67616	0.30676	0.33782
8	0.11753	-1x10 <sup>-14</sup>	0.09414	-3.16928	16.61409	0.16614	0.96333

RMSE = root mean square error, MBE = mean bias error, MABE = mean absolute bias error, MPE = mean percentage error, MAPE = mean absolute percentage error, MARE = mean absolute relative error, R<sup>2</sup> = coefficient of determination.

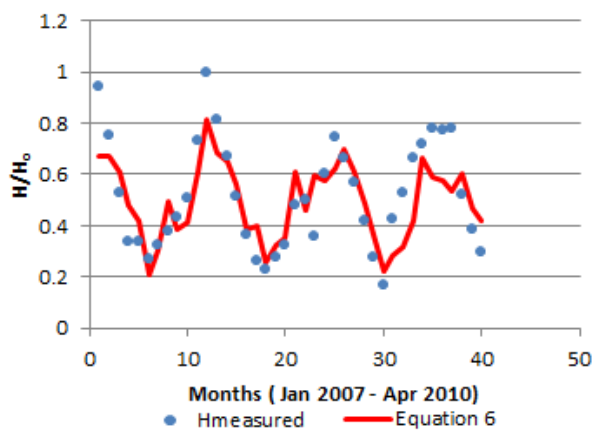


**Figure 13: Proposed multivariate model using  $T_{max}$  to estimate  $\frac{H}{H_0}$  for Durban, where  $T_{max}$ ,  $H_{measured}$  and  $\frac{H}{H_0}$  represent the maximum temperature, observed values of global solar radiation and the extra-terrestrial radiation-global solar radiation ratio respectively.**

Error analysis for the proposed equations for Johannesburg shows low RMSE and MBE values, which make the above equations suitable. It is evident that  $T_{max}$  equations have a stronger dependency to clearness index values. Equation 8, which is a cubic function of  $T_{max}$ , is proposed for Johannesburg and

illustrated in Figure 14. The proposed model accurately fitted the historic data, with a high correlation coefficient and low error indicators and there were a few underestimations which may have resulted from the effects of any of the three variables included in the equation.

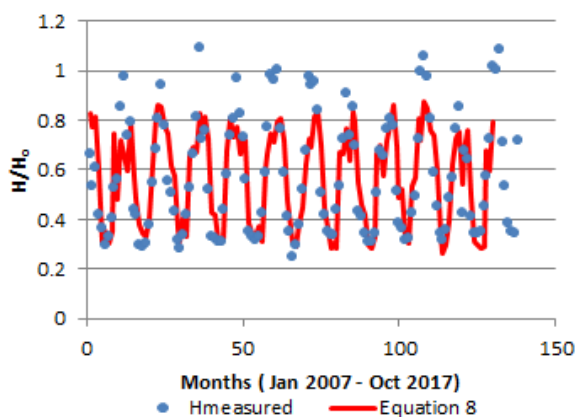


**Figure 14: Proposed multivariate model using  $T_{max}$  to estimate  $\frac{H}{H_0}$  for Johannesburg, where  $T_{max}$ ,  $H_{measured}$  and  $\frac{H}{H_0}$  represent the maximum temperature, observed values of global solar radiation and the extra-terrestrial radiation-global solar radiation ratio respectively.**

**Table 10: Proposed multivariate equations.**

No.	Equation
1	$\frac{H}{H_o} = 0.048(\Delta T) + 2.633\left(\frac{RH}{100}\right) + .174\left(\frac{S}{S_o}\right) - 1.876$
2	$\frac{H}{H_o} = 0.310(\sqrt{\Delta T}) + 2.599\left(\frac{RH}{100}\right) + 0.885\left(\frac{S}{S_o}\right) - 2.361$
3	$\frac{H}{H_o} = 0.032(T_{max}) + 1.462\left(\frac{RH}{100}\right) + 0.235\left(\frac{S}{S_o}\right) - 1.390$
4	$\frac{H}{H_o} = 0.319(\sqrt{T_{max}}) + 1.463\left(\frac{RH}{100}\right) + 0.231\left(\frac{S}{S_o}\right) - 2.168$
5	$\frac{H}{H_o} = -0.016(\Delta T)^2 + 0.475(\Delta T) + 13.621\left(\frac{RH}{100}\right)^2 - 13.963\left(\frac{RH}{100}\right) + 1.237\left(\frac{S}{S_o}\right)^2 - 1.612\left(\frac{S}{S_o}\right) + 0.808$
6	$\frac{H}{H_o} = 0.002(T_{max})^2 - 0.085(T_{max}) + 7.513\left(\frac{RH}{100}\right)^2 - 8.183\left(\frac{RH}{100}\right) - 0.910\left(\frac{S}{S_o}\right)^2 - 1.110\left(\frac{S}{S_o}\right) + 3.533$
7	$\frac{H}{H_o} = 0.003(\Delta T)^3 - 0.12(\Delta T)^2 + 1.67(\Delta T) - 9.02\left(\frac{RH}{100}\right)^3 + 31.06\left(\frac{RH}{100}\right)^2 - 25.38\left(\frac{RH}{100}\right) - 8.77\left(\frac{S}{S_o}\right)^3 + 19.99\left(\frac{S}{S_o}\right)^2 - 14.53\left(\frac{S}{S_o}\right) + 2.0$
8	$\frac{H}{H_o} = 8.9 \times 10^{-5}(T_{max})^3 - 0.004(T_{max})^2 + 0.047(T_{max}) - 22.51\left(\frac{RH}{100}\right)^3 + 50.56\left(\frac{RH}{100}\right)^2 - 35.24\left(\frac{RH}{100}\right) - 9.17\left(\frac{S}{S_o}\right)^3 + 20.59\left(\frac{S}{S_o}\right)^2 - 14.7\left(\frac{S}{S_o}\right) + 11.3$

No. = number,  $\frac{H}{H_o}$  = extra-terrestrial radiation-global solar radiation ratio, RH = relative humidity,  $T_{max}$  = maximum temperature,  $\frac{S}{S_o}$  = relative sunshine duration,  $\Delta T$  = temperature difference.

**Table 11: Error indicators for proposed equations.**

Equation	RMSE	MBE	MABE	MPE	MAPE	MARE	R <sup>2</sup>
1	0.13726	-6.6x10 <sup>-16</sup>	0.11001	-6.71925	25.21744	0.25217	0.59623
2	0.13758	-9.6x10 <sup>-16</sup>	0.11045	-6.79374	25.39489	0.25395	0.93908
3	0.12468	-1.3x10 <sup>-16</sup>	0.10076	-5.39414	22.82711	0.22827	0.94996
4	0.12490	9.4x10 <sup>-17</sup>	0.10090	-5.39830	22.89302	0.22893	0.94979
5	0.18160	0.14	0.14929	-20.75960	28.27592	0.28276	0.29317
6	0.11116	1.44x10 <sup>-15</sup>	0.08474	-4.43616	17.83656	0.17837	0.96023
7	0.11077	9.7x10 <sup>-15</sup>	0.08462	-4.43619	17.68162	0.17682	0.73701
8	0.10744	2.4x10 <sup>-15</sup>	0.08199	-4.22186	17.64309	0.17643	0.96285

RMSE = root mean square error, MBE = mean bias error, MABE = mean absolute bias error, MPE = mean percentage error, MAPE = mean absolute percentage error, MARE = mean absolute relative error, R<sup>2</sup> = coefficient of determination.

First order equations using  $\sqrt{\Delta T}$ ,  $T_{max}$  and  $\sqrt{T_{max}}$  indicate high R<sup>2</sup> values with low error indicators shown in Table 11. Equations containing  $T_{max}$  again show a stronger relationship to  $K_T$  values. For Pietermaritzburg, Equation 6 is proposed. The model's efficiency is depicted in Figure 15 and indicates a well-suited model. Sunshine duration data was unavailable for certain months as a result of technical limitations from the data source and hence the analysis was completed only for the period 2007–2014.

The above analysis is evidence that non-linear, multivariate models are more efficient in estimating GSR than linear, single variable models. Strong R<sup>2</sup> coefficients are detailed for the proposed multivariate equations. Low error indicators (RMSE, MBE and MPE) describe the suitability of these models for

GSR prediction over the long-term. The MAPE error values can be explained by the rounding and averaging of hourly and daily recordings to obtain monthly average values. It was found that the dependence of  $\frac{H}{H_o}$  on  $T_{max}$  is stronger than that of  $\Delta T$  (derived from the H-S model), while relative sunshine duration  $\frac{S}{S_o}$  is a strong indicator of the GSR experienced across the study sites. Higher order equations (both single and multivariate relationships) prove to be more accurate. The equations suggested for the five study sites demonstrate their suitability for the estimation of GSR over the long term, i.e., forecasting, horizon and are summarised in Table 12.



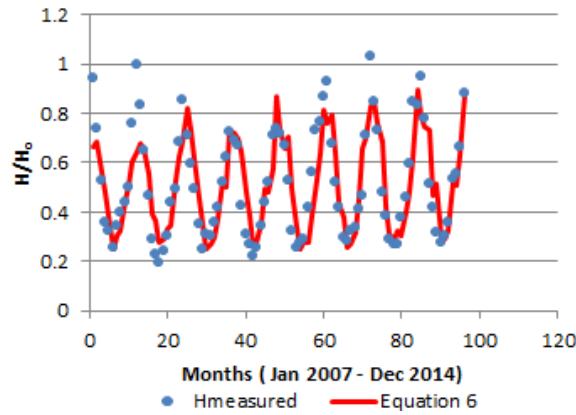


**Figure 15: Proposed multivariate model using  $T_{max}$  to estimate  $\frac{H}{H_0}$  for Pietermaritzburg, where  $T_{max}$ ,  $H_{measured}$  and  $\frac{H}{H_0}$  represent the maximum temperature, observed values of global solar radiation and the extra-terrestrial radiation-global solar radiation ratio respectively.**

**Table 12: Summary of multivariate equations for each study site.**

Site	Equation
BFN	$\frac{H}{H_0} = 0.040(T_{max}) - 0.307\left(\frac{RH}{100}\right) + 1.151\left(\frac{S}{S_0}\right) - 0.979$
CT	$\frac{H}{H_0} = 4 \times 10^{-4}(T_{max})^3 - 0.03(T_{max})^2 + 0.71(T_{max}) + 13.33\left(\frac{RH}{100}\right)^3 - 19.66\left(\frac{RH}{100}\right)^2 + 7.52\left(\frac{RH}{100}\right) + 2.25\left(\frac{S}{S_0}\right)^3 - 0.46\left(\frac{S}{S_0}\right)^2 - 0.368\left(\frac{S}{S_0}\right) - 5.41$
DBN	$\frac{H}{H_0} = -1.4 \times 10^{-3}(T_{max})^2 + 0.108(T_{max}) + 13.097\left(\frac{RH}{100}\right)^2 - 16.833\left(\frac{RH}{100}\right) - 1.180\left(\frac{S}{S_0}\right)^2 + 1.6025\left(\frac{S}{S_0}\right) + 3.399$
JHB	$\frac{H}{H_0} = 7.5 \times 10^{-4}(T_{max})^3 - 0.06(T_{max})^2 - 1.27(T_{max}) - 6.143\left(\frac{RH}{100}\right)^3 + 11.25\left(\frac{RH}{100}\right)^2 - 6.43\left(\frac{RH}{100}\right) - 18.59\left(\frac{S}{S_0}\right)^3 + 36.74\left(\frac{S}{S_0}\right)^2 - 23.7\left(\frac{S}{S_0}\right) + 15.8$
PMB	$\frac{H}{H_0} = 0.002(T_{max})^2 - 0.085(T_{max}) + 7.513\left(\frac{RH}{100}\right)^2 - 8.183\left(\frac{RH}{100}\right) - 0.910\left(\frac{S}{S_0}\right)^2 - 1.110\left(\frac{S}{S_0}\right) + 3.533$

BFN = Bloemfontein, CT = Cape Town, DBN = Durban, JHB = Johannesburg, PMB = Pietermaritzburg,  $\frac{H}{H_0}$  = extra-terrestrial radiation-global solar radiation ratio, RH = relative humidity,  $T_{max}$  = maximum temperature,  $\frac{S}{S_0}$  = relative sunshine duration.

## 5. Conclusions

This study analysed the impact of single variable, linear estimation models on the available GSR within South Africa in comparison to multivariate, non-linear regression models which incorporate variations of meteorological parameters. The investigation to propose linear and non-linear analysis of multivariate models for the estimation of global solar radiation (GSR) received across five South African cities indicated that the empirical Hargreaves-Samani and Angstrom-PreScott models proved to be reliable methods for estimating the amount of GSR in shorter study periods (i.e., one calendar year), but lacked accuracy for long-term estimations. This work further indicated that models that make use of a single meteorological variable and most linear models are not able to adequately predict GSR for the selected cities over periods longer than ten calendar years. Meteorological parameters used for this research were substantially easy to obtain, except for

sunshine data measurements that are not always available because of the costly equipment they demand. This study provided insights on the estimation of GSR in South Africa, which can be accurate, easily employed, and subsequently cost-effective. The proposed models are unique to each of the selected cities and may be incorporated into the design and installation processes of solar photovoltaic (PV) technologies to enhance their efficiency, while endorsing their application. Furthermore, the proposed economical models are appropriate for the feasibility study of solar PV technologies in South Africa.



## Acknowledgements

The assistance of the Agricultural Research Council and South African Weather Service to collate relevant data for this study is acknowledged.

## Author roles

*Tamara Rosemary Govindasamy*: project initiator, research formulation, data collection, write-up, analytical techniques and implementation

*Naven Chetty*: research formulation, project supervision, technical advice, write-up input plus analysis techniques and processing

## References

- [1] Department of Minerals and Energy. 2003. White Paper on Renewable Energy. Available from: [https://un-fccc.int/files/meetings/seminar/application/pdf/sem\\_sup1\\_south\\_africa.pdf](https://un-fccc.int/files/meetings/seminar/application/pdf/sem_sup1_south_africa.pdf)
- [2] Dlamini M. D., Varkey A. J., Mkhonta S. K. 2017. Models for calculating monthly average solar radiation from air temperature in Swaziland. *International Journal of Physical Sciences* 12: 247-254. DOI: <https://doi.org/10.5897/IJPS2017.4679>
- [3] Maleki S. A. M., Hizam H., Gomes C. 2017. Estimation of hourly, daily and monthly global solar radiation on inclined surfaces: Models re-visited. *Energies* 10(1), 134. DOI: <https://doi.org/10.3390/en10010134>
- [4] Zhandire E. 2017. Predicting clear-sky global horizontal irradiance at eight locations in South Africa using four models. *Journal of Energy in Southern Africa*, 28 (4): 77-86. DOI: <https://dx.doi.org/10.17159/2413-3051/2017/v28i4a2397>.
- [5] Da Silva V. J., Da Silva C. R., Almorox J., Junior J. A. 2016. Temperature based solar radiation models for use in simulated soybean potential yield. *Australian Journal of Crop Science*, 10 (7): 926-932. DOI: <https://dx.doi.org/10.21475/ajcs.2016.10.07.p7301>
- [6] Falayi E.O., Rabiou A.B. 2012. Solar radiation models and information for renewable energy applications. *Solar radiation, E. B. Babatunde, IntechOpen*. 111-130. DOI: <https://doi.org/10.5772/35390>.
- [7] Fu Q. 2003. Radiation (solar). University of Washington, Seattle, WA. USA. Elsevier. 1859-1863.
- [8] Meenal R., Boazina P. G., Selvakumar A. I. 2016. Temperature based radiation models for the estimation of global solar radiation at horizontal surface in India. *Indian Journal of Science and Technology*, 9(46). DOI: <http://dx.doi.org/10.17485/ijst%2F2016%2Fv9i46%2F101922>.
- [9] Samani Z. 2000. Estimating solar radiation and evapotranspiration using minimum climatological data. *Journal of Irrigation and Drainage Engineering*, ASCE 126(4): 265-267.
- [10] Allen R.G. 1991. Self-calibrating method for estimating global solar radiation from air temperature. *Journal of Hydrologic Engineering*, New York, 2:56-57.
- [11] Hargreaves G. H., Samani Z. A. 1982. Estimating potential evapotranspiration. *Journal of Irrigation and Drainage Engineering*, ASCE, 108(IR3):223-230.
- [12] Almorox J., Bocco M. Wellington E. 2013. Estimation of daily global solar radiation from measured temperatures at Canada de Luque, Corboda, Argentina. *Renewable Energy*, 60(C): 382-387.
- [13] Dlamini M. D., Varkey A. J., Mkhonta S. K. 2017. Models for calculating monthly average solar radiation from air temperature in Swaziland. *International Journal of Physical Sciences*, 12: 247-254.
- [14] Sarkar N.I., Sifat A. I., Paul S., Hossain S., Rahman M. 2016. Solar radiation estimation using temperature data for Dhaka, Bangladesh. *Proceedings of the 5th International Conference on Informatics, Electronics and Vision (ICIEV), Dhaka, 2016: 204-208*. DOI: <https://dx.doi.org/10.1109/ICIEV.2016.7759996>
- [15] Almorox J., Hontoria C., Benito M. 2011. Models for obtaining daily global solar radiation with measured air temperature data in Madrid (Spain). *Applied Energy*, 88:1703-1709.
- [16] Renewable energy scenarios for municipalities in South Africa. January 2018. South African Local Government Association: Opportunities in renewable energy and energy efficiency for municipalities in South Africa.
- [17] Musango J. K., Amigun B., Brent A. C. 2011. Sustainable electricity generation technologies in South Africa: Initiatives, challenges and policy implications. *Energy and Environment Research*, 1 (1): 124-138. DOI: <https://dx.doi.org/10.5539/eer.v1n1p124>
- [18] S.K. Solanki and M. Fligge. 1998. Solar irradiance since 1874 revisited. *Geophysical Research Letters*, 25(3): 341-344.
- [19] Sayigh A. A. M. 1977. Solar radiation availability prediction from climatological data. *Journal of Solar Energy Engineering*, -1: 61-82. DOI: <https://dx.doi.org/10.1016/B978-0-12-620850-4.50010-7>
- [20] Viorel B (Ed). 2008. *Modeling solar radiation at the earth's surface: Recent advances*. Springer, Germany. Chapter 1.
- [21] Campbell G. S., John M. N. 1998. *An introduction to environmental biophysics*. 2<sup>nd</sup> Ed. Springer, New York.
- [22] Tijjani B.I. 2017. Comparison between first and second order Angstrom type models for sunshine hours in Katsina Nigeria. Bayero. *Journal of Pure and Applied sciences*, 4(2): 24-27. DOI: <http://dx.doi.org/10.4314/bajopas.v4i2.5>.

- [23] Ituen Eno E., Esen Nisken U., Nwokolo Samuel C., Uto Ema G. 2012. Prediction of Global solar radiation using relative humidity, maximum temperature and sunshine hours in Uyo in the Niger Delta Region, Nigeria. *Advances in Applied Science Research*, 3(4): 1923-1937.
- [24] Meinel A. B., Meinel M. P. 1976. *Applied solar energy. An introduction*. Chapter 8. Addison-Wesley, Michigan.
- [25] Academy of Science of South Africa. 2014. The state of energy research in South Africa. ASSAF, Pretoria.
- [26] Sendanayake S. Miguntanna N. P., Jayasinghe M. T. R. 2014. Estimating incident solar radiation in tropical islands with short term weather data. *European Scientific Journal*, 10 (3): 40-412  
DOI: <http://dx.doi.org/10.19044/esj.2014.v10n3p%25p>.
- [27] Prescott J. A. 1940. Evaporation from water surface in relation to solar radiation. *Transactions of the Royal Society of Australia*, 46: 114-118.
- [28] Angstrom A. 1924. Solar and atmospheric radiation. Report to the International commission for solar research on actinometric investigations of solar and atmospheric radiation. *Journal of the Royal Meteorological Society*: 121-126. DOI: <https://doi.org/10.1002/qj.49705021008>.
- [29] Teke A., Yilidirim H. B. 2014. Estimating the monthly global solar radiation for Eastern Mediterranean Region. *Energy Conversion and Management*, 87: 628-635.
- [30] Günther M., Janotte N., Mezrhab A., Pottler K., Schillings C., Wilbert S. and Wolferstätter F. 2011, Advanced CSP Teaching Materials, Solar Radiation. *Adv CSP Teach, Mater, Enermena*. Chapter 2: 7-82.
- [31] Srivastava R. C., Pandey H. 2013. Estimating Angstrom-Prescott coefficients for India and developing a correlation between sunshine hours and global solar radiation for India. *ISRN Renewable Energy*, (2013). DOI: <http://dx.doi.org/10.1155/2013/403742>.
- [32] Allen R. G., Pereira L. S., Raes D., Smith M. 1998. Crop evapotranspiration (Guidelines for computing crop water requirements). *Food and Agriculture Organization of the United Nations, Irrigation and drainage paper no. 56*, Rome. European Environment Agency. Available from: <http://www.fao.org/docrep/x0490e/x0490e00.htm>
- [33] Sarkar M. N. I., Sifat A. I. 2016. Global solar radiation estimation from commonly available meteorological data for Bangladesh. *Renewables* 3(6). DOI: <https://doi.org/10.1186/s40807-016-0027-3>.
- [34] Marwal V.K., Punia R.C., Sengar N., Mahawar S., Dashora P. 2012. A comparative study of correlation functions for estimation of monthly mean daily global solar radiation for Jaipur, Rajasthan (India), *Indian Journal of Science and Technology*, 5(5): 2729-2732.
- [35] Robaa S.M. 2008. Evaluation of sunshine duration from cloud data in Egypt. *Energy*, 33(5): 789-795.
- [36] Adeala A. A., Huan Z., Enweremadu C. C. 2015. Evaluation of solar radiation using multiple weather parameters as predictors for South Africa provinces. *Thermal Science*, 19 (2): 495-509.
- [37] Ya'u M. J., Gele M. A., Ali Y. Y., Alhaji M. 2018. Global solar radiation models: A review. *Journal of Photonic Materials and Technology*, 4(1): 26-32.
- [38] Itodo I. N., Yohanna J. K. 2011. Correlation between global solar radiation, ambient air temperature and sunshine hours for Makurdi, Nigeria. *Proceedings of the Solar World Congress, Solar Radiation Availability and Variability. 2011*. DOI: <https://dx.doi.org/10.18086/swc.2011.24.17>
- [39] Nia M., Chegaar M., Benatallah M. F., Aillerie M. 2013. Contribution to the quantification of solar radiation in Algeria. *Energy Procedia*, 36: 730-737.
- [40] van den Besselaar E. J. M., Sanchez-Lorenzo A., Wild M., Tank A. M. G. K., de Laat A. T. J. 2015. Relationship between sunshine duration and temperature trends across Europe since the second half of the 20<sup>th</sup> century. *Journal of Geophysical Research: Atmospheres*, 120 (20): 10 823-10 836. DOI: <https://doi.org/10.1002/2015JD023640>.
- [41] Chen J.L., Li G.S. 2013. Estimation of monthly average daily solar radiation from measured meteorological data in Yangtze River Basin in China. *International Journal of Climatology*, 33: 487-498.
- [42] Rivington M., Bellocchi G., Matthews K. B., Buchan K. 2005. Evaluation of three model estimations of solar radiation at 24 UK stations. *Agricultural and Forest Meteorology*, 132: 228-243.
- [43] Jury M. R. 2013. Climate trends in southern Africa. *South African Journal of Science*, 109 (1-2): 1-11. DOI: <http://dx.doi.org/10.1590/sajs.2013/980>.
- [44] Burton M., Cooke S., Godfrey A., Neville L., Pauker E., Le Roux-Rutledge E. 2010. Africa talks climate: The public understanding of climate change in ten countries. Executive Summary. BBC World Service Trust, London, UK, 20.
- [45] South Africa climate and weather by regions. Available from: <http://www.cosechaypostcosecha.org/data/articulos/ConvenioSudafrica/ClimateAndWeather.pdf>.